THE UNIVERSITY OF HULL

Two novel methods of measuring cosmic distances in the Universe

being a Thesis submitted for the Degree of Doctor of Philosophy

in the University of Hull

by

Mikkel Ortving Lindholmer, M.Sc. (University of Copenhagen)

November 2020

Pleasure to me is wonder - the unexplored, the unexpected, the thing that is hidden and the changeless thing that lurks behind superficial mutability. To trace the remote in the immediate; the eternal in the ephemeral; the past in the present; the infinite in the finite; these are to me the springs of delight and beauty.

– Howard Phillips Lovecraft, *The Defence Remains Open! (1921)*

Acknowledgements

I would like to take this as an opportunity to acknowledge and thank the many people that has supported and helped me complete this thesis. Perhaps chief among these are my supervisor Kevin Pimblett as well as, for the last year, my former colleague and senior Yjan Gordon both of whom have had a great understanding and endless patience while I was writing the thesis. Both of their feedback has without a doubt made me a better researcher and has helped me improve as a writer while writing this thesis. I would especially like to thank Kevin for the opportunity he gave me to work at Hull University in a great environment and with some of the most interesting scientific ideas I have had the pleasure of working on.

I had enough luck to be working in one of the best environments imaginable together with many different colleagues including, but not limited to, James Keegans, Gareth Few, Tom Lawson, Chris Jordan, Lawrence Bilton, and Mikkel Kristensen.

Lastly I would like to thank my family for their support as well as their many packages of Danish food, without which I would likely have gone mad while living in England.

Declaration of Originality

This thesis is submitted as a part of the fulfilment of the degree of Doctor of Philosophy from the University of Hull.

I declare that the work submitted as part of this thesis is original and produced by myself with the supervision of Dr Kevin Pimbblet and Elke Roediger. For work, results, plots, or anything else not done by me the sources have been cited and referenced.

Some of the work here has already been published in peer reviewed journal articles. This work has all been authored by myself with the help of Dr Kevin Pimbblet and is presented in this thesis in a format that closely resembles the published work.

Chapter 2 has been published as Lindholmer & Pimbblet (2019) Astronomy & Astrophysics, EDP Scien while chapter 3 presents work that I am currently preparing for submission to the journal Astronomy & Astrophysics as the lead author with Dr Kevin Pimbblet and Dr Yjan Gordon as co-authors. Chapter 4 is work only presented in this thesis and is not currently in preparation for submission to any journal.

Candidates signature:

Date:

Contents

List of Figures

List of Tables

Abstract

We present two novel methods of distance measurement using photometric techniques. We compare the methods to each other and independently created methods to measure photometric redshifts.

The first method we present in this thesis is based on SFR of galaxies which are typically either star forming, quenched, or in transition between the two. This causes the SFR measurements to group up into two distinct and well defined groups in SFR-$M_\star$ space. We measure how these groups evolve with redshift and see a distinct non degenerate evolutionary path which makes it possible to use it for distance measurements. Since this method requires measurements of several different galaxies we apply this method to several galaxy clusters to test it and see how well it works.

The second method uses BL Lac objects to measure distance. While using these objects is not by itself a novel concept, we do extract the host galaxy magnitudes needed to measure the distance in a way that has not before been done on this large an amount of data. We also present several thousand new BL Lac candidates in the SDSS BOSS catalogue which has not previously undergone a systematic and dedicated search for BL Lacs. By doing this we also find many more radio quiet BL Lac like objects which have previously not been detected in a high enough number to properly analyse through the use of statistics.

Finally we compare the two methods to each other as well with an independent photometric redshift method as well as measure the Hubble constant to be able to compare the methods to the distance ladder as a whole. Here the SFR method does not match up well to the independent methods giving worse results, but the BL Lac method give results with similar precision to the independent methods.

1. Introduction

1.1 Cosmology

The story so far: In the beginning the Universe was created. This has made a lot of people very angry and been widely regarded as a bad move.

– Douglas Noel Adams, *The Hitchhiker's Guide to the Galaxy (1979)*

Cosmology is the study of the growth of the Universe. Since the Universe is dynamic and evolving rather than static, measuring any given distance across a length scale of the Universe naturally requires an understanding of the fundamentals of cosmology. This chapter reviews these prerequisites before going on to the areas of observational astronomy and galaxy evolution in order to give the reader a solid background before presenting our original works in the later chapters.

1.1.1 The Big Bang

The name, The Big Bang, was first coined by an opponent of the theory, Fred Hoyle, during a broadcast in 1948 (see Kragh 2013) and it was referred to as a model of dynamical evolution before then. The model itself is a product of many different discoveries since 1912 and even today we continue to see changes to the model and our understanding of it. The earliest signs of an expanding Universe were likely recorded by Slipher (1915) who found evidence that spiral nebulae were receding from Earth. He furthermore noted a systematic redshift of these nebulae. While them having motion relative to us is not something surprising today, at the time, the Universe was believed to be static and astronomers were still uncertain about the existence of extragalactic objects meaning that a systematic redshift was hard to explain. In 1917 Einstein published his general theory of relativity (Einstein 1917) which resulted in a Universe that was either shrinking or expanding. Since this was contrary to the basic notion that the Universe is static he considered that there might have been an error in his theory and
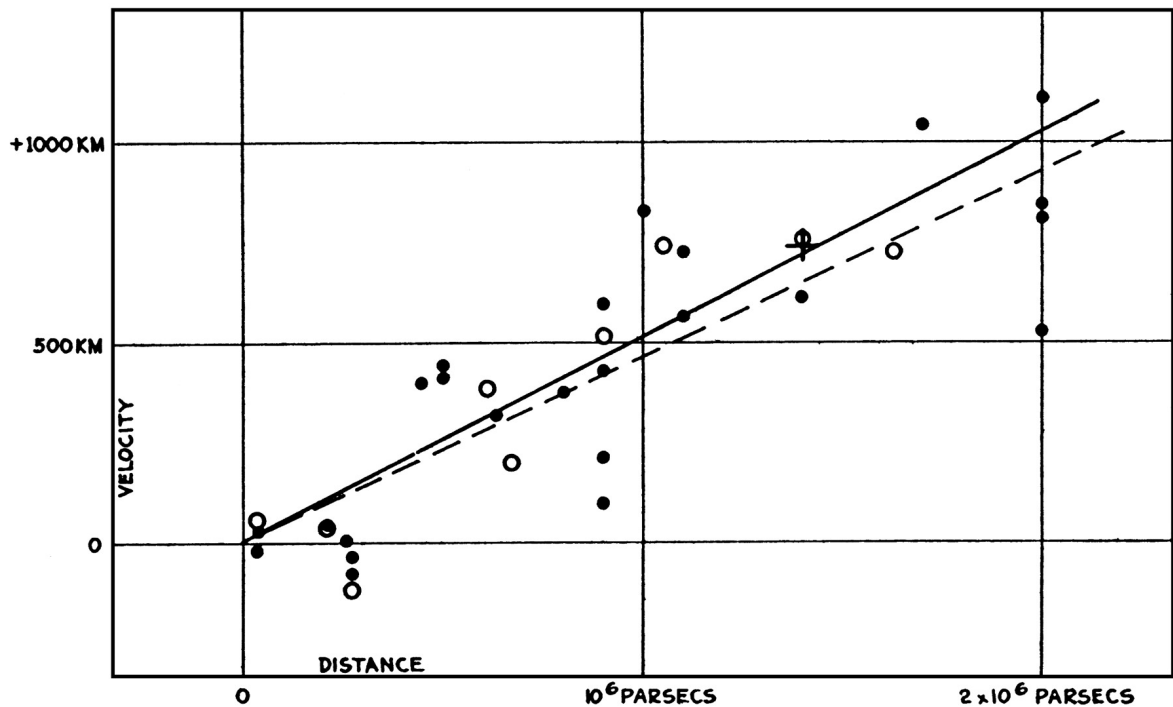
Figure 1.1: The original plot from Hubble (1929), showing the relation between velocity and distance of extra galactic nebulae. The black circles and full line represent the solution if the nebulae are used individually whereas the white circles and striped line represent a solution where the nebulae have been grouped into nine groups based on their proximity. We can clearly see from this plot that there is a correlation between distance and velocity which is what Hubble (1929) postulated. These results pointed to a Hubble constant of 500 km/s/Mpc.

added an extra constant for the Universe to remain static.

With this the groundwork for the Big Bang model has been laid. However it still took 10 years before Georges Lemaître published his paper explaining the redshift of these spiral nebulae (see Lemaître 1927). According to him the Universe was expanding rather than static and his model predicted that as objects got further away from us their redshift would increase. Two years later Edwin Hubble provided observational evidence that this was case, essentially providing a foundation for Lemaître's theory. Hubble used the redshifts of the observed objects to calculate their velocity relative to us and by cross checking with distance measurements discovered that the redshift was directly proportional to the distance of each objects (see Fig. 1.1, Hubble (1929)). Together with Milton Humason he formulated Hubble's law, now known as the Hubble–Lemaître law, which relates redshift to distance from us (see Hubble & Humason 1931). This law is consistent with Einstein's general theory relativity and assuming an homogeneous and isotropic Universe it suggests that the Universe itself is expanding rather than all objects simply moving away from each other into an empty space. In 1931, Lemaître took this expansion to its natural beginning and suggested that an ever expanding Universe must have started in an infinitesimally small point (see Lemaître 1931). Naturally this was challenged as the idea of an ever-changing Universe was hard to accept and a rival theory was made to challenge it. This theory would become known as the Steady State theory.

The Steady State theory was first suggested by Hermann Bondi, Thomas Gold, and Fred Hoyle (see Bondi & Gold 1948; Hoyle 1948). According to this theory new material was constantly being constantly created as the Universe expanded. This was done to keep the density of matter in the Universe constant despite the objects in the Universe constantly moving away from each other. While the theory developed by Lemaître had had some success in explaining the abundance of different elements it failed to explain elements heavier than helium which could not have been created in large amounts during the Big Bang and therefore would have to be explained with supernovae or similar processes which where also present in the Steady State Theory (see Hamblin 2005). This gave some, perhaps undeserved, credibility to the Steady State theory and combined with measurements of the Hubble constant

that according to this early Big Bang model indicated the age of the Universe to be only 2 billion years meant that the Steady State theory seemed very plausible. It is during the time that these competing theories were debated that Fred Hoyle mockingly refereed to it as the Big Bang theory. Unfortunately for Hoyle precise measurements of the Cosmic Microwave Background proved to be indisputable evidence for the Big Bang theory (see Weinberg 1972). The fact that it shows as a black-body radiation to a very high degree suggests that some mechanism must have made it all at once and likely from a highly homogeneous Universe. This suggests a smaller, denser, and much hotter Universe in line with what the Big Bang theory predicted[1].

This evolution has led to the currently accepted model, the hot Big Bang model, which was adopted to better describe and explain the five key parameters observed in the Universe (see Roos 2008). These parameters are the Hubble Constant H_0, density parameters for matter and radiation Ω_m and Ω_r, the spacial curvature Ω_K, as well as the cosmological constant Ω_Λ (see Ade et al. 2014; Uzan 2016). To describe how the Universe evolves it is easiest to look at how the different density parameters evolve and consequentially which parameter is dominant in the Universe.

Since the Big Bang model suggests that the Universe was once an infinitesimally small point it is important to realize that the evolution of each of these parameters are correlated to the size of the Universe and therefore use that instead of time. To do so it is easiest to visualize with a scale factor. We will define this scale factor as a for which it follows that

$$d(t) = a(t)d_0 \tag{1.1}$$

where $d(t)$ is the proper distance at a given epoch t and d_0 is the distance at the reference time t_0. We here easily see that by definition $a(t_0) = 1$. Since the energy density of radiation can be described by $\rho \propto a^4$ (see Roos 2008) and since no other energy density follows a more extreme proportionality it follows that in the earliest stages of the Universe it was dominated by radiation. At this stage the Universe would have looked much different from how it is today. The temperature, T, of the Universe would have been so large that

---

[1]Edgar Allan Poe also seems to suggest this in his poem Eureka (Poe 1848) although this has in more recent years been discarded as mere coincidence

the energy of single photons could produce particle-antiparticle pairs. As the Universe then expands the temperature rapidly cools which has several different consequences; mainly that the particle anti-particle production stops and that some interactions which were efficient at higher temperature stop being efficient (Alpher et al. 1953) and therefore leaves relic particles (Alpher et al. 1953) which it is no longer efficient to produce or break down (see Alpher et al. 1948). This decoupling process happens as the relic particles decouple from the temperature of the Universe and is generally believed to happen in three main steps (see Uzan 2016 for more information on these steps):

1. For $T > 1$ MeV, (age of the Universe $(t) < 1$ s) the neutrons, protons, electrons, positrons and neutrinos are kept in statistical equilibrium by the weak interactions

$$n \longleftrightarrow p + e^- + \bar{\nu}_e, \qquad n + \nu_e \longleftrightarrow p + e^-, \qquad n + e^+ \longleftrightarrow p + \bar{\nu}_e. \qquad (1.2)$$
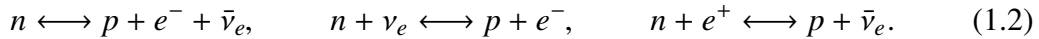
   As long as these equilibria hold we can predict the abundance of each of the elements and can as such predict the neutron to proton ratio to be described by

$$n/p = e^{-Q_{np}/k_B T} \qquad (1.3)$$

   where $Q_{np} \equiv (m_n - m_p)c^2 = 1.29$ MeV. The abundance of the other light elements can be described in a similar way (Alpher et al. 1953).

2. At about T $\approx$ 0.8 MeV (t $\approx$ 2 s) the weak interactions freeze out and below this temperature the number of neutrons and protons change only from the neutron β-decay until the Universe is cooled to T $\approx$ 0.1 MeV where p+n reactions happen faster than their dissociation (Peebles 1966).

3. For 0.6 MeV $> T >$ 0.05 MeV (3s $< t <$ 6 min) the synthesis of light occurs by two-body reactions. This allows for helium to be created through first creating deuterium and then combining two deuterium atoms (Peebles 1966).

As the Universe expands and cools down the energy density of radiation drops below the energy density of matter. This is due to the equation of state of radiation following the expansion of the universe so that $\Omega_r \propto a^4$ compared to matter for which it follows that $\Omega_m \propto a^3$ where

a is in both cases a denoting the size of the Universe. This happens around 47,000 years after the big bang (Ryden 2003). Despite this the Universe is still optically dense to radiation for another 300,000 years (see Alpher & Herman 1948; Gamow 1948; Ryden 2003). After the Universe cools further down the deuterium isotope is too fragile to be created in great enough abundances that helium can be produced and the process therefore also freezes out. As long as the temperature of the Universe remains larger than the ionisation energy of the hydrogen atom (13.6 eV), matter is ionized and photons are coupled to the electrons through Compton scattering (see Compton 1923; Uzan 2016). As the temperature decreases further the formation of neutral atoms happens and photons decouple from matter giving rise to the relic radiation otherwise known as the cosmic microwave background (CMB, see Penzias & Wilson 1965; Fixsen 2009).

Another effect of this decoupling can be observed in the form of baryon acoustic oscillations (BAO, Eisenstein et al. 2005) which refer to the sounds waves in the primordial matter. These sound waves occurred due to excitations from the perturbations in density. As the Universe then cooled and radiation decoupled from matter the speed of sound would have abruptly decreased and the propagations of these waves would have nearly ended (Eisenstein et al. 2005). Their direct effect can be seen in the CMB as well as a slight preference for galaxies to form at the peaks of these acoustic waves due to those locations already containing higher mass from dark matter (Eisenstein et al. 2005). Measuring the distance between these peaks at a given time hints at the expansion of the Universe and as such a direct hint at the Hubble parameter at the observed objects (Eisenstein et al. 2005).

1.1.2   Expansion of the Universe

As mentioned in chapter 1.1.1 Einstein discovered the theory of general relativity (see Einstein 1917) and by doing so created the fundamentals for an expanding or shrinking Universe. He did however not like this model and initially added a constant to ensure the Universe were static:

$$\Lambda = \frac{1}{R^2} = 4\pi G \rho \tag{1.4}$$

where G is the gravitational constant and the volume of the Universe is given by $2\pi^2 R^3$ (Einstein 1917). However this model proved inadequate at explaining the shifts of known spectral lines exhibited in early observations of galaxies Hubble (1929) which we described in the previous chapter. Using this Edwin P. Hubble was among the first to measure the systematic increase in velocity with distance and figure out that it had a linear relation of $v = H_0 r$ which using the z from before can be rewritten to

$$z = H_0 \frac{r}{c}. \tag{1.5}$$

This has become known has the Hubble-Lemaître law and one of the direct consequences of it is that the Universe is expanding.

Following Einstein's discovery, in 1922 Alexander Friedmann found several solutions (see Friedman 1922) that used general relativity to create an expanding Universe keeping in line with Hubble's law. Unfortunately this discovery did not gain much recognition before they were independently derived by Georges Lemaître in 1927 gaining Lemaître recognition as the father of the Big Bang model.

Today the standard cosmology model uses the Friedmann-Lemaître equations as well as the Robertson-Walker metric which were published in 1935 (see Robertson 1935) and matches the general geometrical structure of the Einstein tensor $G_{\mu\nu} = 8\pi G T_{\mu\nu}/c^4$ where $T_{\mu\nu}$ is the stress-energy tensor that describes the density and flux of energy and momentum (see Lovelock 1971). Covering general relativity to the point of explaining what these are would be outside of the scope of this thesis. Fortunately, however, we need only cover the case for a comoving observer with a velocity four-vector of $v = (1, 0, 0, 0)$ in an homogeneous and isotropic Universe and in this specific case we only need two equations to describe the expansion of the Universe:

$$\left(\frac{\dot{a}}{a}\right)^2 \equiv H^2 = -\frac{kc^2}{a^2} + \frac{8\pi G}{3}\rho, \qquad \frac{2\ddot{a}}{a} + H^2 = -\frac{kc^2}{a^2} - \frac{8\pi G p}{c^2} \tag{1.6}$$

where H is the Hubble parameter and p is the pressure of the Universe (see Roos 2008). These equations inherently contain the contraction or expansion of the Universe, $\dot{a}$, which the first equation is shown to increase with the density of matter, ρ, while the second equation shows

that the density of matter, together with the pressure, also decelerates this expansion. We can use the first equation to eliminate the $\ddot{a}$ in the second equation to obtain the covariant conservation equation:

$$\dot{\rho} + 3H(\rho + pc^{-2}) = 0. \tag{1.7}$$

By making the assumption that ρ and p are linearly related by the equation of state, $\omega \equiv p/\rho c^2$, one can rewrite 1.7 to take the form $\dot{\rho} + 3H\rho(1+\omega) = 0$. From statistical mechanics we know that the equation of state for a radiation filled Universe has $\omega = 1/3$ whereas the Universe today will have $\omega = 0$ (see Roos 2008). This directly confirms what we stated earlier since using these values for ω equation 1.7 implies that $\rho_m(a) \propto \Omega_m \propto a^{-3}$ and $\rho_r(a) \propto \Omega_r \propto a^{-4}$.

By integrating 1.6 we find a relation between time and size of the Universe, $a(t)$. Since observations have shown that to a good degree of confidence $k = 0$ (see Eisenstein et al. 2005) we will, in this work, focus on this case of flat space where $k = 0$ and the integration can be done easily. In this case we find that in a radiation dominated Universe which we had in the early days of the Universe $a(t) \propto t^{1/2}$ whereas a matter dominated Universe has $a(t) \propto t^{2/3}$ (see Roos 2008). We can directly see now that as t approaches 0 so does the scale and therefore also the energy density. It is from this singularity that the model got the name the Big Bang. Although the result is of interest we must remember that quantum mechanics does not allow for results with exactly zero scale or time implying that this result is a theoretical nuance rather than an observed one. It is however quite understandable that this is the case since general relativity, which all of this is based upon, does not include quantum mechanics and will therefore break down whenever we approach territory where quantum mechanics becomes important.

In the static Universe, first proposed by Einstein, $a(t)$ was constant and the age of the Universe therefore infinite. In order for this to be the case in a Universe where ρ is positive Eq. 1.6 implies that k must be positive (see Roos 2008). This in turn leads to the result that the Universe is contracting and p is negative. In order to keep the Universe static Einstein therefore added Λ, the cosmological constant, which corresponded to a correction in geometry adding enough repulsion that the Universe once again was static. However as we previously noted Hubble later showed that the Universe is expanding making the cosmological constant

unnecessary at the time. Since then studies using supernovae as well as other methods have indicated that the Universe might in fact be accelerating in its expansion (see Riess et al. 1996; Peebles & Ratra 2003; Seo & Eisenstein 2003; Bernstein & Jain 2004; Eisenstein et al. 2005; Taubenberger et al. 2019; Inserra et al. 2021). This expansion has been attributed to dark energy and mathematically works similarly to Einstein's cosmological constant (see Eisenstein et al. 2005). Due to this the cosmological constant has been reinserted although it now represents dark energy rather than a constant to keep the Universe static. For this work we only need to note that this cosmological constant has been described as dark energy which has the properties of being an ideal fluid with energy density $\rho_\Lambda = \Lambda/8\pi G$ and negative pressure $p_\Lambda = -\rho_\Lambda c^2$ (see Roos 2008). This in turn implies that for positive Λ the dark energy acts as a universal repulser which counteracts the effects of gravity on physical matter. In a Universe dominated by this dark energy we expect the equation of state for the Universe to have $\omega = -1$ resulting in a exponentially expanding Universe. Observations tell us that we are not living in this kind of Universe yet. It should however be noted that the energy density of dark energy does not decrease with the size of the Universe and so the Universe is likely to end up in a state where it is dominated by dark energy.

Having defined how the Universe expands when dominated by different types of energy densities we can finally combine it all together. To do so we first normalize all energy densities to the critical density, $\rho_c = 3H_0^2/8\pi G$, which is defined such that if the total energy density of today, ρ_0, is equal to the critical density then the Universe is flat. Using this definition we can now define the energy density in dimensionless parameters

$$\Omega_m(a) = \frac{\rho_m}{\rho_c}, \qquad \Omega_r(a) = \frac{\rho_r}{\rho_c}, \qquad \Omega_\Lambda = \frac{\rho_\Lambda}{\rho_c}, \qquad \Omega_0 = \frac{\rho_0}{\rho_c}. \tag{1.8}$$

We can now address the Hubble parameter from Eq. 1.6. By rewriting it we see that it is a function of a and by making use of the dimensionless parameters we just defined we can see that

$$H(a) = H_0 a(\Omega_k a^{-2} + \Omega_m a^{-3} + \Omega_r a^{-4} + \Omega_\Lambda)^{1/2} \tag{1.9}$$

where Ω_k is the energy density added due to curvature of space for which $\Omega_k = 1 - \Omega_0$ Roos (2008). This finally gives us the evolution of the size of the Universe. Alternatively by

integrating Eq. 1.9 from $a = 0$ to $a = 1$ we can find the age of the Universe or the look back time by integrating from present day, t_0 to a given time, $t(a)$. An important thing to note from 1.9 is that the Hubble constant is not quite a constant but rather a parameter that changes with the size and energy densities of the Universe as seen in figure 1.2. This is quite important for several types of distance measurements which we will get back to later as we first need to build up knowledge about how exactly we measure distances in the Universe. Since the Universe stretches over enormous distances several different methods are required to measure objects at different distances as some methods work better at certain distance intervals and other methods are all together impossible to use at certain distances. This build up and co dependence of different measurements is what we call the distance ladder which we shall now take a look at.

1.2   The distance ladder

There are no safe paths in this part of the world. Remember you are over the Edge of the Wild now, and in for all sorts of fun wherever you go.

– J.R.R. Tolkien, *The Hobbit, or There and Back Again (1937)*

As we mention in the previous section, by trying to settle the great debate and testing if the 'island Universes' were external or internal to the Milky Way, Hubble measured the movement and distance to several galaxies and by doing so provided evidence that the Universe was expanding. He did this by measuring the redshift of galaxies and then measuring the distance to the galaxies by looking at Cepheids. Both of these form some of the fundamental steps of the distance ladder. To understand this distance measurement and the core of this work we therefore turn our attention to the distance ladder. The first step of the distance ladder begins at measuring the distance to the Sun.

1.2.1   Distance to the sun

Aristarchus of Samos deduced in his time that the Earth must orbit the Sun (see Batten 1981). In his time he thought that there must be a difference in time between half moons since the moon would have to form a right angle with the sun whenever it happened (see Fig. 1.3).
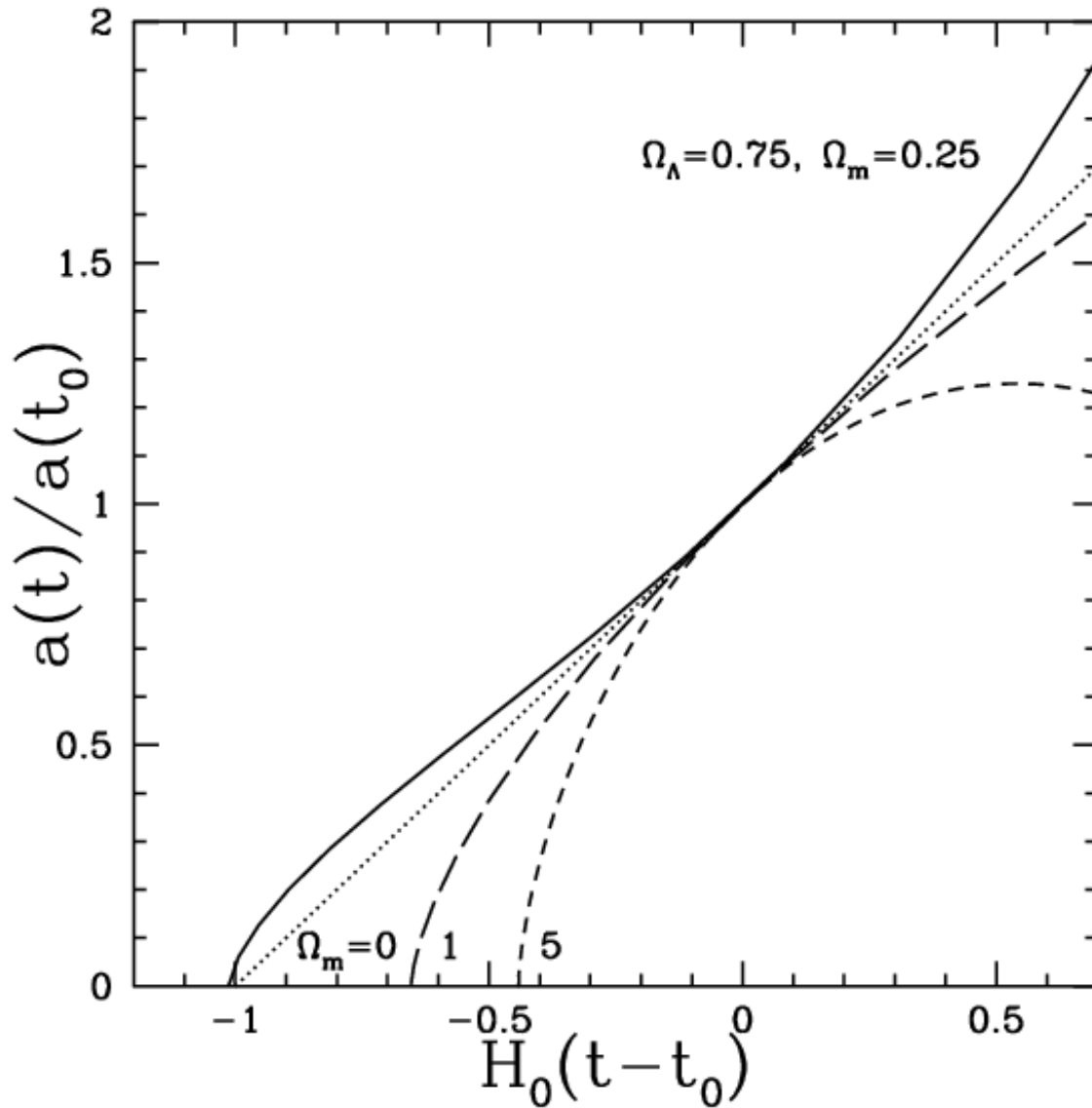
Figure 1.2: Plot lot of how the Hubble parameters evolves with size of the Universe. The different lines in the graph represent different types of Universes. $\Omega_M = 5$ represents a closed Universe which has a very high matter density to the point where the Universe collapses again causing a 'Big Crunch' and possible new Big Bangs, $\Omega_M = 1$ represents a Universe with similar energy density to ours but where all of it is matter, $\Omega_M = 0$ represents an empty Universe, and finally $\Omega_M = 0.25, \Omega_\Lambda = 0.75$ represents our current model of the Big Bang including both dark energy and radiation. Frieman (2008)
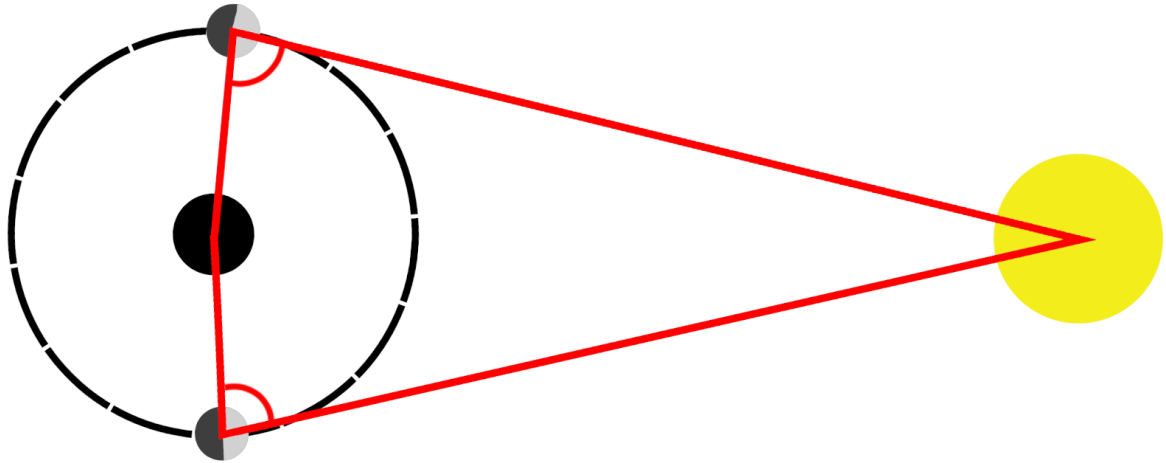
Figure 1.3: Not to scale diagram of the Sun, Moon and Earth. The black circle represents the Earth, the yellow circle the Sun, and the grey circle the Moon with one of its sides lit up. Aristarchus of Samos used the right angles between the Earth, Moon and Sun, which are highlighted in red, to calculate the distance to the Sun.

Using the time measurements of his time he deduced this difference to be 12 hours which would result in an angle, θ, of $\theta = \pi/2 - 2\pi \cdot 12$hours/month and $\cos\theta = d/D$ where d is the distance to the moon and D is the distance to the sun. This resulted in a ratio of $D = 20d$. We know now that this difference in time is closer to half an hour which results in $D = 390d$ or about 150 million kilometres or 1 astronomical unit (AU). Unfortunately the ideas of Aristarchus were discarded by his contemporaries and it was not until Copernicus presented his heliocentric model that Aristarchus gained proper recognition (Kish 1978).

1.2.2   Nearby stars - up to 12 pc

The next step of the process is then to measure the distance to nearby stars. This was first done by Friedrich Bessel in 1838 where he used parallax (see Bessel 1838), that was previously used to measure distance to planets, to measure the distance to these nearby stars. He did so by measuring the angles to stars six months apart (see Fig. 1.4). If a given star had an angle difference of a single arcsecond (1/3600th of a degree) he calculated that this distance, a parsec (pc), would be about 206,265 AU away. In 1917 Joan Voûte used this method to measure the distance to Proxima Centauri (see Voute 1917). He found a difference in angle of 0.755" ± 0.028" which results in a distance of 1.301 pc. More interestingly, perhaps, is
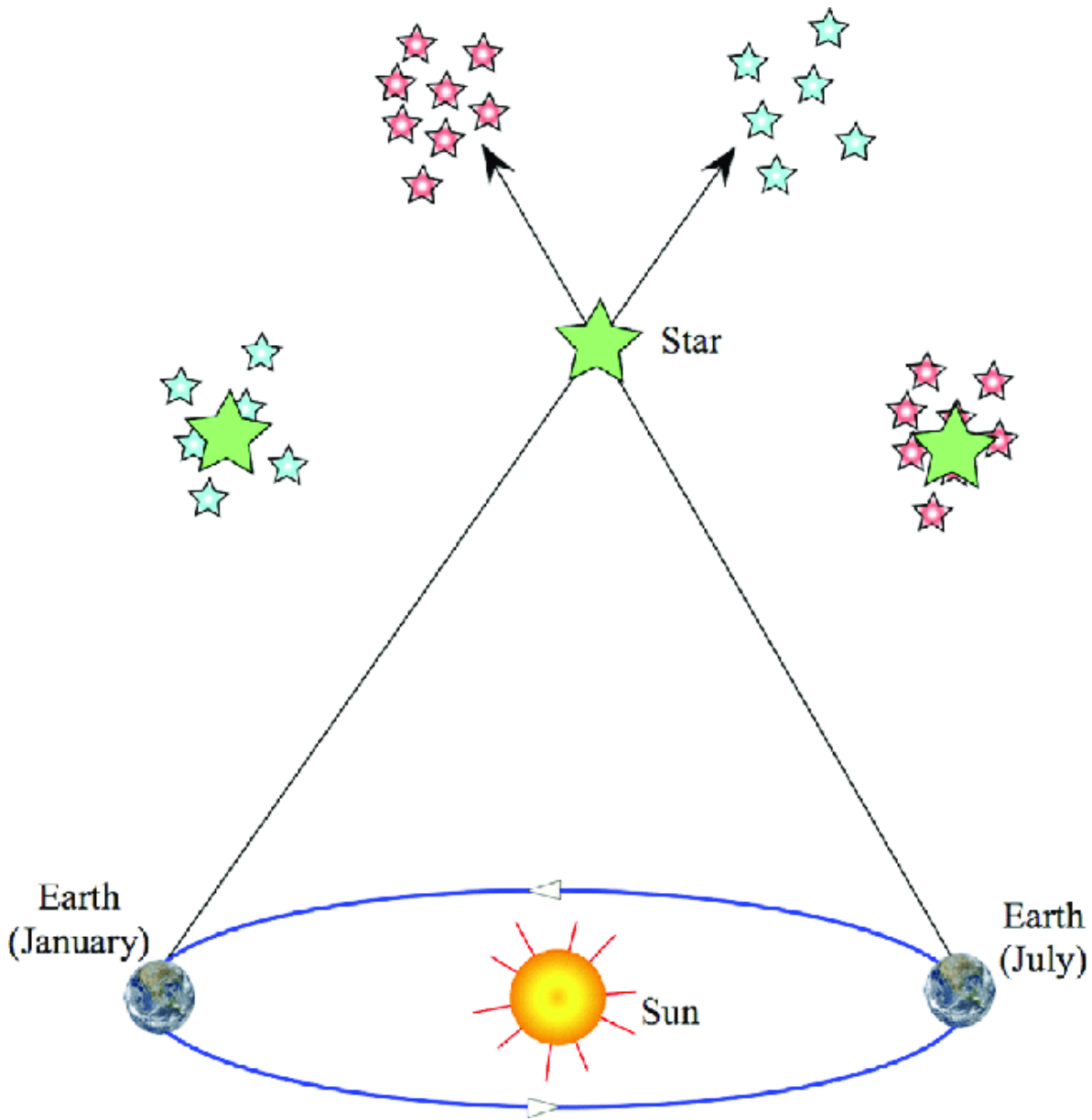
Figure 1.4: The parallax to a given star is defined by half angle of the vertex of the triangle created between the given star and the earth's orbit around the sun. Doing this we can measure the distance to the star based on the distance between the earth and the sun. In this method we use that the angle difference, p, is related to the distance to the star, d, as $p = 11AU/d$. Similarly this method can be used by measuring with two different telescopes at the same time. Taken from Mahmood et al. (2016)

the parallax measurement of Polaris. This star has a much smaller angle difference of only 7.54 ± 0.11 milliarcseconds (mas, van Leeuwen 2013) but its type, namely a Cepheid star, makes it a very intriguing target for distance measurements as we shall see in just a moment (see van Leeuwen 2013). It is this very dependence on the previous step, measuring the distance to the sun, that gives us the first two steps of our distance ladder and how we go further up the distance ladder. In essence a more accurate measurement of the distance to the sun, the first step of our distance ladder, gives us a more accurate measurement of a parsec which gives a more accurate measurement of later steps in the ladder. In more recent years, astronomy missions such as Hipparcos (van Leeuwen et al. 2007) and Gaia (Gaia Collaboration et al. 2017) have both proven instrumental in collecting data and hundred of thousands of stars and their parallax data including several hundred cepheids. Both missions also greatly improved the accuracy at which parallax was measured. There are a few methods which are independent of this such as redshift but discounting those methods we see a clear ladder where each step builds on top of the previous step and a change in previous steps changes the size of the entire ladder. We shall go through some of the major of these steps until we finally reach the largest of the steps as well as where the later chapters of this work fit in.

1.2.3   Cepheid variables - ~100 pc to ~33 Mpc

Our next step lies in measuring Cepheid variables. These are a special type of star that varies in luminosity and whose pulsation period is strongly related to its luminosity (see fig 1.5, Hubble (1927)). These were the objects used to settle the great debate (see Smith 2009) about the existence of extragalactic objects and as such hold special importance in the history of astronomy. Although observers had been aware of what we now know are galaxies separate from the Milky Way since Messier and Herschel (see Messier 1781; Herschel 1802) these were thought to be objects inside our own galaxy for more than 100 years. It was only in the early 1900s that astronomers began collecting evidence that there were objects beyond our own galaxy (see Curtis 1917). It was this evidence that started the 'great debate' which lasted a few decades before Hubble presented strong evidence, using Cephied variables, that
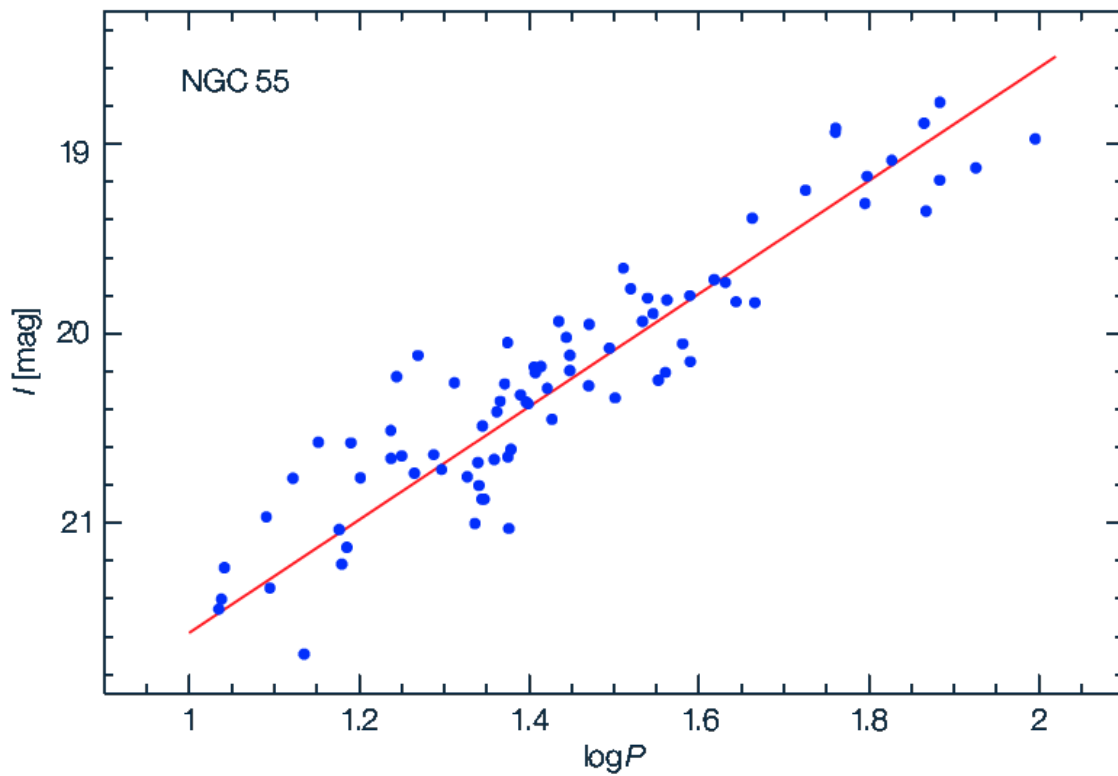
Figure 1.5: The relation between Cepheid magnitude and period for Cepheids in NGC 55. In this case the I-band is used and the period is in days. The red line shows the fit which is clearly linear in nature indicating that Cepheids are indeed standard candles. Plot taken from Gieren et al. (2005)

there were objects much further away than the reaches of the Milky Way. Before this the Milky Way was believed to have a diameter of less than 30,000 light years (Shapley & Curtis 1921) which at the time suggested that if spiral nebulae were beyond the reaches of the Milky Way then they would have to rotate at speeds faster than the speed of light (see Hetherington 1993). The brightness of some of these objects also suggested that if they were extragalactic in nature then they would have absolute magnitudes beyond anything else seen in the sky. While some arguments were made counter to this it was not until Hubble used Cepheid variables (Hubble 1927) to show that some of these were at astonishingly large distances relative to other observed objects that the 'great debate' was finally settled in favour of extragalactic objects. It is after this that, as we noted in the previous chapter, Hubble discovers that many of these galaxies have their light 'stretched' and that the further away they are the more stretched the light becomes. We are, however, getting ahead of ourselves as that step in the distance ladder is not until later. Indeed our next step lies at the Tip of the Red Giant Branch (TRGB).

1.2.4   Tip of the Red Giant Branch - ~500 pc to ~14 Mpc

The TRGB sequence marks a well understood abrupt transition of low-mass RGB stars onto the lower-luminosity horizontal branch (see Fig. 1.6, Sakai (1999)). These stars enter this phase when they begin having a hydrogen burning shell surrounding a helium core which is supported by electron degeneracy pressure. Their transition away from the TRGB is initiated by a helium flash where the star quickly loses luminosity as it once again becomes gas pressured in its core. The whole process is well understood (see Sakai 1999) making them excellent standard candles. Furthermore they are very easy to pick out due to their distinct features in colour-colour plots (see Fig. 1.6). The I band, a set of wavelength around 7625 Å, has proved to have a very tight spread of absolute luminosities and provides a good standard candle (Bellazzini et al. 2001). However since it requires us to measure the entire path of the TRGB and measuring the same star as it approaches the TRGB and leaves it over a period of some million years is impossible we have to get creative. Normally we use this method to measure the distance to entire galaxies since they will have many stars which are in the
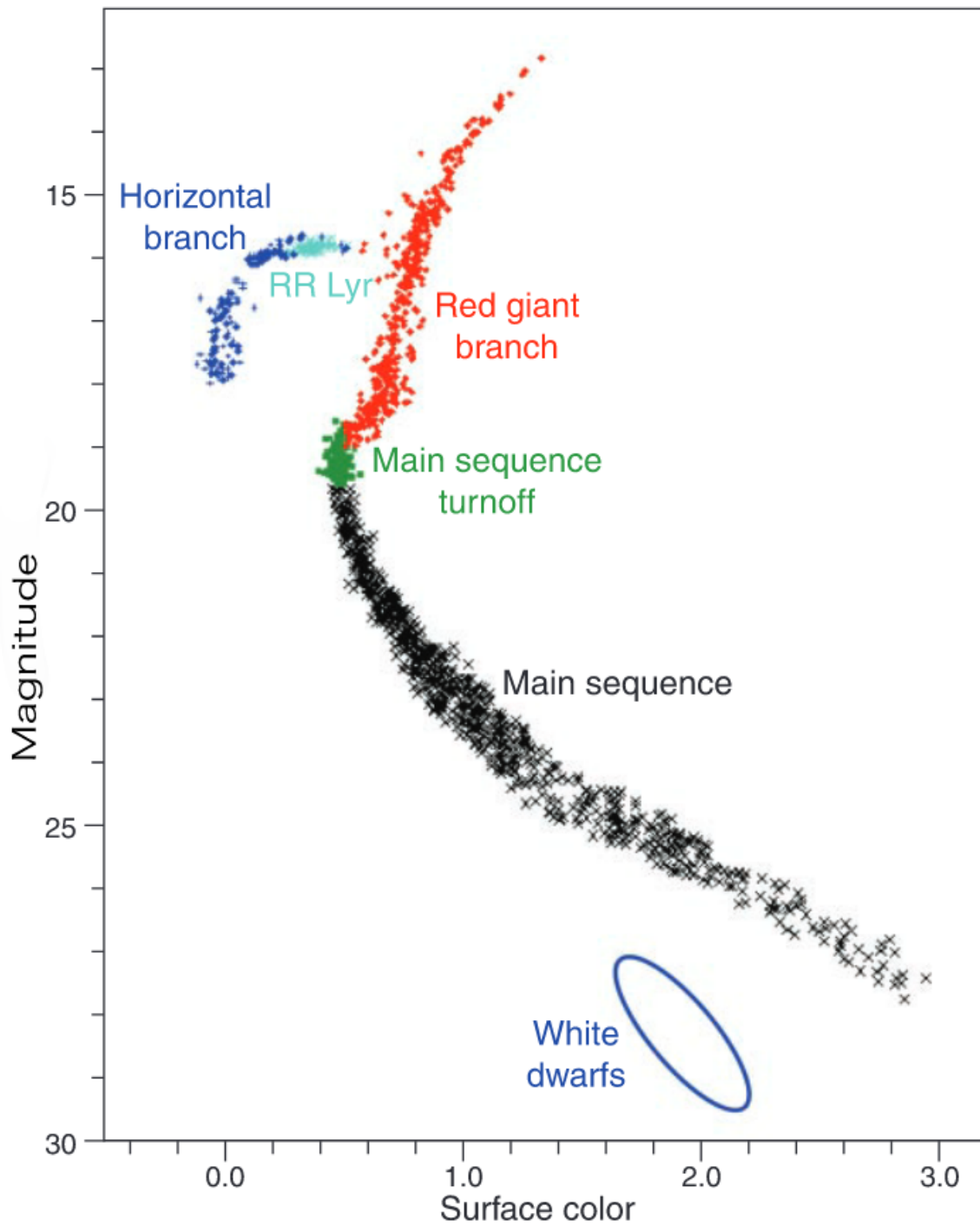
Figure 1.6: Colour-magnitude plot of stars in a typical globular cluster. The red giants branch is marked by red dots while other types of stars are marked by different markers. We are mainly focused on the very tip, the top right, portion of the red giants. This tip will always be at approximately the same absolute magnitude making it an excellent standard candle. There are no white dwarfs in this case since they are too dim. Taken from Krauss (2003)

TRGB at the same time thus creating good picture of what path each of them will take or have already taken. This is our first step of the distance ladder where we use multiple objects to collectively measure the distance to a group of objects rather than measuring the distance to a single object. Depending on the method we go back and forth between using groups of objects like this or single objects similar to how we measured the distance to Cepheids. It is therefore important to note that there are strengths and weaknesses of each of these. Since almost all galaxies will have stars at the TRGB this method can be used for almost all galaxies however compared to measuring single objects we need to define which objects to include in the group of objects, in this case which stars, we use for the measurement. In the case of messy or sparse groups this can become difficult. On the other hand measuring single objects does not require us to define groups of objects but rather to find these specific objects. In the case of Cepheid stars these appear regularly enough that can find one that lies close to or inside most of what we want to measure the distance to but on the higher steps of the distance ladder some of these objects become more sparse or too dim and are therefore not always available to use as a measurement. An example of this would be Type Ia supernovae (SNe) which are the next step in our ladder.

1.2.5   Supernovae - ~6 Mpc to 3200 Mpc

Supernovae had already been observed during the 'great debate' but since their absolute luminosity would reach $M = -16$ they were initially considered to be evidence against the presence of extragalactic objects (see Pigatto 2005). Baade & Zwicky (1934) later showed that there existed a distinction between novae seen our galaxy and the extragalactic supernovae. Their evidence even strongly suggested that the dispersion of peak luminosities of these supernovae where small at about 1.1 magnitudes and suitable candidates for being standard candle. Today this dispersion has been narrowed down partly due to a stretch factor (see Fig. 1.7) but also because we understand the mechanics of the particular kinds of supernovae, namely type Ia SNe, where instead of a single large star nearing the end of its life cycle these supernova comes from a binary system where a white dwarf star is accreting mass from a larger star nearing the end of its life cycle. As this happens the white dwarf will
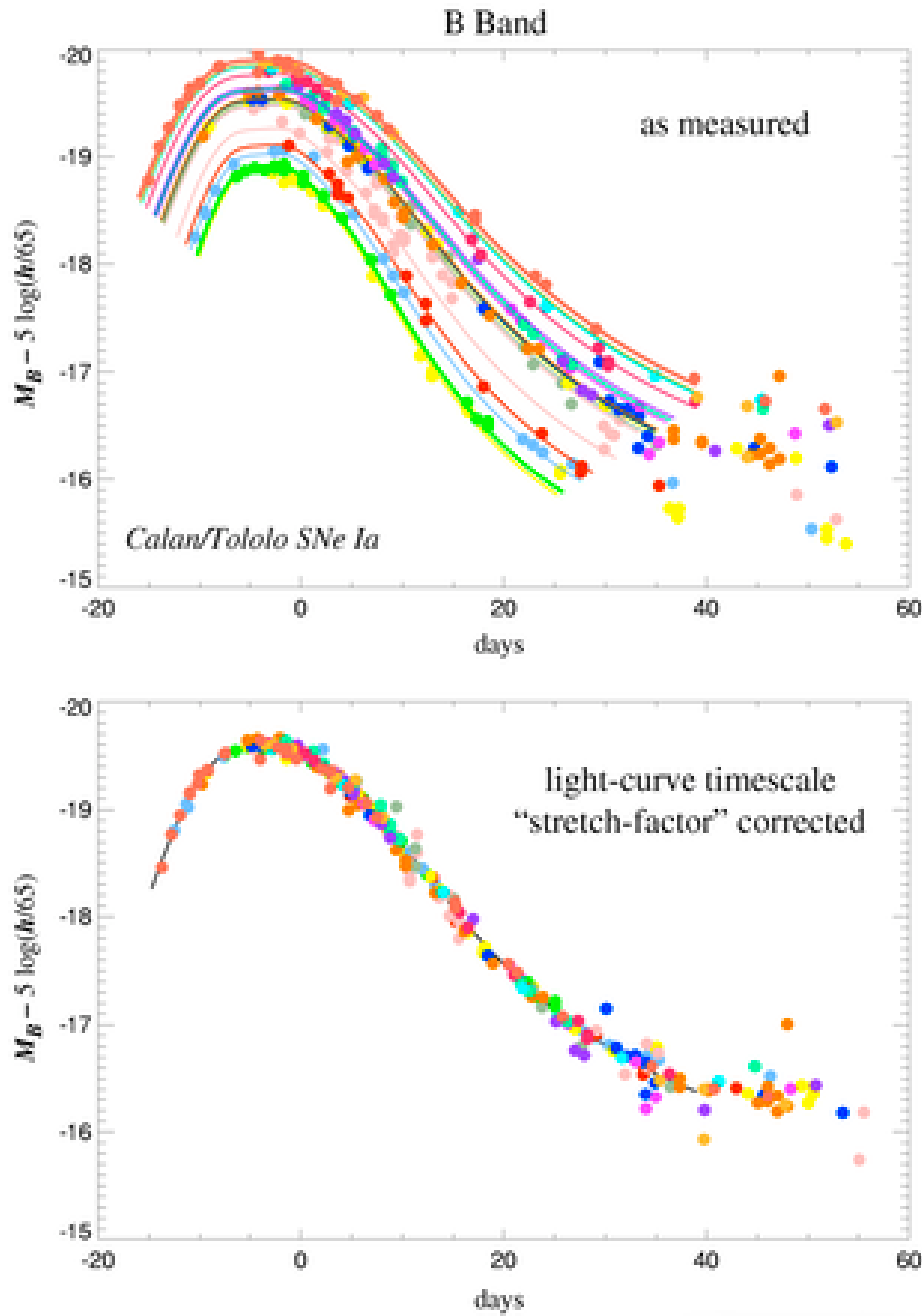
Figure 1.7: Top is the light curves of several supernovae which are colour coded based on the speed at which they top out and begin dimming. Bottom is a unified plot where a stretch factor (see Lapuente 1997) has been applied based in the speed at which a given supernovae dims. The correlation is very obvious and is the reason it can be used as a standard candle. Plot is from Garcia-Bellido (2004)

reach Chandresekhar limit (named after Subrahmanyan Chandrasekhar but first discovered by Anderson 1929; Stoner 1929) of about 1.4 $M_\odot$ (Anderson 1929; Stoner 1929) where the white dwarf is no longer stable. Since this limit is the same for any given white dwarf this instability and following supernovae always happens at the same conditions and results in the same brightness every single time. This made them a subclass of supernovae with very tight dispersion of luminosities, and thus established them as an important step on the distance ladder. By pure luck Baade's sample contained no type II supernovae which have significantly lower luminosity than type Ia supernovae. It is only in 1941 that Minkowski (Minkowski 1941) classifies type II supernovae as another category of objects due to the presence of hydrogen in their spectra. With the distinction of type I and II made and an increasingly large list of spectroscopically defined type I supernovae that the dispersion in peak magnitudes sharpened to about 0.7 magnitudes. The sample was however still impure and contained supernovae with no silicon lines (Pruzhinskaya & Lisakov 2016). These objects are now classified as type Ib and Ic supernovae leaving the group of type Ia SNe to form a very homogeneous set which is very tightly packed in peak luminosity measurements and thus a good indicator of distances.

1.2.6   Magnitudes and distances

This concludes our examples of the distance ladder obtained from apparent and absolute magnitudes of specific objects. Before we move on it is then perhaps prudent to talk a bit about how exactly distance is related to absolute and apparent magnitude. Naively one might use that the intensity of light is related to distance by $I \propto 1/d^2$. In a vacuum this is definitely correct and space is mostly vacuum. In astronomy we mainly use magnitudes. The Greek astronomer Hipparchus established this scale such that the brightest object he could see had an apparent magnitude of 1 and the dimmest objects a magnitude of 6. In terms of actual intensity this corresponds to a difference of a factor of 100 (see Pogson 1856; Ptolemy 1998). We can therefore write that

$$100^{\frac{m-M}{5}} = \frac{F_{10}}{F} = \left(\frac{d}{10pc}\right)^2 \tag{1.10}$$

where F_{10} is the flux measured at a distance of 10 parsecs, F is the flux measured at a distance of the observer, d, m is the apparent magnitude, and M is the magnitude measured at a distance
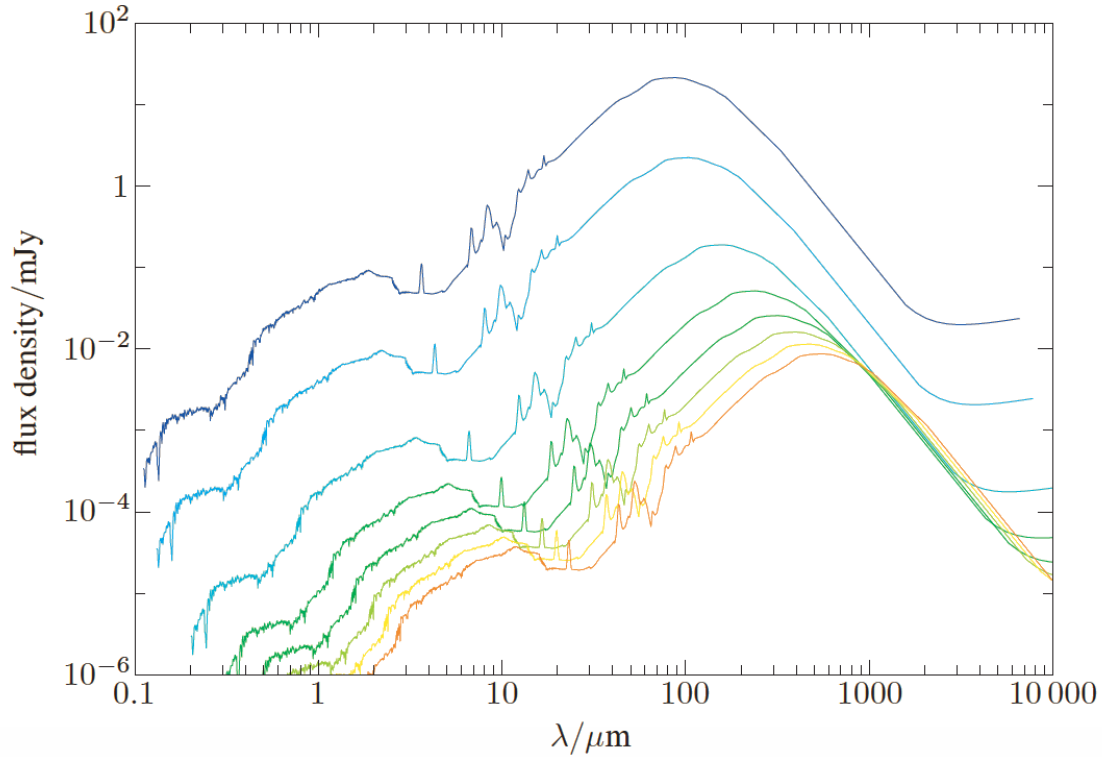
Figure 1.8: Plot showing the spectral energy distribution of M82 if it was located at different redshifts. The colours from blue to red refer to redshifts of 0.1, 0.3, 1, 2, 3, 4, 5, and 6. Note how if we observe the same set of wavelengths the galaxy will appear to have different magnitudes independent of the dimming due to distance. This is resolved by a k-correction which in some circumstances can end up being positive for certain wavelengths. Figure taken from Serjeant (2010).

of 10 parsecs. This equation is somewhat unintuitive and rather unwieldy. Fortunately it can be rewritten in terms of logarithms to look like this:

$$M = m - 5\log_{10}(d_{pc}) + 5 \tag{1.11}$$

which intuitively shows what we expect, namely that as the distance increases the apparent magnitude must become dimmer if the object is to have a constant absolute magnitude. If we assume that space is a vacuum this is all we need and as long as we can find a standard candle we can measure the distance. Fortunately the Universe is much more interesting than this. In the actual Universe we have a few more factors to consider than this. The main ones among these are extinction and k-corrections. We will now turn our attention to these as well as the evolution correction which also changes our measurements in some cases relevant to

this work.

Although there is some uncertainty in the origin of the term 'k-correction' Kinney et al. (1996) attributes it to a paper by Carl Wilhelm Wirtz from 1918) who refers to it using the German word for constant, *konstante*. In practice it is a correction to the magnitude of a given bandpass so that the given object is measured in its rest frame so that similar objects have the same magnitudes regardless of their respective velocities and distances relative to us (see Fig. 1.8). As such this type of correction was used even before it got its current name. Mathematically it is simply subtracted from equation 1.11:

$$M = m - 5\log_{10}(d_{pc}) + 5 - K_{Corr}. \tag{1.12}$$

At face value this makes the correction easy to understand both conceptually as well as mathematically. Unfortunately we cannot observe the entire spectrum of every object so we have to rely on observations of similar objects. However since there are many different types of objects and almost all of these evolve with time it is hardly ever possible to find a k-correction based solely on observations of similar objects. Instead we have to turn to theoretical simulations of the different types of objects. For a given galaxy this can be a monumental task since one has to keep track of different types of star populations, their ratios, metallicities as well as their ages and even then there are several other factors that can play a role in the evolution of the galaxy. Unfortunately it is well outside the scope of this work to go through each these and many works not specifically focused on studying k-corrections use approximations to factor out many of the variables since it is impossible to keep track of all the different variables for most galaxies. As we shall see later, for this work, we are only interested in old, red, elliptical galaxies which are relatively easy to approximate compared to many of the other types of galaxies. In the case of these galaxies we can assume them to be mostly consisting of a single stellar population (SSP, Zhu et al. (2010)) so by assuming there are no outside forces that considerably changes the star formation history of the galaxy we are testing we limit the major variables to be only metallicity and age. While this is somewhat doable for galaxies close to us it becomes more difficult with galaxies further away, especially as we reach galaxies whose ages are on the scale of our SSP's. At those times our assumptions of using a ssp and our modelling of the galaxy becomes too poor to get good results.

The e-correction works in a very similar vein and many methods for calculating the k-correction in fact calculate both the e- and the k-correction. The e-correction or evolution correction is also a factor added on to equation 1.11 and attempts to correct for the evolution of a given object. This is because even if two objects are corrected to be in rest frame if one of them is older it will have evolved to some degree and changed its observational properties. We therefore apply an e-correction to make up for this change in a way that a given standard candle will have the same properties at different distances despite the actual observed objects being at different stages of their evolution. Both of these corrections do not need to be applied for objects close to us, but for objects far away from us we can see a significant contribution from both of the corrections. While the observed objects at more extreme redshifts are generally very bright and the corrections being somewhat small in comparison it is important to note that since we are working with standard candles it does not matter how bright the object is but only how tightly correlated objects of a given type of standard candle is in magnitude.

Before moving let us then take a look at the extinction of objects. At the set of wavelengths used in this work extinction mainly refers to extinction of light from dust and gas in our own galaxy. This effect was first noticed by Trumpler (1930) as he realized that distances to globular clusters differed when using photometric methods compared to geometric methods. At the time he found that the extinction was consistent with a loss of 0.67 mag/kpc. The source of the extinction he observed is now known to be due to dust grains in the inter stellar medium. Furthermore the effect of extinction makes the objects appear redder since the blue light has stronger interactions with both dust and gas (Binney 1998). This has an effect when using standard candles that rely on colour differences or magnitudes in specific bands. Since this work mainly focuses on magnitudes we can fortunately disregard the absorption lines from the dust and just add a constant to the measured magnitude. Furthermore although there is good observational proof of intergalactic dust (Outram et al. 2001) the extinction mainly comes from our own galaxy and all the objects we use are mostly impacted by galactic dust we can simply refer to maps of extinction based solely on position of a given object in the sky (for an example see Schlegel et al. 1998; Kohyama et al. 2010).
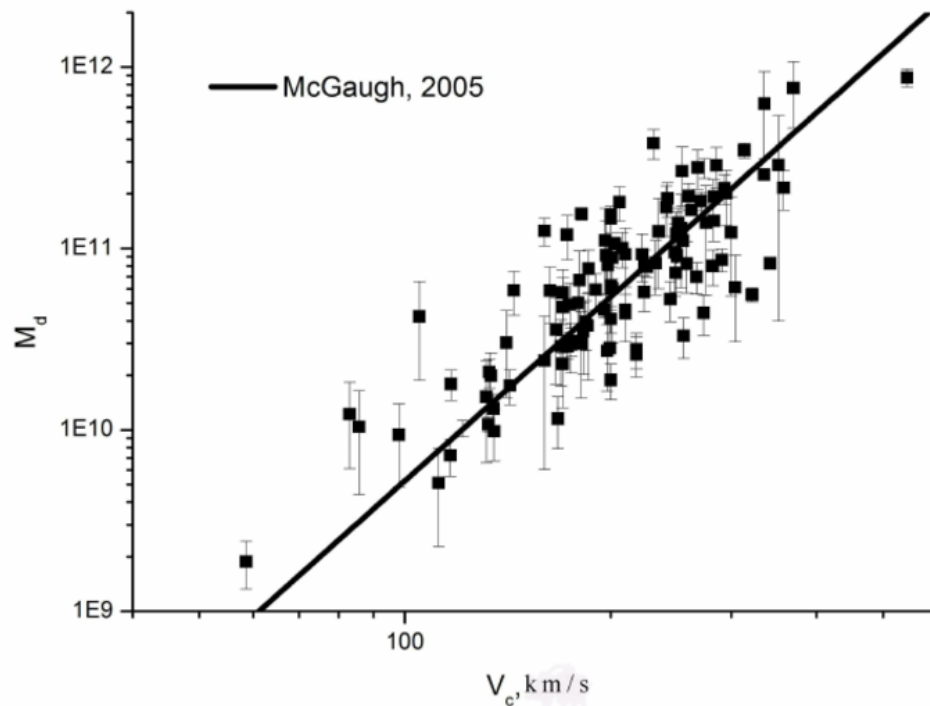
Figure 1.9: Tully-fisher relation for several different spiral galaxies. The relation shown here is between disk mass and rotational speed of the disk. The straight line represents data from McGaugh (2005) and gives us the underlying relation between the two parameters. While the plot has larger error bars than the previous methods we have mentioned it is important to remember the relative ease of measuring the Tully-Fisher relation. Figure taken from Zasov et al. (2011)

1.2.7   Tully-Fisher and the Fundamental plane - ~8 kpc to ~100 Mpc

Besides these methods we can also look at the overall properties of galaxies. Unlike the methods previously discussed these methods are rooted in empirical evidence and our theoretical understanding and simulations are often not yet advanced enough to infer these results using purely theoretical methods. Perhaps the most famous relation of properties is the Tully-Fisher relation (Tully et al. 1975) which relates mass and luminosity (see Fig. 1.9). Intuitively we expect heavier galaxies to be brighter than lighter galaxies simply due to the larger amount of stars in a heavier galaxy. While there is relation it is weak which does seem to become better if we smartly select our method of measuring luminosity and mass (see McGaugh et al. 2000). Originally the relation was between the luminosity of the galaxies and the width of the 21 cm line. This width in the emission line is caused by the rotational velocity of the objects in the galaxies. Since heavier galaxies can contain objects with greater relative velocities than their lighter counterparts we can use theoretical methods to calculate a relation between this velocity dispersion and the mass of the galaxy effectively resulting in a relation between luminosity and mass. Similarly we can expect that there is likely a relation to the number and mass of the stars to the amount of light they emit. Unfortunately it does seem that different types of galaxies have different mass to light ratios and the slope and scatter of the relation even changes with band pass used to measure luminosity (see McGaugh et al. 2000). Freeman (1999) and McGaugh et al. (2000) suggested that using baryonic mass instead of total mass gives a better relation but even there, there are changes depending on the pass bands used. Nonetheless this relation is still of great importance to astronomy since it provides a fast and easy measurement of distance, mass or both as well its strength in testing theoretical predictions.

The Tully-Fisher relation can unfortunately not be used for galaxies which are not rotationally supported. Elliptical galaxies fall into this category and while the Tully-Fisher relation cannot be used on them we have found relations in the properties of regular ellipticals. Perhaps the most important of these is the fundamental plane (see Colless et al. 2007; Jones et al. 2009; Magoulas et al. 2009; Campbell et al. 2014; Springob et al. 2014). According to this there is a relation between the surface brightness, effective radius and central velocity

dispersion in these types of galaxies. This relation can be derived through the virial theorem (see Busarello et al. 1997) if we assume a constant mass to light ratio for the galaxy similarly to what we did in the Tully-Fisher relation. Unfortunately the fundamental plane of galaxies seems to be a function of environment in addition to the properties of the galaxy making it a somewhat harder to use as a distance measurement. Additionally when used in this way we need to measure the observed radial size of the galaxy so it cannot be used on galaxies which are observed as point sources. It still, however, remains an important tool in measuring the distance as well as other properties of galaxies.

To summarize we can divide the different distance measurement methods into three broad categories. The first category is often referred to as the primary indicators. These methods are directly applicable and rely on little or no previous methods. Examples include using radio pulses or parallax to measure the distance. The next step then are the secondary indicators. This includes Cepheid variables, TRGB and most spectroscopic methods. In essence they rely on primary indicators and then extrapolate based on the findings of those indicators. Taking this a step further we arrive at tertiary indicators. These are the methods used to measure distances furthest away. The closest objects we can use for calibrations of these indicators are usually not within range of primary methods so we are forced to use secondary indicators for calibration. These indicators include type Ia supernovae and the Tully-Fisher relation.

1.3   Active Galaxies and Quasars

After the 'great debate' it was obvious that several of the 'nebulae' objects that were previously detected were in fact galaxies. The systematic study of these objects and their spectral lines started with Seyfert (1948). Among his sample where 6 galaxies with point like nuclei which had emission lines on top of the normal G-type spectrum. However the line width for these spectrum were extremely large and Seyfert (1948) attributed this to Doppler shifts requiring speeds of 8,500 km/s, far beyond what was otherwise detected. Although the these types of objects had a few things in common they also had many differing aspects of their spectral lines, even when comparing lines from the same object. NGC 1068 had similar profiles for both its forbidden and permitted lines with widths of roughly 3000 km/s (see Seyfert 1943;

Osterbrock & Parker 1965) whereas NGC 4151 had narrow forbidden and permitted lines but broad hydrogen lines corresponding to velocities of 7500 km/s (see Seyfert 1943). Due to this work today we classify galaxies with high surface brightness, strongly ionized emission lines, and a quasar like nuclei as Seyfert galaxies (Seyfert 1943; Sandage 1971; Shields 1999). Unfortunately the work of Seyfert (1948) was not enough to really start the investigation of quasars even if it laid a good foundation. This investigation starts with some key observations from radio astronomy so let us take a look at that.

1.3.1   Early observations

Jansky (1932) studied sources of static in trans-Atlantic radio communications. He recorded three sources from which this static originated. Local thunderstorm, distant thunderstorms and "a steady hiss type static of unknown origin". He believed this static to be associated with the sun. Continuing these measurements Jansky (1933) observed that this unknown static moved around azimuth each day and that the direction of static changed throughout the year consistent with the Earth's orbit around the Sun. He inferred that the static came from the center of the Milky Way although there were some static from the entire disk. Unfortunately there were still no astronomers taking serious note of this work and it mainly fell on different engineers (see Shields 1999 for more information). This culminated with Baade & Minkowski (1954) where they report observations of six forbidden lines which are strongly emitting compared to the $H\alpha$ line they observed in a radio emitting object. At the time they thought the Hubble constant had a value of $H_0 = 540$ km/s/Mpc which for the redshift of Cyg A, the galaxy they observed, would indicate a radio luminosity of 8×10^{42} erg/s in the radio and slightly lower in optical luminosity. At the time these values were considered enormous even though measurements today show that the real values are even bigger than first thought. After this radio astronomy detected several radio sources both in the plane of the Milky Way and isotropically distributed across the sky. The former of these objects were classified as 'Class I' while the latter was thought to be extra galactic in nature and classified as 'Class II' (Fanaroff & Riley 1974).

Astronomers began finding more of these objects in the third Cambridge survey (3C, Edge et al. (1959)) in the 1960's and beyond. Several radio sources where observed to coincide with stellar-like objects. These objects showed broad emissions lines at unexpected wavelengths, and excess ultraviolet emission compared to stars. Due to their similarity they were classified as quasi-stellar objects (QSOs, Matthews & Sandage (1963)).

In 1963 Maarten Schmidt was studying the spectrum of the quasar 3C 273. This object would appear and disappear with precise periods and was therefore determined to be a two component object. One of the components had a fairly typical spectrum for a Class II objects while the other component seemed to have a very small extension on the sky and a very unusual radio spectrum. Both of these objects coincided with a star like object that had a faint jet pointing away from it Schmidt (1963). At first this stellar object was thought to be a foreground object but careful observations showed that it was not an ordinary star. Schmidt noticed four emission lines in the optical spectrum which were decreasing in strength and spacing towards the blue end of the spectrum. He found that these four lines agreed with the expected wavelengths of hydrogen lines at a redshift of $z = 0.16$ (Schmidt 1963). While this was not an unprecedented redshift it was larger than what was expected for stellar objects and still extremely far away for any type of object. Based on this he postulated that these objects were not stars but rather extragalactic in nature. This implied they had optical luminosities which were much brighter than any type of star observed by a factor of at least 10 while the radio brightness were larger than that of entire galaxies (see Hazard et al. 1963; Schmidt 1963; Oke 1963). We now know that these objects where in fact supernovae but at the time these events were poorly understood.s

These objects were, however, still not understood. Their relative small size coupled with the widths of the spectral lines suggested masses of $\geq 10^9 M_\odot$. Hoyle & Fowler (1963) had previously done some work to examine super massive stars in the context of extra galactic radio sources and had found that such masses were unlikely to be stable. Despite this Matthews & Sandage (1963) as well as Smith & Hoffleit (1963) proposed a model in which a central object emitting optical continuum is surrounded by an emission-line region and a larger radio emitting region. In their model a central mass of $10^9 M_\odot$ would provide adequate energy for

a lifetime of $\geq 10^6$ years aligning with the jet of 3C 273. They noted that this mass would correspond to a Schwarzchild radius of about 10^{-4} pc and that such nuclei could have host galaxies surrounding them which were hidden due to the bright nature of their nucleus.

Sandage (1965) reported his discovery of a large population of objects similar to these QSOs but without radio emission. Sandage estimated that these objects were far greater in number than their radio loud counterparts by a factor of about 500. While this number has since been reduced they are still more numerous (see Best et al. 2005 for a deeper explanation on this ratio).

The objects we focus on in 3, namely BL Lacartae objects, were first reported by John Schmitt in 1968 (see Schmitt 1968). He found the object, already named BL Lacartae, to be a variable star and having an unusual radio source. Subsequently the objects was found to have rapid variations in radio flux and linear polarization. The object was also observed to have a continious spectrum with neither absorption or emission lines.

This started a search for more of these objects and by 1976 more than 30 such objects had been discovered (Stein et al. 1976). At the Pittsburgh BL Lac conference in 1978 a great deal of interest was placed line strengths, redshifts and the physical location of the BL Lac in its host galaxy (Urry 1999). Ten years later at the Como BL Lac conference several of the topics were on the evolution of BL Lacs, their unification with other blazars, and their luminostity functions as multi wavelength observations of these objects became more common (Urry 1999). Since then it is now understood that BL Lacs are at the center of the host galaxies and have been inserted in the unified model discussed in the next section (Urry 1999).

1.3.2   The physics of quasars

At this time it was commonly accepted that QSOs were of extragalactic origin as well as that there was a parallel between QSOs and Seyfert galaxies. While it was hypothesized that they were due to a similar physical phenomenon there was no good explanation of the energy source capable of producing what was observed.

Structure

The first observational property to give rise to explanations of the nucleus were emission lines (see Woltjer 1959; Souffrin 1969; Burbidge et al. 1966a; Oke & Sargent 1968). Woltjer (1959) had derived an electron density of $N_e \approx 10^4 \text{cm}^{-3}$ and temperatures of $T \approx 20,000$ K based on ratios of [S II] and [O III] in Seyfert galaxies (see Kewley et al. 2001; Kauffmann et al. 2003 for more recent approaches using the same method). The regions responsible for this emission were resolved for nearby galaxies and were found to be of the order of 200-350 pc in diameter (see Walker 1968). Oke & Sargent (1968) found a mass of about $10^5 M_\odot$ for the nucleus of NGC 4151 while Burbidge et al. (1959) found that the nuclear emission lines of NGC 1068 were broader than what would be expected for the velocity dispersion of the galaxy. The latter discovery led to the conclusion of the material being in a state of expansion. This still begged the question why forbidden lines and permitted lines were behaving differently. In some galaxies permitted lines would have broad wings while the forbidden lines were not showing these broad wings. Galaxies with broad wings would become known as Seyfert 1 galaxies while those without were called Seyfert 2 (see Khachikian & Weedman 1974). Several solutions were proposed to explain this phenomenon (see Souffrin 1969; Burbidge et al. 1966b; Weymann 1970) however it was ultimately the proposal by Woltjer (1959) that found the greatest support from evidence (see Shields 1974). According to Woltjer there were two separate regions of gas moving at different velocities. In this model there would be a small region of dense fast moving clouds, which produced the broad permitted lines, as well as a region of slow moving cloud which produced the narrower forbidden emission lines. This led to an obvious question: what was the shape this inner, broad line region (BLR)? Observations had not provided real constraints and theories ranged from an accretion disk to swarms of clouds which could be either falling in, orbiting or flying away from the central nucleus (see Shields 1977; Collin-Souffrin 1987). Symmetry of optically thick lines like Lyα and Hα pointed to motions being circular or random rather than radial (see Ferland et al. 1979). This would however imply large masses for the central object due to the estimated radius of the BLR region. In addition an orbit around a central nucleus should in some cases produce a double peaked line profile (see Shields 1978). These problems were somewhat

solved with the emergence of echo mapping of the BLR. This method uses the time delays between continuum and line variations due to the travel time of light across the BLR (see Blandford & McKee 1982). This method indicated that the BLR was smaller and denser than what was previously thought (see Ulrich et al. 1984) and thus a smaller central mass was made plausible.

Parallel to this, the question of the energy source of these active galactic nuclei (AGN) were being discussed. Early explanations focused on high densities of supernovae (see Burbidge 1961; Spitzer & Saslaw 1966;) while others focused on starburst models (Terlevich & Melnick 1985) or a single supermassive star (Hoyle & Fowler 1963). All these models were capable of producing relativistically accelerated particles and ejecting gas clouds at velocities necessary to produce the observations from the BLR. Hoyle & Fowler (1963) suggested that "a magnetic field could be wound toroidally between the central star and a surrounding disk" which would then store large amounts of energy resulting in explosions and jets which had also been observed. Finally Salpeter (1964) and Zel'dovich (1964) independently proposed the idea of energy production due to accretion onto a supermassive black hole. This process was energetic enough to explain the luminosities from the QSOs while keeping the black hole at a reasonable mass. The model did not get popularized before Lynden-Bell (1969) pointed out that dead quasars in the form of black holes must be common in galactic nuclei given the energy output of quasars and their large population in the earlier Universe. Lynden-Bell noted that different parameters of black hole mass and accretion rate of disks around these black holes could explain most of the phenomena in high energy astrophysics such as galactic nuclei, Seyfert galaxies, quasars, and cosmic rays.

Types

With the physical mechanisms and structure established let us now turn to the different types of QSOs observed. These are mostly split based on their continuum. Initially this was mainly done in the optical spectrum although variations in radio and X-ray were noticed. Oke (1963) noticed that the energy distribution was not shaped as a black body since it became redder

towards the infrared part of the spectrum. This in turn led to the conclusion that a substantial part of the spectrum was the result of non-thermal radiation (e.g. synchrotron or inverse-Compton) rather than thermal emission. This discovery would set the scene for much debate in the years to come as astronomers argued the relative importance of the two processes for different parts of the optical spectrum (see Shklovskii 1964; Visvanathan & Oke 1968; Rieke & Low 1972). The main observable factors for this debate were the energy distribution in the spectra, variability and polarization. While the idea of a nonthermal component to the continuum in the optical part of the spectrum was widely accepted it was hard to completely measure since this component would be brightest in the infrared where observations still had low sensitivity. Measurements were however good enough to show a universal trend of getting brighter towards the infrared part of the spectrum (see Johnson 1964; Low & Johnson 1965; Wisniewski et al. 1967; Rieke 1978). This infrared emission was attributed to dust in the case of Seyfert 2 galaxies whereas astronomers were not as sure in the case of Seyfert 1 galaxies (see Neugebauer et al. 1976; Stein & Weedman 1976).

Edelson & Malkan (1987) studied high variability of AGN in the infrared part of the spectrum. The highly polarized objects had a variability with a period of a few months with variations of up to 15% for "normal" quasars and Seyfert galaxies. These "normal" galaxies showed characteristics similar to another category of objects known as blazars. In this category of blazars there are two distinct objects. BL Lacertae objects and optically violent variables (OVV) where the former has a nonthermal continuum but almost no line emission or other significant features in their optical spectrum while OVVs have the standard emission lines expected of QSOs (see Angel & Stockman 1980; Padovani & Giommi 1995). All blazars are dominated at all wavelengths by a variable, polarized nonthermal continuum making them an excellent fit for what Edelson had observed. Blazars are however separate from other types of AGN by the fact that they are highly variable in all parts of the spectrum whereas AGN were considered to have systematically less variability in the red end of the spectrum (see Angel & Stockman 1980). Some AGN appeared to be borderline blazar (see Impey et al. 1989) and further studies showed evidence of a thermal infrared component in the less luminous blazars (see Impey & Neugebauer 1988). It is in fact this unification of

blazars and AGN that would lead to the final, unified model that we will discuss in below.

Unified models

With the acceptance of disk like structures around the black hole (see section 1.3.2 for more information on this discovery) the question of observer's angle relative to this disc was immediately evident. The first place to look was in the radio part of their spectrum. As we explained in 1.3.2 some AGN were radio loud while other, radio quiet, objects had nearly no radio emission. Since these kind of radio sources would radiate isotropically their presence of absence could not be attributed to orientation of the viewer. Furthermore radio loud AGN seemed to be associated with elliptical galaxies whereas radio quiet AGN were associated with spiral galaxies (see Smith et al. 1986; Hutchings et al. 1989). Moreover some extreme features could only be explained by orientation. Chief among these are the blazars where Blandford & Rees (1978) argued that BL Lac objects were radio galaxies viewed directly down the axis of the relativistic jet. Blandford argued that the relativistic beaming caused the nonthermal continuum to be very bright when observed whereas the emission lines would be dim in comparison. The same object, Blandford argued, would have normal emission line equivalent widths and the radio spectrum would be dominated by the extended lobes rather than the core if viewed from the side.

Rowan-Robinson (1977) also argued for the possibility that the BLR of Seyfert 2 galaxies was obscured by dust causing it to be impossible to observe. Antonucci & Miller (1985) found the polarized flux of NGC 1068, a Seyfert 2 galaxy, to have a similar spectrum to a Seyfert 1 galaxy. This Antonucci argued was due to the BLR and central continuum source being obscured by a dusty torus. What Antonucci explained this as the light from the nucleus scattered by the torus and sent our direction in a process that polarized the light. This type of geometry had already been suggested by various astronomers (see Antonucci 1984; Osterbrock 1978) and therefore quickly gained popularity to become the accepted model of AGN as seen in fig 1.10.
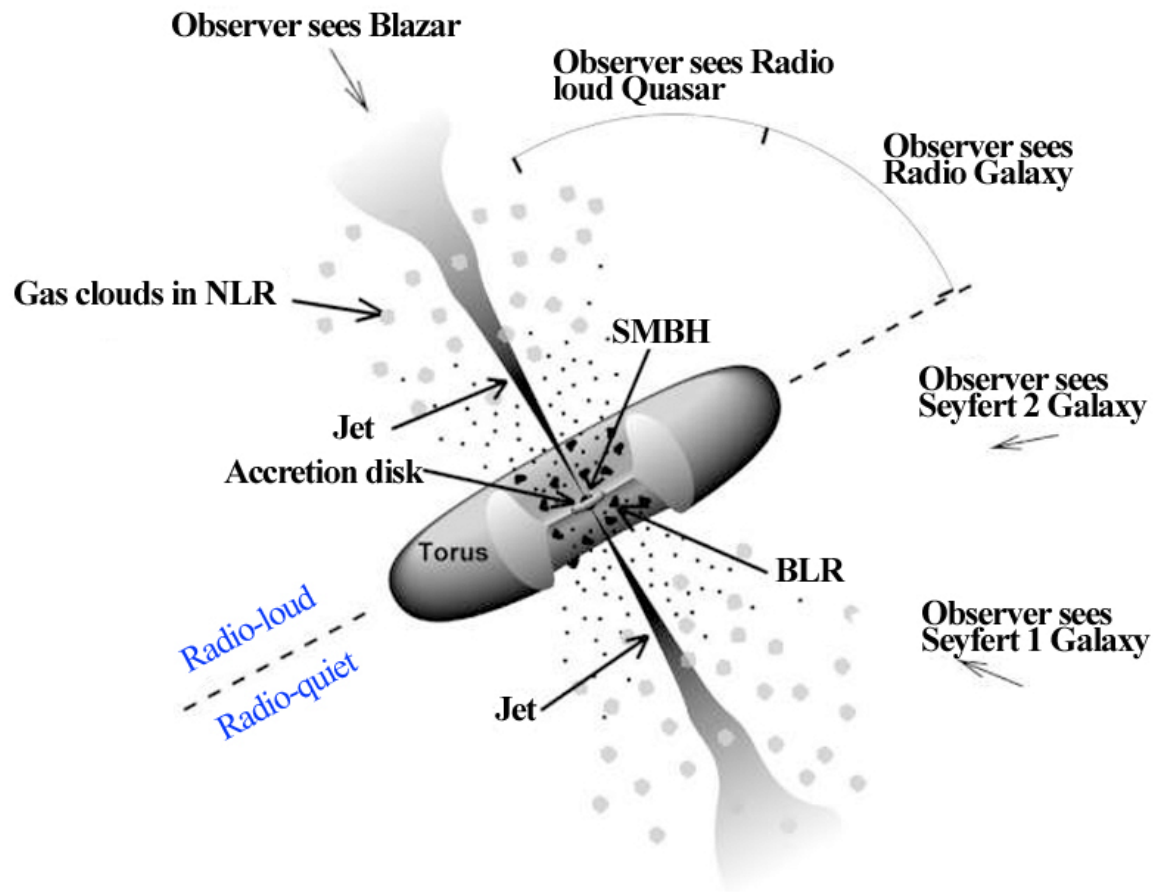
Figure 1.10: The AGN unified model. Key to this model is how different angles of observations provide different 'types' of objects observed. Lower part shows radio quiet AGN while the upper part of the diagram shows radio loud AGN. Credit: Fermi and NASA: https://fermi.gsfc.nasa.gov/science/eteu/agn/

BL Lacs

Since 3 focuses on BL Lacs it is prudent to take an extra look at the specific physics regarding them. As mentioned in 1.3.2 and 1.3.2 BL Lacs are a type of blazar where we are looking directly down the jet. Asssuming that this is the case what we observe has to follow from physics in the jet. Although there are various models that each explain our observations, in this explanation we will focus on the "leptonic models". In these models a relativistic electron-positron jet up-scatters low energy photons to high energy states via the Inverse Compton effect. This results in a highly polarized emission region which moves with relativistic velocities along the jet. Since our assumption is that we are looking directly down the jet we therefore expect to observe radiation which is highly beamed into the observers line of sight (Mücke et al. 2003). The photons can then come from either the accretion disk (Dermer & Schlickeiser 1993), the BLR clouds (Sikora et al. 1994), a dusty torus (Błażejowski et al. 2000), or be produced by interactions in the electron-positron population (Maraschi et al. 1992). In these models it is plausible that the emision from the jet dominates dominates in objects with weak accretion disk radition which aligns with observations of BL Lacs being dominated by polarized emision (Mücke et al. 2003). While this model does explain our observations well there are alternative models such as the "hadronic models" (see Cerruti et al. 2015) or the Synchrotron Proton Blazar which is discussed in Mücke et al. (2003).

1.4 History of star formation

As we mention in 1.3.2 radio loud AGN are located elliptical galaxies which would suggest that these AGN are in some way influenced or influencing their host galaxy. This is perhaps clearest when looking at Madau plots (see Fig 1.11). These plots relate redshift to star formation rate density (SFRD) where they show a clear peak at around $z = 2$. Perhaps as interesting as these plots are the results of including AGN activity in the plots. When comparing mass accretion history of massive black holes we find a good correlation between this and SFRD as shown in Fig 1.11.

This correlation clearly shows that there is a connection between AGN activity and star formation rates (SFR). It still leaves the question of whether this is causation or just

correlation. This is not a simple question to answer. Contributing starburst origins purely to AGN is problematic (Terlevich & Melnick 1985; Terlevich et al. 1992) although observations does suggest link between powerful AGN triggering and star formation (Bongiorno et al. 2012; Feltre et al. 2013). It does however seem that the link disappears in moderate powered AGN (Shao et al. 2010; Rosario et al. 2012). As such it is perhaps easier to look at outside factors which could trigger or quench both of these processes simultaneously. To do so let us first look at the environment of these galaxies namely galaxy clusters.

1.4.1   Star formation in galaxy clusters

Galaxies in galaxy clusters, which are essentially tens to hundreds of galaxies packed in dense environments, have been observed to have different properties than galaxies in a less dense environment would such as lower star formation rate (see Hubble 1936; Dressler 1980). Further studies have suggested that star formation couples strongly with environment whereas morphology of the galaxy is only a secondary correlation (see Kauffmann et al. 2004; Christlein & Zabludoff 2005; Bamford et al. 2009; Weinmann et al. 2009). This would suggest that as galaxies fall into the clusters they must undergo a transformation that causes them to align with the observed properties of cluster galaxies. Although this process is not yet fully understood several mechanisms have been suggested to cause this transformation. Among these are strangulation (see Weinmann et al. 2006; Weinmann et al. 2009; van den Bosch et al. 2008) that is the mechanism by which diffuse gas reservoirs surrounding the galaxy are stripped and ram-pressure (see Gunn & J. Richard 1972; Farouki & Shapiro 1980; Quilis 2000) that strips the galaxy of cold gas in disc. Both these diffuse gas reservoirs and the cold gas are used for star formation and without them galaxies are far less star forming than if they are still intact.

Whatever the exact process or combination thereof a key product of them is two distinct populations of galaxies (see Brammer et al. 2009; Muzzin et al. 2013). One is the star forming, main sequence galaxies which have high SFR compared to the other group which are quenched galaxies that have little star formation and mostly contains old stars. While a given cluster will have galaxies that fall in the middle of these categories the majority
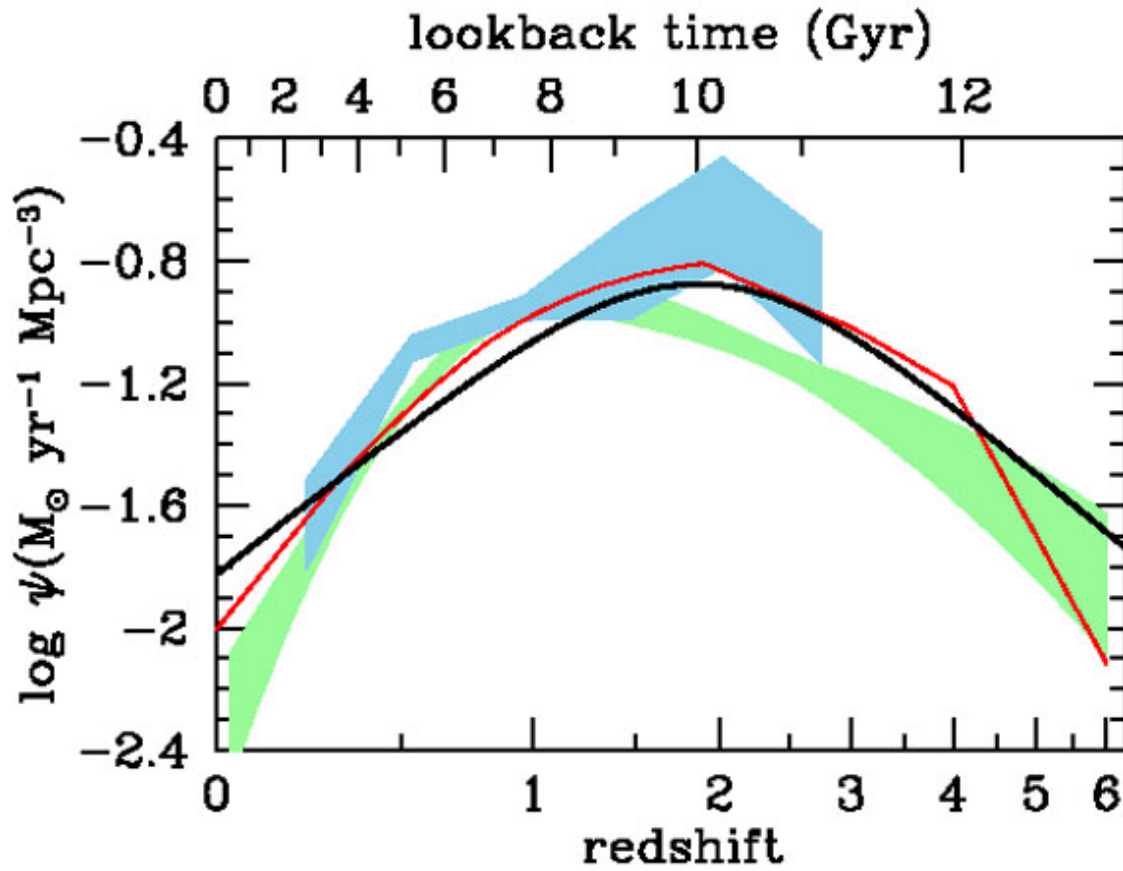
Figure 1.11: Madau plot of the best-fit star formation history (thick solid curve) over which is plotted the accretion history of massive black holes. X-ray based results are fitted in the red curve (Shankar et al. (2009)) and the light green shading (Aird et al. (2010)) while infrared data is highlighted in the light blue shade (Delvecchio et al. (2014)). The shading indicates $\pm 1\sigma$ uncertainty ranges. The rates of black hole accretion has been scaled to fit with the star formation for visual comparison. Plot taken from Madau & Dickinson (2014).
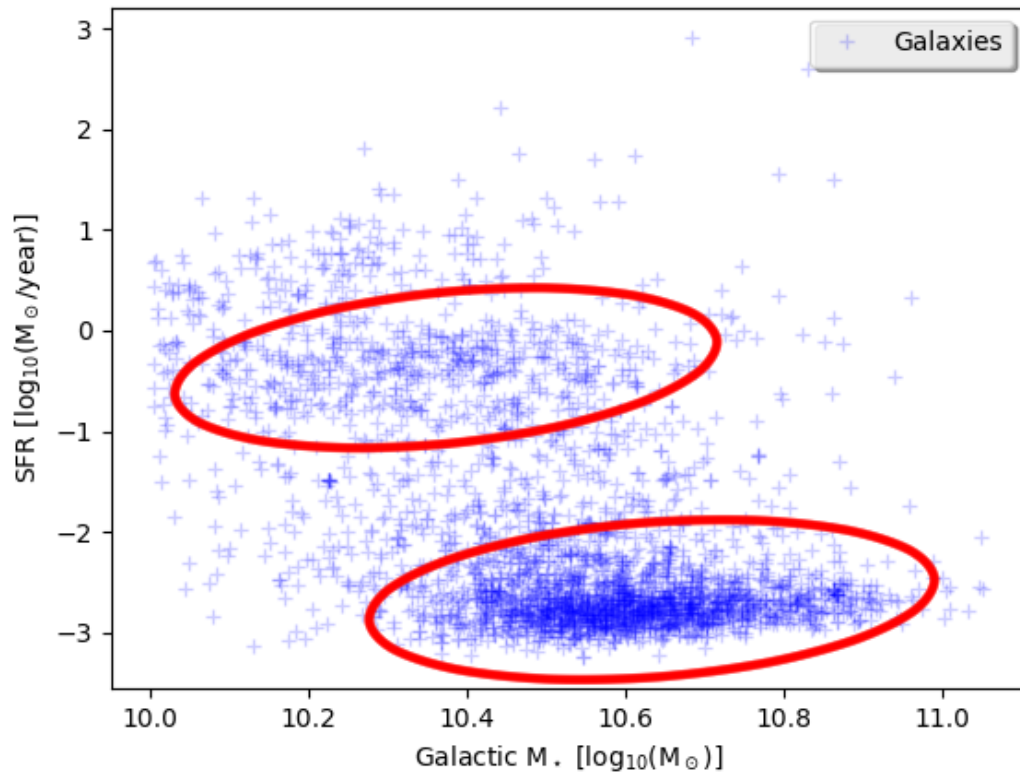
Figure 1.12: SFR-Mass$_\star$ plot of galaxies in SDSS DR8 in the redshift range of 0.152 to 0.153. We have here added transparancy to the points for a better visualization of densities of points. SFR is taken from MPA-JHU (Brinchmann et al. 2004). The main sequence galaxies are located in the top circle whereas the quenched galaxies are located in the bottom circle. Both populations are clearly distinct at and has a slight slope indicating more massive galaxies have higher SFR.

of galaxies will fall into one of them as we shall see in chapter (2). One way to observe this is to look at colour-colour diagrams where each population will appear as a group with main sequence galaxies appearing bluer while quenched galaxies appearing redder due to their stellar population (Dickinson et al. 2003). Perhaps more important to this work is the SFR-$M_\star$ plot as seen in fig 1.12. In this plot we can clearly see two 'groups' of galaxies as well as several galaxies in the process of getting quenched. We also clearly see that more massive galaxies, on average, have higher SFR creating a slope in both the quenched as well as the main sequence population. While the implications of this is certainly interesting, in that quenching happens at small time-scales compared to the lifetime of the galaxies as well as it not being unlikely to be a repeating process, a single cluster does not give us the complete picture.

Similar to how galaxies can change in type from star forming to quenched, the star forming and quenched populations have both changed over the course of the history of the Universe. From observations it appears that most massive galaxies ($\log(M_{star}/M_\star) > 11$) assembled their stellar mass rapidly at the early history of the Universe ($z > 2$) (Marchesini et al. 2009; Brammer et al. 2011) although it appears high star formation rate (SFR) objects are generally more abundant at higher redshift for every type of galaxy (Noeske et al. 2007a). Observations do however suggest that the SFR of galaxies does not increase significantly between redshift of $z = 4$ and $z = 1$. Another interesting aspect is that there does not seem to be a change in how much more star forming massive galaxies are relative to less massive galaxies in the era of decreasing star formation from $z = 1$ to present day (Karim et al. 2011).

1.5   Thesis motivation

As we have presented in this section 1.2 there exist several methods for measuring the distance to objects of phenomena in the Universe. Besides the ones presented in that section there exist many more methods that each have their own advantages and disadvantages ranging from only being able to measure at certain distance intervals, their uncertainties, or how universal their use is at their given distance intervals.

Characterising the uncertainty is one of the more important aspects of the distance ladder method. It is especially the combination of methods that are important. When using secondary or tertiary methods they are usually calibrated using primary methods such as redshift or parallax which results in uncertainties not only from the method but also the uncertainty of the methods used to calibrate them. In most cases several methods can be used to calibrate secondary and tertiary methods and by doing so creating better calibrations of the method.

This makes it important to discover and create new distance indicators for use in, and for the calibration of, the distance ladder. While it certainly is important to have distance indicators at distances which previously had few indicators it is perhaps equally important to have many indicators that overlap with each other for exactly the reason of calibrating and checking previous methods as well as giving future methods more ways to calibrate themselves on. It is exactly this that the work in this thesis tries to do where we present new ways to calibrate new and previous methods as well give an example of how exactly this is done using previously established methods.

1.6   Summary of future chapters

Now that we have laid the groundwork and build up some of the necessary knowledge to understand the following chapters as well as how to connect them to the broader discoveries in astronomy we turn to the rest of the thesis. In chapter 2 we test a new method for measuring distances to galaxy clusters. This is done by looking at the SFRs as well as the masses of galaxies. As we mentioned earlier we expect galaxies in clusters to be split into to groups of quenched and main sequence galaxies. By getting an accurate measure of the center of these groups we can correlate a given cluster with a redshift that contains galaxies with an equal amount of SFR for both of the groups. Both SFR and mass can be measured by the use of photometry, making this an excellent method for distance measurement in observations where photometry is not done due to cost or other considerations or as a test independent of redshift. It also provides a test for simulations of galaxy clusters as it can predict how main sequence and quenched galaxies should be grouped and how their SFR should evolve with time. This

work has been published as Lindholmer & Pimbblet (2019).

Chapter 3 presents work on identifying BL Lacs in Sloan Digital Sky Survey (SDSS) and Baryon Oscillation Spectroscopic Survey (BOSS) data. While these objects have been observed several times and are understood theoretically they are hard to detect due to the unusual characteristic of their spectrum stemming from lack of features. We follow the work of Plotkin et al. (2010) which we update to the use SDSS and BOSS data for more accurate results. We then take the spectrum of the BL Lac and subtract the contribution of the AGN to end up with a spectrum similar to what we would expect the host galaxy to have if there had been no AGN. We do this since these host galaxies have been observed to have very similar magnitudes. By using these magnitudes and correction for extinction, e- and k-correction we can then measure the distance to these galaxies. We note how this breaks down at higher redshift to a degree that poorly fitted e- and k-corrections cannot account for. This then possibly suggests that this relation of constant luminosity does not hold at higher redshifts although some of this could be attributed to completeness rather than host galaxies with the expected magnitude simply not existing. This work is currently in preparation and has not been published yet.

In chapter 4 we compare the two methods presented in this thesis. While we do not expect to get any scientifically publishable results from this exercise it is none the less important to be able to see our results in the larger picture and see how they compare to each other. Due to the small region of overlap between the two methods a direct comparison is unlikely to give many test cases and we therefore also make use of an independently created method. This his method makes use of Bayesian statistics to measure photometric redshifts based on colour magnitudes from multiple filters and is presented in Benítez et al. (2004). By making this comparison we can connect our methods to the wider pool of distance measurement methods that has been created by the scientific community and figure out how well we do compared to them. Finally, chapter 5 summarises the works presented in this thesis and goes on to look at the future direction research in this area could take as well as some predictions of future results based on surveys that are currently in development. Using the estimated sensitivity of these surveys we do a few calculations to test how much data from them could effect the

methods we have presented here. We also do a test to see how well our measurements are able to predict the Hubble constant. This is an especially interesting of research as it currently seems that there is a rift between photometric methods to measure the constant and ones based on the CMB. Since the methods presented here are photometric it is quite likely that they will favour the results from other photometric methods but it still provides an useful test on how well our methods are able to calculate distances.

2. Redshift measurement through star formation

The flame that burns Twice as bright burns half as long.

– Lao Tzu, *Tao Te Ching (late 4th century BC)*

2.1 Prologue

It is well documented that the typical star formation rate has waned for most galaxies since redshift $z = 1$ (Karim et al. 2011). We used this as a measurement of distance since we can directly correlate that to a large number of galaxies where the distance has already been determined. The following chapter is the work published as "Redshift measurement through star formation", Astronomy & Astrophysics, 629, A7 (Lindholmer & Pimbblet 2019). This paper was first authored by myself and co-authored by Kevin Pimbblet. I was responsible for data reduction and analysis as well as writing up most of the paper. Kevin provided the initial idea for the paper, the initial draft of the introduction, as well as scientific feedback. There have been made minor adjustments to the paper to fit in with the thesis such as the removal of the abstract.

2.2 Introduction

The main sequence of galaxies is a relationship between the star formation rate (SFR) or specific star formation rate (sSFR) relative to its stellar mass ($M_\star$). The main sequence has been observed at both low and high redshift, using deep and (or) wide-field surveys (e.g., Guzmán et al. 1997; Bell et al. 2005; Reddy et al. 2006; Salim et al. 2007; Daddi et al. 2007; Noeske et al. 2007b; Elbaz et al. 2007; Rodighiero et al. 2011; Wuyts et al. 2011; Salmi et al. 2012; Whitaker et al. 2012; Guo et al. 2013; Guo et al. 2015; Pannella et al. 2015; amongst others) and has received attention by theoreticians in recent years (e.g., Sparre et al. 2016; Obreja et al. 2014; Dutton et al. 2010; Bouche et al. 2010).

Noeske et al. (2007b) presents one of the most comprehensive reviews of the main sequence of galaxies. They use data from the All-Wavelength Extended Groth Strip International Survey (AEGIS; Davis et al. 2007) to show that despite some scatter in SFR-$M_\star$ space, star-forming galaxies form a relationship with less active red sequence galaxies lying below, although these are likely to be active galactic nuclei (AGN; Weiner et al. 2007). Noeske et al. (2007b) notes that the slope of this relationship tends to flatten out at higher redshift, which could be due to completeness issues in AEGIS. At lower redshift, the scatter in the relationship is constant out to at least $z \approx 1.0$ (see also Speagle et al. 2014). It should be noted that the galaxy main sequence evolves in redshift, such that at higher redshifts the main sequence has a higher SFR. This is not due to the outer envelope of the relationship changing; it is the actual relationship itself that translates in the SFR-$M_\star$ plane (see also Zamojski et al. 2007).

It has been observed that the galaxy main sequence is a relationship that has a multi-wavelength appearance, from the optical through the infra-red and radio. It is argued (cf. Pannella et al. 2015; Tasca et al. 2015; Rodighiero et al. 2014; Karim et al. 2011; Elbaz et al. 2011; Brinchmann et al. 2004 Noeske et al. 2007a) that the reason behind the relationship between redshift and SFR-$M_\star$ can be attributed to a staged galaxy formation, which is an expression of the widely discussed downsizing phenomena (e.g. Cowie et al. 1996; Brinchmann & Ellis 2000; Heavens et al. 2004; Thomas et al. 2005 Bundy et al. 2006; Bell et al. 2005; Fontanot et al. 2009; Eliche-Moral et al. 2010). In simple terms, the argument is that as galaxies have decreasingly less mass they are likely to have their major star formation (SF) episodes occur at decreasing redshift.

More recent work has focussed on both the intrinsic scatter of the star-forming galaxies in the main sequence, as well as the issue of whether there is any evolution in the slope of the relationship over time. Turning first to the scatter, Noeske et al. (2007b) find an intrinsic scatter of around 0.35 dex in SFR about the main sequence that includes 34% of the galaxy population. Several figures for the scatter of the main sequence reported elsewhere show that this value is typical for a wide variety of redshift ranges (cf. Rodighiero et al. 2011; Whitaker et al. 2012, but see also Guo et al. 2013). However, it should be noted that there have been reports that the scatter can increase with higher galaxy stellar mass. Guo et al. (2015) show

that higher mass galaxies at low redshift ($z < 0.03$) have more scatter in their sSFR than lower mass ones do.

The slope of the main sequence appears to be constant over both galaxy stellar mass and redshift (see Karim et al. 2011), as long as the selection effects are taken into account (Guo et al. 2013). Guo et al. (2013) make it clear that selection effects have a large impact on the evolution of the slope in regards to redshift. Once this is taken care of it has been reported several times that the slope is fixed at about unity out to high redshifts in the SFR-$M_\star$ plane (e.g. Elbaz et al. 2007; Noeske et al. 2007b; Daddi et al. 2007; Gilbank et al. 2011; Salmi et al. 2012).

We predict a number of significant uses of the galaxy main sequence. For example, with greater precision we could use it as an extra check on redshift for galaxy cluster in cases where measuring redshift is not achievable, for example due to a paucity of spectroscopy. We can additionally use it to identify other atypical clusters like the Coma cluster (Pimbblet et al. 2014), and potentially further explore the cause of their deviation from SFR expectation values.

The plan of this work is as follows. In Sect. 2.3 we present the data used for both finding clusters and getting the SFR and mass of each of the member galaxies. In Sect. 2.4 we go through our method of analysing the galaxy main sequence and its evolution in redshift. In Sect. 2.5 we present our results and test how precise the method is. In Sect. 2.6 we conclude our findings and discuss the implications and uses of them. Throughout this work we use the Spergel et al. (2007) ΛCDM cosmology in which $\Omega_M = 0.238$, $\Omega_\Lambda = 0.762$, and $H_0 = 73 km s^{-1} Mpc^{-1}$.

2.3   Data

To find the general relationship between redshift and SFR-$M_\star$ plane of the main sequence (Sect. 2.4) we use Sloan Digital Sky Survey (SDSS) data release 8 (DR8), as it is the latest available data release where all the masses and SFR have been calculated homogeneously (Brinchmann et al. 2004 and Kauffmann et al. 2004). The data are split into bins of $z = 0.001$ in width, up to $z = 0.20$, and analysed separately. Hence each of these bins are complete to

the spectroscopic limit and provide a stellar mass limit that is approximately constant within any given bin, although clearly the stellar mass limit and completeness does vary significantly from bin to bin over the redshift range probed. Since SFR and $M_\star$ are a key part of the process, we only use galaxies that have those values available. Importantly, we note that the galaxy main sequences should have the same locus in both the discrete redshift bins and any given galaxy cluster.

The cluster sample used in this work (Sect. 2.5) is selected from the X-Ray Clusters Database Base de Données Amas de Galaxies X (BAX; Sadat et al. 2004). We select clusters with luminosity $L_X > 0.3 \times 10^{44}$erg/s and within a redshift range 0.0 to 0.20. Additionally, Base de Données Amas de Galaxies X (BAX) is used to identify the rough X-ray centre of the galaxy cluster centre and therefore the corresponding galaxies in SDSS DR8 that are potentially part of the cluster.

To determine cluster membership, we used the method outlined in Diaferio (1999) to identify which galaxies and substructures are part of these clusters. We imposed a minimum limit of 50 galaxies per cluster to ensure we have sufficient galaxies to work with. This gives us a total of 129 clusters for which we find more than 50 galaxy entries in SDSS DR8 although a significant number of them are so messy in the SFR-$M_\star$ plane that our method either does not detect the ridges or the detection we make has an standard deviation of above $0.05 \log_{10}(\text{SFR} /\text{M}_\odot/\text{year})$.

In our analysis, we aim to measure both the star-forming sequence of galaxies, as well as the quenched sequence on the SFR-$M_\star$ plane where possible. Therefore for the redshifts that we examine, we need to ensure that the data and their completeness enable us to measure both. We did this by creating log histograms of sSFR for the redshift bins. We fitted a line to the linear portion of the log histogram and extrapolated to determine where the completeness drops below an acceptable level. We removed all galaxies that are part of those low completeness bins from our analysis. This sometimes results in part of the quenched ridge being completely eradicated, and in those cases we acknowledge it is not possible to locate the quenched ridge. In most cases, however, we were able to fit both the star-forming ridge and the quenched ridge, or a sufficient part of the quenched ridge, as desired.

Even where some of the completeness issues affect the star-forming ridge, the star-forming ridge can be fit and the number of galaxies removed from this ridge due to completeness is inconsequential to the fit performed. Upon checking the resulting data after cuts, we see that some of our data are slightly under $\log(\text{SFR}) = 0.1$ M$_\odot$/year, which seems to align fairly well with SDSS data used by others (see Schreiber et al. 2014, Renzini & Peng 2015), as well as data from other sources (Davies et al. 2016).

2.4 Method

The outline of our method is first to find an estimate of the inclination of the ridges of the SFR-$M_\star$ plane. We then more precisely identify the location of the ridge and translate that into a 'standardized' SFR. The standardized SFR is then applied to ridges found in the galaxy cluster sample to determine the distance to them. We use the same method for both analysing redshift bins and subsequently the galaxy clusters. The only difference comes from scaling depending on the number of galaxies in the observed bin or cluster. We can do this since we can assume that the galaxies in galaxy clusters are, in general, a good representation of the redshift bin in which they are located.

2.4.1 Inclination

To determine a rough inclination we start by sampling the overdensity of all the areas in the SFR-$M_\star$ plane. We then assume that the point with the largest overdensity should be on or close to the top of the ridge that represents the galaxy main sequence. After this we fit a line through that point and the largest densities in the SFR-$M_\star$ plane as seen in Fig. 2.1, where the highest density point is located in the star-forming ridge. This gives a rough estimate of the inclination of the galaxy main sequence that is then used as an initial guess for fitting the galaxy main sequence.

Using the initial guess of the inclination we then place angled lines across the galaxy main sequence and measure the density along the lines with the ultimate goal of determining a double Gaussian fit along them. These lines are used to measure the exact location of the ridge and therefore need to be close to perpendicular to the ridge. However since the range of
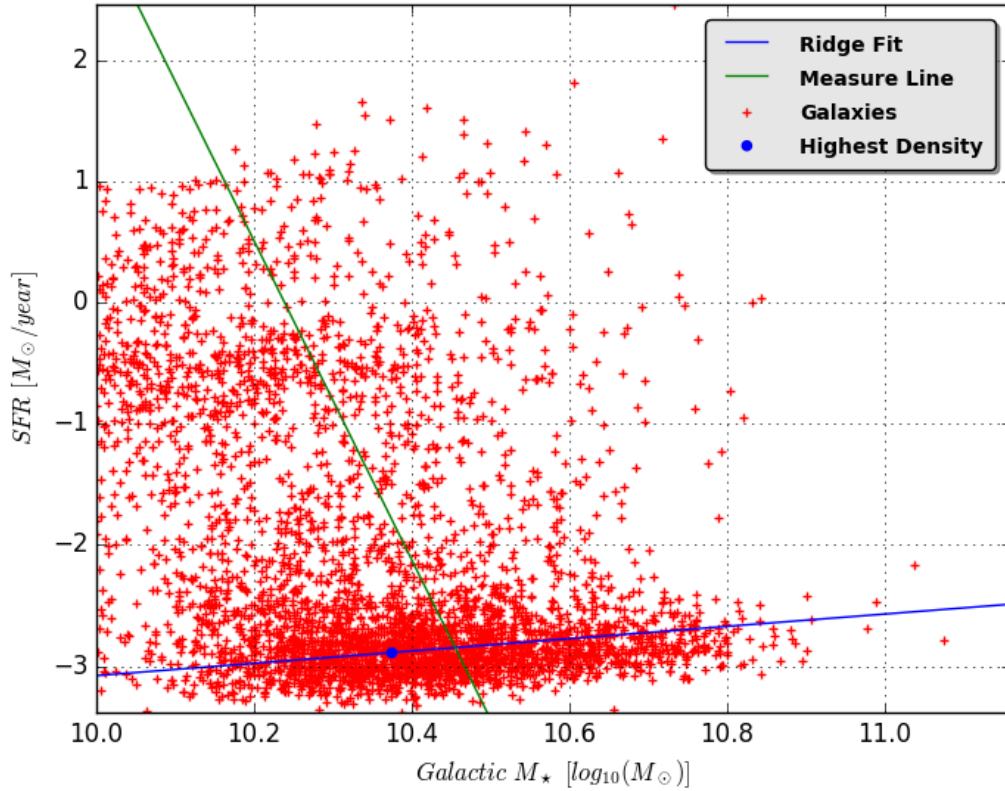
Figure 2.1: All the galaxies where SFR and mass have been measured in the redshift bin $0.092 < z < 0.093$. The red crosses are individual galaxies while the green circle shows the point of highest density and the blue line shows our rough fit of the density ridge. It can clearly be seen that there is an overdensity along the solid blue line. By inspection it can also be seen that there is another overdensity around -0.8 SFR ranging from $10^{10.8} M_\odot$ to about $10^{11.1} M_\odot$. We make 199 lines that are parallel to the green one and measure overdensities along them to identify where the centre of the ridge is. By combining all these 200 measurements we can get a good idea of where the ridges are. The angle of the green line to the ridge has been optimized such that we have the smallest variance across all the redshift bins.

observed values is far larger for SFR than it is for $M_\star$ using a perpendicular line to the galaxy main sequence would not be correct. As such we correct for this by adjusting the lines to be steeper in SFR.

2.4.2   Fitting

We then measure the density along the lines. This gives us a rough double Gaussian curve where the centres of the Gaussians are located at the quenched sequence and the star-forming sequence (see Fig. 2.2). Besides these regions most of the other galaxies are located in the transition region, the so-called "green valley". Sometimes it is not possible to get a clean double Gaussian fit due to completeness removing the quenched ridge along the line we are fitting, or if the star-forming ridge is sparse, or if the green valley has a significant artefact along the line we are measuring. In such cases we remove the Gaussian with the largest amplitude, since it is the most significant one and then remeasure with a new double Gaussian where we allow the fit to reduce one of the Gaussians to zero amplitude. One Gaussian will then represent the remaining ridge while the remaining noise should be hard to fit to any shape. A poor model of the noise is acceptable since this is meant to detect what part of our measurement is the remaining ridge and the ridge should appear roughly as a Gaussian. We then do a test to check the likelihood that we actually found a ridge and remove any measurements with a signal to noise ratio that is too low. By then plotting the centre of each of the Gaussian fits in the SFR-$M_\star$ plane we can then see a pattern emerging in the form of one or two lines depending on how well the star-forming sequence has been fitted (Fig. 2.3). By fitting a line to one of these sequence points we then arrive at a fit for the ridge.

2.4.3   Ridge fitting

For the initial fits of the ridges we have freely fitted the inclination of the ridge. This creates some scatter in the inclination we have fitted due to uncertainties and selection criteria, especially at lower redshift. When analysing the scatter at low redshift it is obvious that it is mainly towards higher inclination. This is because there are few galaxies far below the quenched sequence and the area around $10^{10} M_\odot$ has the largest number of galaxies, causing the ridge to typically be fitted better in that area. To avoid this systematic error we only use
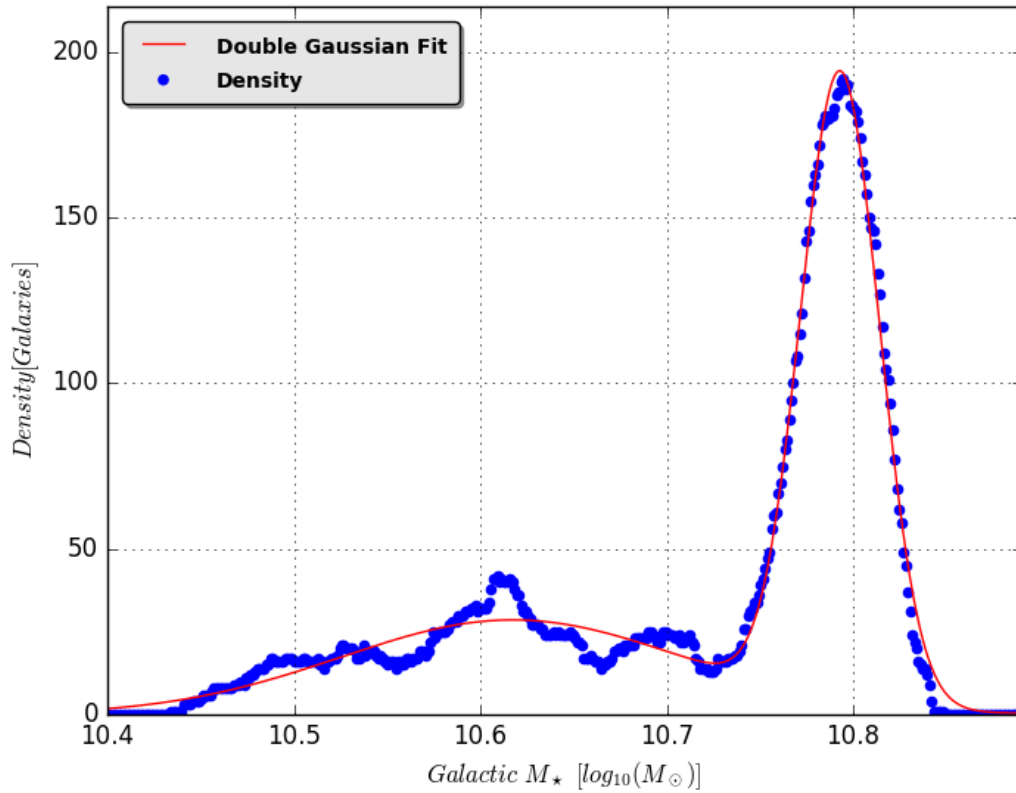
Figure 2.2: Example of how we fit at one point in a ridge. The blue dots represent the density around each point measured across the ridge (see the green line in Fig. 2.1) and the red line is our fit. The quenched ridge top is located around 10.84 and our fit to it is well within accepted errors. The star-forming ridge top is located at around 10.72 and is also well within our accepted range. The green valley is not fit very well in this plot, but this is not important as we are not trying to measure anything in that area.
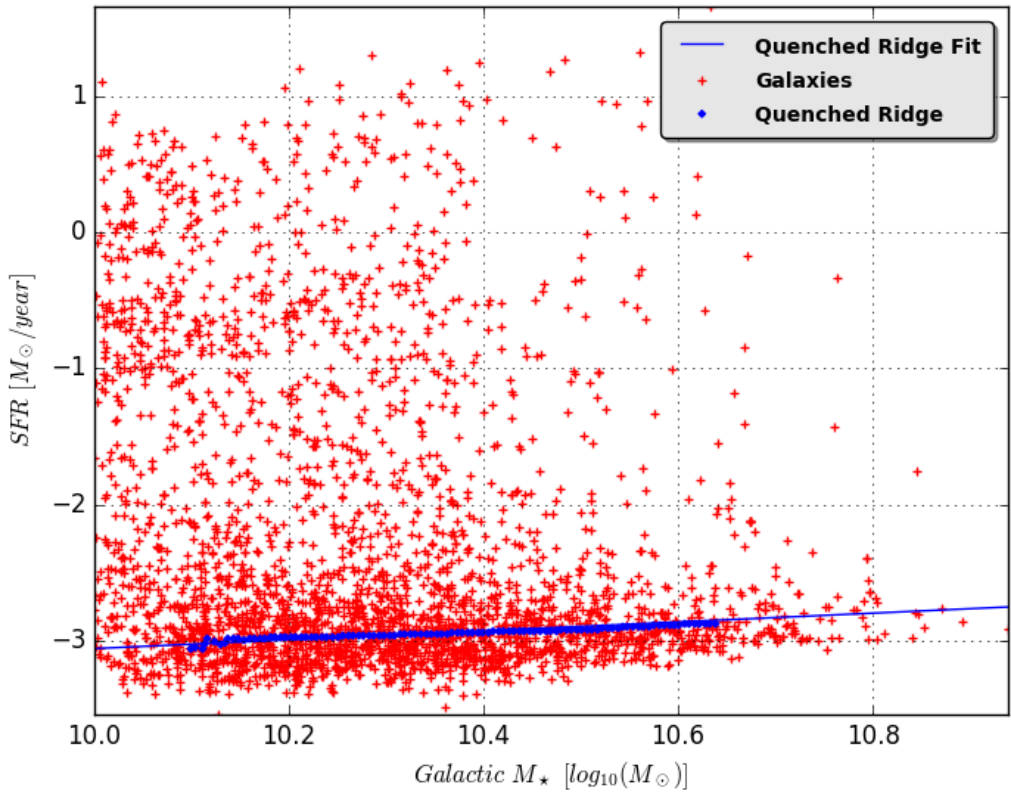
Figure 2.3: Fit to the quenched ridge along the blue line while the star-forming ridge is too sparse to get a clear detection of. The blue diamonds are the locations the Gaussian fits have indicated which line up well for the quenched ridge line.

the area where we see little scatter in the inclination (redshift $0.1 < z < 0.18$) to give us an expected value for the inclination for all of our data. We find that this value is constant as suggested by Guo et al. (2013). As further demonstrated by Guo et al. (2013) we can expect this to also be true for lower redshift and we therefore assume that it works there as well.

To measure the position of the ridge in the SFR-$M_\star$, plane we use a standardized measure of the SFR. This is simply done by calculating the SFR of our ridge fit at the $10^{10} M_\odot$ point. Doing this allows us to get a measure of how the galaxy main sequence evolves in redshift. By using the same inclination for all the data we arrive at a relationship in SFR-redshift space with very little scatter. We then fit this relationship to a straight line, using two free parameters. This can then be used as an expected value to compare to standardized measures of cluster SFR.

2.5 Results and discussion

In this section we will go over the results we get from the method when comparing our results obtained from redshift bins to the galaxy clusters. We will first present the fit to the redshift bin ridges to ensure that they are good and we highlight the few locations which are less than optimal. After this, we present the evolution of the ridges in redshift and make a fit to this evolution. Finally, we try to apply this method to a sample of clusters to test the method's viability in measuring the redshift of the clusters.

2.5.1 Ridge fitting

Since we are trying to create a general method to use for many different sets of galaxies at different redshifts, we have decided to use a single set of parameters across all the bins. By doing so we retain a generally low dispersion in the fits as it makes sure that there are no systematic errors due to using different parameters. As can be seen in Fig. 2.4, we mostly obtain good fits for both the ridges with a few outliers and even fewer ridges that we do not find at all. The main exceptions to this are at around redshift $z < 0.05$ where the bins do not contain many galaxies and we end up with sparse ridges. For the redshift bins very close to us we cannot fit anything below redshift $z = 0.021$ as the ridges are too irregular and the
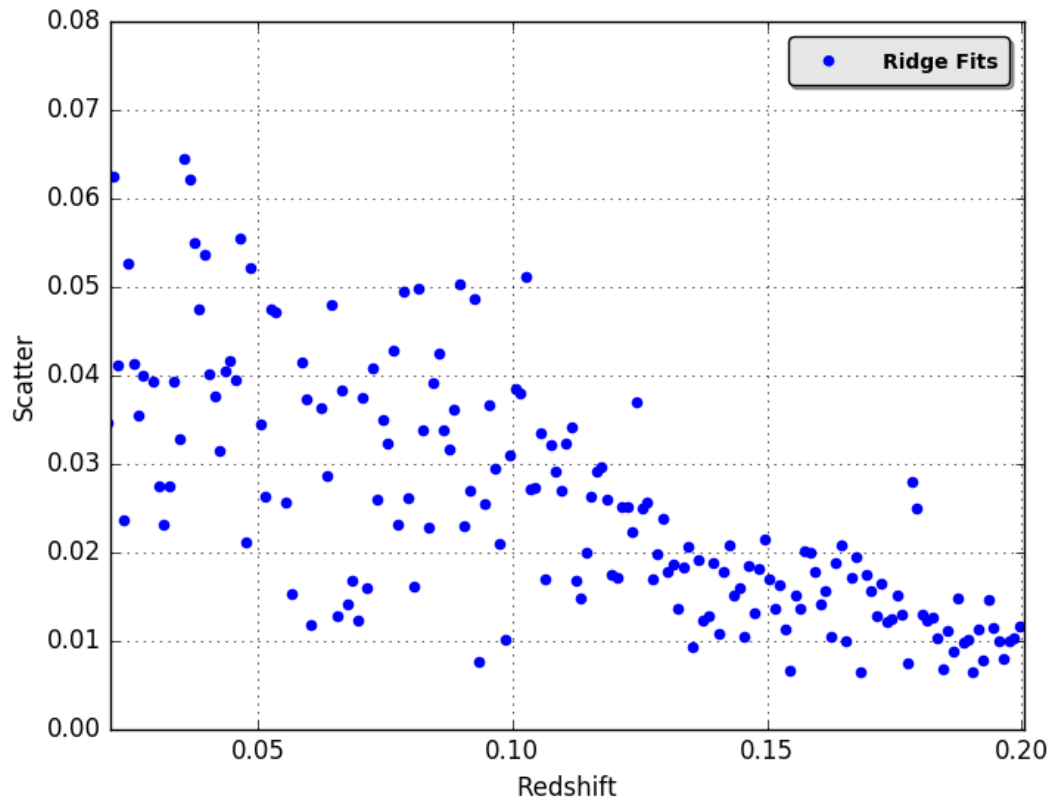
Figure 2.4: Standard deviation of the fit of the ridges in each of the redshift bins. At redshifts of $z < 0.021$, the method does not detect any ridges due to the number of galaxies in the bins. We also see increasing irregularity in the ridges below about redshift $z < 0.05$. Besides this we the star-forming ridge having very high dispersion at redshifts above $z < 0.15$ due to being very sparse at these redshifts.

method can no longer fit them to satisfying precision. For the star-forming ridge we see a large increase in dispersion at higher redshift. This is mainly due to how sparse the ridge becomes at this point, making it harder to detect.

2.5.2   Evolution of ridges in redshift

By plotting each of our measured ridge SFRs, we can then see a relationship between the SFR and redshift (Fig. 2.5). It is obvious that the relationship is linear for the whole range of redshifts for the star-forming ridge and linear in about half the redshift range for the quenched ridge. It could be argued that a logarithmic fit would make a better fit for the quenched ridge but it seems more likely that there is another answer for the high redshift part of the quenched ridge, since the SFR values for the ridge stay almost constant in that part. This is likely due to a few different factors such as difficulty in observing the quenched ridge at this redshift or due to us using a shallower incline in the SFR-$M_\star$ plane than appropriate or that the ridges are not linear in the SFR-$M_\star$ plane but actually curve downwards at higher mass ranges as suggested by Schreiber et al. (2014) and Ciesla et al. (2017). This would lead to higher estimates as we go to higher z since we only detect the high mass end of the ridge in that region. This fit does not seem to be widely accepted as people are still using linear ridges in some papers (Renzini & Peng 2015 and Davies et al. 2016).

2.5.3   Comparison with observed clusters

We can now apply the relationship between the measured ridge SFR and redshift to our galaxy cluster sample to find their redshifts. By using our method with the exact same parameters as when using bins, we find a few clusters where a ridge can be measured. The clusters are very close to the expected value in SFR compared to their known redshift (see Fig. 2.6), with all of them coming within 1σ or very close to it. We even find a measurement for the Virgo cluster despite being unable to get a measurement in the redshift bin containing the cluster. This is due to the Virgo cluster not being messy and because the requirements for the redshift bins are harsher than for the clusters. Unfortunately when converting the uncertainty to redshift, it ends up being a large range of redshifts and becomes useless in determining exact an redshift compared to other, more precise, methods. The main cause of this appears to be the number
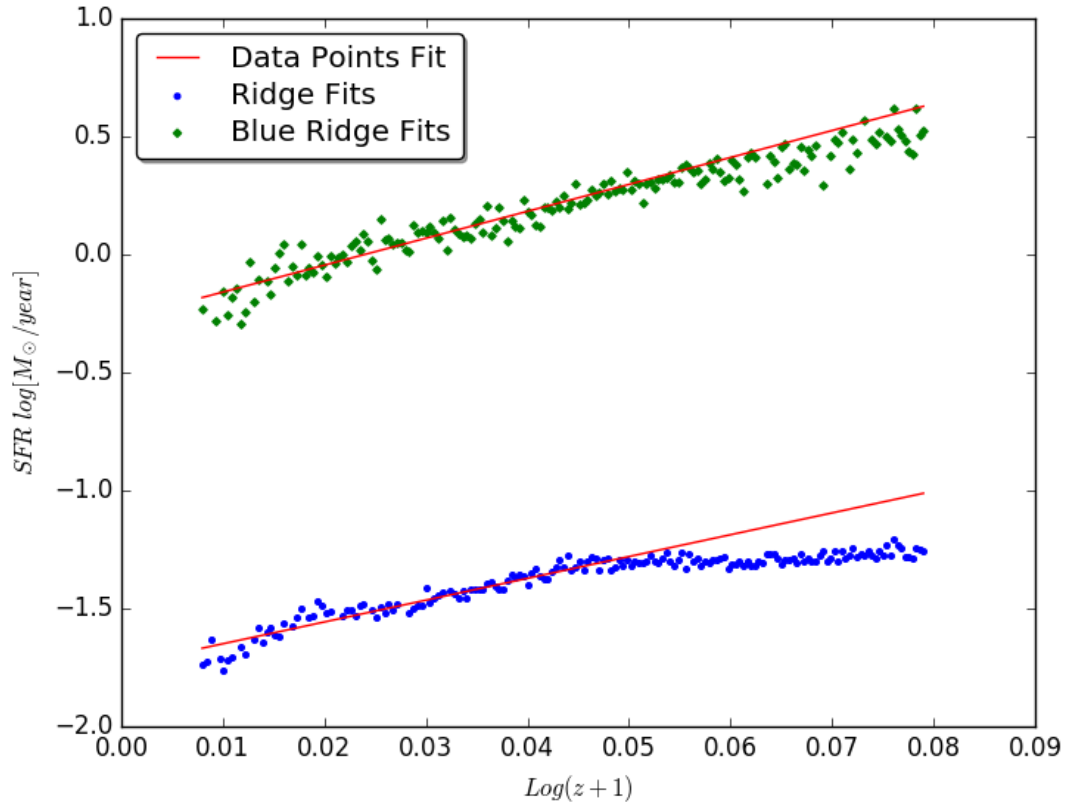
Figure 2.5: Evolution of star-forming ridge (represented by the green diamonds) and the quenched ridge SFR with redshift. For the star-forming ridge the best fit seems to be a linear one whereas for the quenched ridge it seems that above about redshift $\log(z + 1) = 0.055$ the measurements diverges from the linear fit. This could be due to a systematic error in the measurement of star formation rates at higher redshifts or due to the completeness test removing the left part of an already small quenched ridge.
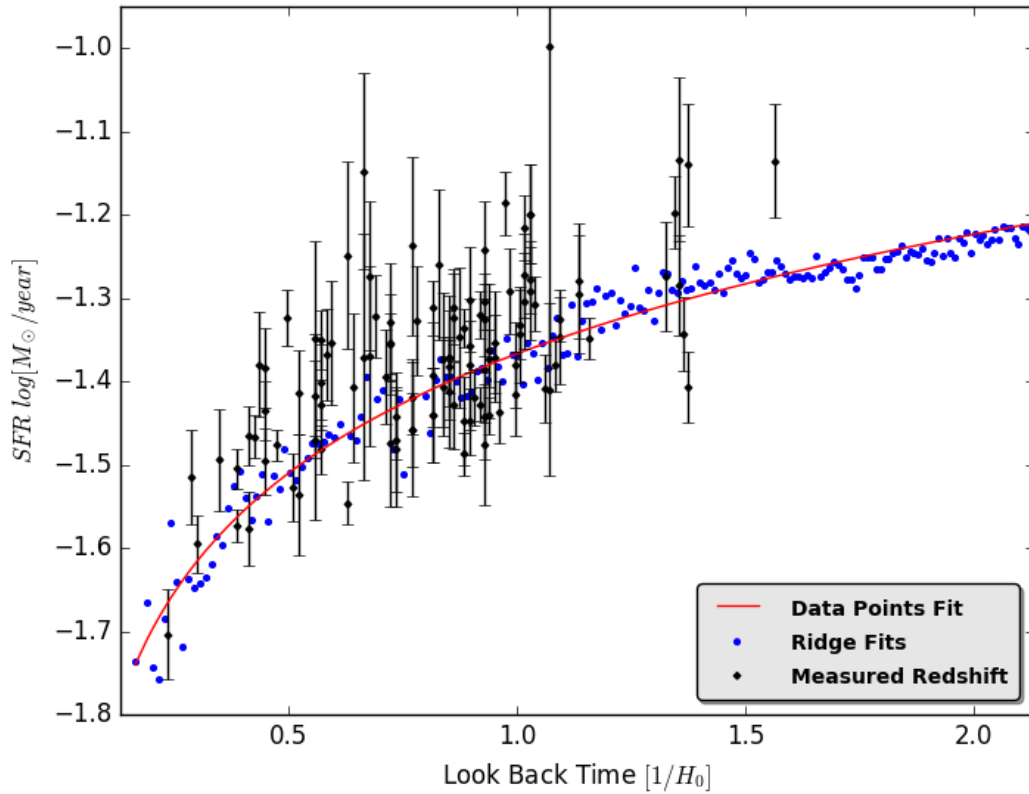
Figure 2.6: Comparison of our fits to the redshift bin data and fits to a sample of galaxy clusters. They are all within our expectation; our fit for the Virgo cluster is sufficiently close that it even extends to lower redshifts beyond what we can do with the redshift bins.

of galaxies per cluster. To obtain reliable results, this method requires at least 100 members per cluster. Due to the low member count of many of the clusters this means that even in the best cases the results from the clusters are only as precise as the worst cases for the redshift bins, with the clusters typically having $> 200\%$ higher variance in their measurement.

It should be noted that a lot of clusters in our sample have fewer than 100 members with masses above $10^{10} M_\odot$. The number decreases further since we also need the SFR of the galaxy, which has not been reliably measured in all cases. For these cases we can still measure the ridges but the measurement becomes dominated by the spread of galaxies, which theoretically should yield the double ridge structure we expect, but due to the low number of galaxies we often see irregular ridges or overdensities in the SFR-$M_\star$ plane that thwart the fits.

2.5.4 Limits

From our experiments, there are clear requirements on the data for our approach to work reliably. The first is that the objects we are measuring have to be at least at a redshift $z > 0.02$. If it is less than this the ridge will become too irregular causing the fit to become inaccurate. There is a similar limit at higher z due to the incompleteness of data.

Applying the method to clusters, we see that we can use clusters with more than 100 galaxies to get good results (standard deviation of $\sigma_{\mathrm{SFR}} < 0.1 \log(M_\odot/\mathrm{year})$. For the quenched ridge the resulting redshift measurements have an uncertainty of $\sigma_z = \pm 0.024 \cdot (z + 1)$ in our worst case but average to $\sigma_z = \pm 0.017 \cdot (z + 1)$ for all cases and go as low as $\sigma_z = \pm 0.01 \cdot (z + 1)$ in the best case. For the star-forming ridge we only find two clusters that satisfy our requirements and they have a standard deviation of $\sigma_z = \pm 0.004 \cdot (z + 1)$ and $\sigma_z = \pm 0.013 \cdot (z + 1)$. To calculate these standard deviations, we have not taken the cluster's redshift into account as we have not been able to get enough galaxy cluster measurements to verify if there is a trend relating uncertainty to redshift. Assuming that this accuracy is adequate the method can find proper redshifts to within that accuracy with > 100 galaxy members in the cluster. The same limits for the redshift bins also apply to the clusters but the number of member galaxies is the primary difference, making it much easier to get

measurements on the bins in most cases.

2.5.5   Comparison to others methods

The analysis that we have presented in this work uses spectroscopy to obtain the critical parameters required to populate the galaxy main sequence plane (star formation rates and stellar masses). Naturally, one could simply apply one of a number of techniques to these spectra to obtain the overall recession velocity of the galaxy cluster itself (e.g. Yahil & Vidal 1977; Zabludoff et al. 1990; Beers et al. 1990; Carlberg et al. 1996; Diaferio 1999). From this point of view, the method presented here should be viewed as an additional way in which the redshift of clusters could be obtained, and not necessarily the easiest or most efficient. However, it is possible to populate the galaxy main sequence plane in different manners, and hence finding the redshift of a galaxy cluster from the main sequence plane alone may be more expedient than undertaking observationally expensive (in comparison to imaging) spectroscopy. For the stellar mass axis, there are a number of authors in the literature advancing methods to compute galaxy stellar mass based on photometric observation alone. For example, Hsieh & Yee (2014) introduce a direct empirical photometric method that can compute stellar mass from a small number of passbands (see also Budavari et al. 2009); Brinchmann & Ellis 2000 map out the relationship between stellar mass and K-band luminosity; others use multi-wavelength broadband photometry to derive very reasonable estimates for stellar masses in their own surveys (for example Taylor et al. 2011; Zibetti et al. 2009; Dye et al. 2008; Bell et al. 2003). However these methods should be used with care at high redshifts where a variety of uncertainties could affect the results (cf. Mitchell et al. 2013). For the star formation rate axis, spectral energy distribution (SED) modelling can potentially yield the required parameter. For example, Flores et al. (1999) use radio, mid- and near-IR, optical, and UV photometry to extrapolate the far-IR luminosity and thus estimate SFRs that are not extinction dependant. The use of SED modelling for photometry has also been applied to other studies to yield SFR, including but not limited to Maraston et al. (2010), Yuan et al. (2012), and Straatman et al. (2016); other methods such as machine learning are yielding very promising results in this area as well (Stensbo-Smidt et al. 2016).

2.5.6   Using this method as an H_0 estimator

While this method relies on redshift as a way to calibrate it is possible to calibrate it using other methods such as SNe and cepheids. Using those indicators we can get an estimate of the absolute magnitude from the galaxies which can in turn be used to infer a distance. The difficult part then comes in the form of finding the SFR without using redshift. This can be done by modelling, especially for red, quenched galaxies which make up a significant part of the galaxie in the quenched ridge, if we make the assumption that an SSP could roughly fit the evolution of the galaxy due to quenched galaxies forming very few new stars to the point of it being negligible. Alternatively one could theoretically study the galaxy as it evolves and count each birth and death of a star to get a more accurate model, but this would take millions if not billions of years to do so there is little pratical application of this approach. Finally the mass of a given galaxy can be inferred from the Fundamental Plane since the quenched galaxies are overwhelmingly going to be elliptical galaxies. With these quantaties a value of H_0 can be inferred by comparison with redshifts since all of these methods have been redshift independent. In this chapter we opted to use redshift data since that data is available in larger quantaties and precision which therefore gives a more clear presentation of the method.

2.6   Conclusion

The method succeeds in finding clear ridges in most of the redshift bins and we were able to determine a clear correlation between the ridge SFR and redshift. We then used the same method to find the redshift for several clusters and were able to find the ridge and get a good measurement of redshift for seven clusters. When comparing these results from the clusters to the fit from the redshift bins. We see that the inclination of the fit is very shallow so the error from the cluster measurements results in a somewhat large range of redshift, with uncertainties $\sigma_z = \pm 0.017 \cdot (z + 1)$. We do not detect any correlation between outliers and any measurable parameter of the clusters such as luminosity or substructuring, suggesting that this dispersion is largely due to lack of data.

Therefore, this method can only be applied to those clusters with many members (each with SFR and stellar mass well determined) to yield a redshift value with a low standard

deviation. Even then, the scatter present in our method means that such a redshift must be regarded as a secondary method at best.

2.7 Acknowledgements

3. Using BL Lacertae Objects as Standard Candles: The need for multiwavelength observations

"It's hard to say which is more satisfying: the search for that missing piece or fitting that piece into place." —Evo Ragus

– Wizards of the Coast, *Call to Mind (2010)*

3.1 Prologue

BL Lac objects have been observed since 1968 (Schmitt 1968; Angel & Stockman 1980; Padovani & Giommi 1995) and have been used for standard candles for about half that time (Scarpa et al. 2000a; Urry et al. 2000). In this chapter we construct an automated method to find and analyse BL Lacs in the Baryon Oscillation Spectroscopic Survey (BOSS) catalogue in order to test their reliability as a standard candle at multiple redshifts. In turn this allows us to demonstrate that previously documented radio quiet BL Lacs, unlike their radio loud counterparts, do not behave as a standard candle and thus likely form a separate population. The following chapter is in writing and is planned for submission to Astronomy & Astrophysics. This chapter (which will be submitted as a paper) was first authored by myself and co-authored by Kevin Pimbblet and Yjan Gordon. I was responsible for data reduction and analysis as well as writing the paper while Kevin Pimblett and Yjan Gordon provided scientific feedback. Minor adjustments to the chapter will be made when submitting it for peer review to a journal to fit with the format of the journal.

3.2 Introduction

With the discovery of Cepheids, standard candles became one of the corner stones of distance measurement in astronomy. Objects which are used as standard candles share the common characteristic of their absolute luminosity being known either from associations with similar

objects, a strong theoretical understanding, or another way of determining the absolute magnitude of the observed object. In the case of Cepheids their luminosity is directly related to their period of variability (Leavitt 1908; Pawlak et al. 2019) and any measurement of extended time of a Cepheid therefore easily tells us its luminosity.

By using Cepheids we can measure the distance to other objects such as BL Lacertae objects (BL Lacs). BL Lacs differ from 'classic' standard candles such as Cepheids where the object is directly measured and instead look at the host galaxy the BL Lac is situated in (see Urry et al. 2000; Falomo et al. 2014). This host galaxy is expected to have an absolute luminosity of about $M_R \approx -22.9 \pm 0.5$ (Sbarufatti et al. 2005). While Sbarufatti et al. (2005) uses that H$_0$ = 70 km/s (and k= 0; Ω_M = 0.3), resulting in a measurement that is not independent of redshift, this is still an interesting example of a standard candle given that while it is fairly easy to observe the magnitude of a single galaxy even if it has to be correlated to a another object it can be difficult to find the correlated object. In the future this problem could be solved by detecting redshift independent standard candles in BL Lac host galaxies which would make BL Lacs a standard candle that is independent of H$_0$. Such standard candles are likely (but not limited) to be type Ia supernovae as BL Lacs in general are fairly distant objects requiring luminous standard candles.

In this case that object is the nucleus of the galaxy which is what astronomers search for when trying to find this type of standard candle. The nucleus of a BL Lac is categorized as a subtype of blazar (see Angel & Stockman 1980; Padovani & Giommi 1995; Xu et al. 2009) which in turn is a type of active galactic nuclei (AGN, see Fig. 3.1). Since we will be using BL Lacs as a standard candles throughout this paper we now turn to how to find this type of AGN before returning to their exact properties as standard candles.

According to the Unified model which was first proposed by Miller & Antonucci (1983, see also Antonucci, 1993) all AGN are powered by a supermassive black hole that accretes mass on to itself and in the process creates radiation (Salpeter 1964). In the case of blazars the viewing angle is almost perpendicular to the disc. This means that a large amount of the photons we observe have been relativistically shifted towards or away from us in the jets of the AGN. This in turn provides some rather unique observational signatures compared
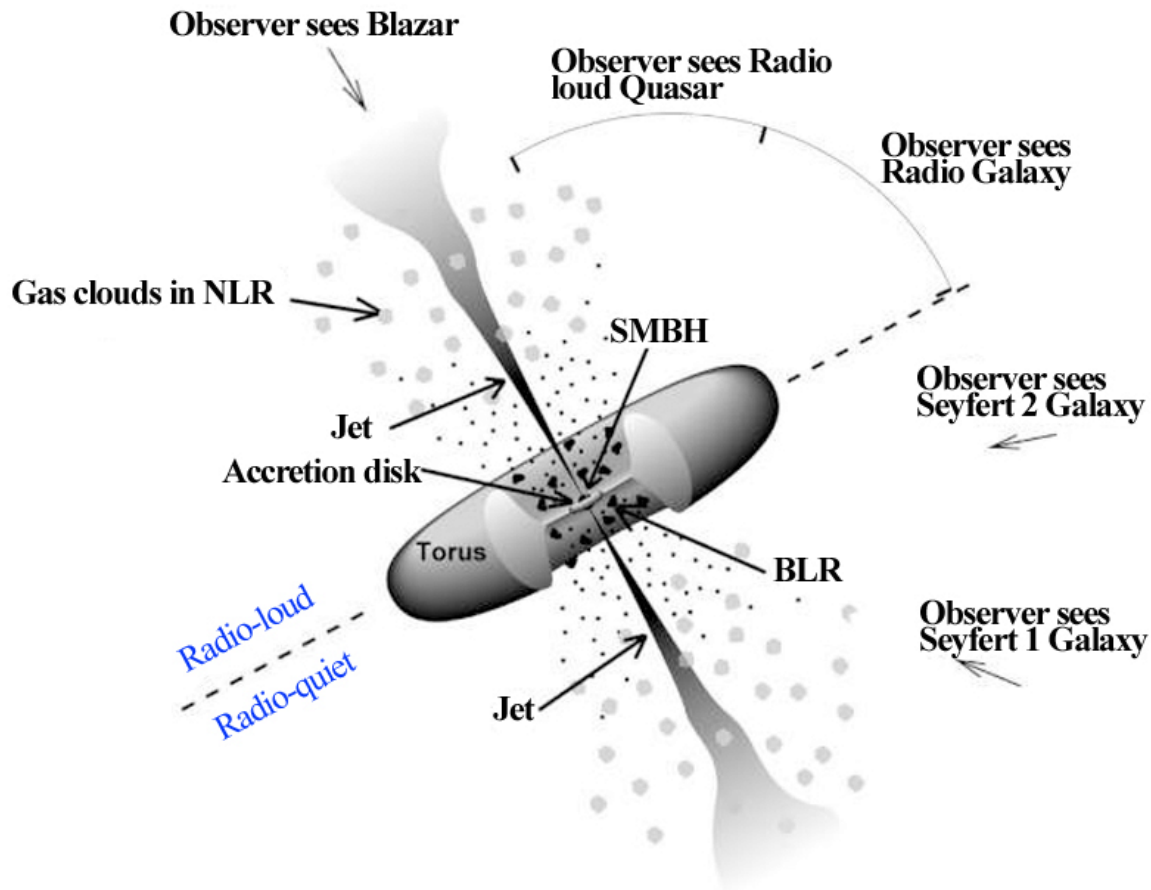
Figure 3.1: Figure representing the AGN unified model. Key to this model is how different angles of observations provide different 'types' of objects observed. Lower part shows radio quiet AGN while the upper part of the diagram shows radio loud AGN. Credit for the figure goes to Fermi and NASA: https://fermi.gsfc.nasa.gov/science/eteu/agn/

to other cosmological phenomenon. The common identifiers of this case are high amounts of non-thermal emission (Böttcher 2007) as well as highly polarized radio and optical flux due to the magnetic field that produces the jets (Antonucci 1984; Osterbrock 1978). Despite these similarities between different blazars they are still split into two distinct groups of Flat-Spectrum Radio Quasars (FSRQs) and BL Lac objects. FSRQs have more emission compared to their BL Lac counterpart at 1-2 orders of magnitude higher for FSRQ's when looking in the radio part of the spectrum. This results in spectra of low spectral index value in the radio part of the spectrum, a high degree of ionization (generally having [O II]/[O III] < 1, see Landt et al. 2004) and broad emission lines from Doppler broadening of hot gas close to the black hole (both are presented in Fig 3.2 for comparison). BL Lacs have spectra with few or no features since their spectra is comparatively more dominated by beamed emission rather than unbeamed emission (Urry & Padovani 1995; Heckman et al. 2005). These objects are rare amongst blazars, constituting only 15% of blazars in the 1Jy sample (Urry & Padovani 1995; Stickel et al. 1994), a catalogue listing 518 found radio sources with flux densities of $S_{5GHz} > 1Jy$ within a 9.811 sr region that excludes the galactic plane and is not expected to have any completeness issues (Kuehr et al. 1981). This rarity means that classifications in big catalogues like SDSS does not typically have build in methods to detect BL Lacs and even more specialized catalogues like the Multi-frequency Catalogue of Blazars (BZCAT, Massaro et al. 2008) rely on a collection of different analyses or specialized surveys to gather all their data. This results in there being no gold standard method for finding BL Lacs but instead a multitude of methods each capable of finding some similarities with each other but are unlikely to be in full agreement on every analysed object.

Due to the nature of BL Lacs not having any spectral features, the basis of many of these methods are often not to use optical spectra. Many of the methods instead use radio or X-ray measurements; flux polarization, especially in radio; gamma rays or simply their variability such as Impey & Brand (1982) looking at polarization and variability in the optical part of the spectrum which results in objects with very long variability periods being removed and possible radio quiet objects being selected; Borra & Corriveau 1984 looking exclusively at polarization in an attempt to avoid bias against radio quiet objects but possibly including
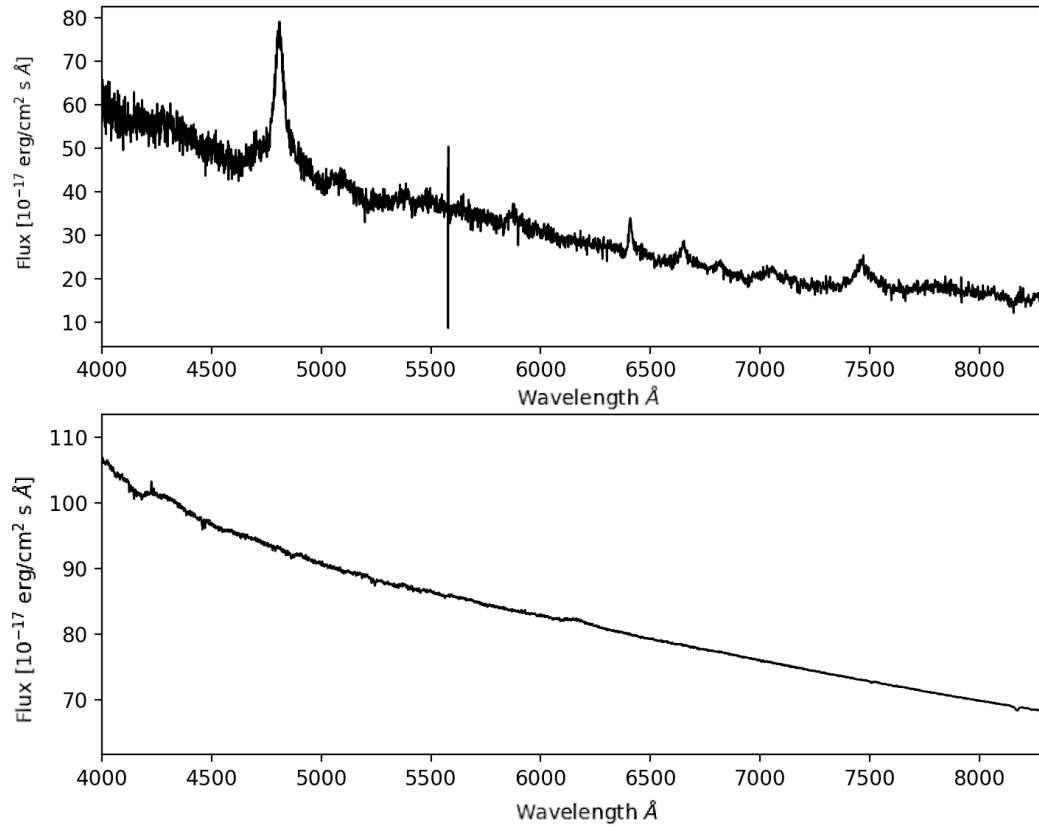
Figure 3.2: Top is a plot of a typical FSQR (BZQJ0059+0006) with common emission lines and excess emission in the UV regime due to the thermal continuum of the accretion disk. Note the line around 5600 Å is an artefact. Bottom is a BL Lac (BZBJ0050-0929) with a spectra that has a few weak emission lines and is otherwise featureless as is expected of this type of object. Both spectra taken from the SDSS DR12 catalogue

RR Lyrae stars or flare stars due to their data reduction method; Jannuzi et al. 1993 mainly looks a polarization but does a follow up check on variability as well as the optical spectrum similarly failing to test radio and X-ray measurements; Muriel et al. 2015 and Ramazani et al. 2017 use gamma rays to identify and measure the distance to BL Lacs but such methods will fail to discover BL Lacs with weak or no gamma ray emission. Furthermore since BL Lacs are far more distinct from other objects in those regimes they do suffer from lower flux sensitivity. In the case of period measurements there also is the problem of the large amount of observation time needed. As such there are several upsides to using methods to identify them at optical wavelengths. This follows the methods first set out in the 2QZ redshift survey (Londish et al. 2002; Londish et al. 2007) which used observations from the Two-Degree Field (2dF, Croom et al. 2004) and the Six-Degree Field (6dF, Jones et al. 2004) quasi-stellar object (QSO) Redshift Surveys respectively. In this survey they found 7 BL Lac objects over an area of $\sim 1,000\,\mathrm{deg}^2$. All of these objects were observed as radio and X-ray sources and have since been shown to have variable optical flux (Nesci et al. 2005). A single possible BL Lac was also found in this survey that lacks both a radio and an X-ray source associated with its optical detection, but it is otherwise similar to typical BL Lacs. This detection along with the small number of detections in other surveys (Collinge et al. 2005; Shemmer et al. 2009) are however not decisive enough to confirm the nature of radio quiet BL Lacs, and in these surveys such objects appear as less than one out of 5 BL Lac candidates. As we demonstrate in this paper these methods have since been updated (see Plotkin et al. 2008; Plotkin et al. 2010) and made more stringent since more data is now available in part due to the SDSS survey and it therefore has become a considerably larger task to test each object individually without removing a large portion of them first.

As more BL Lacs were discovered it was made possible to test for shared traits between BL Lacs which directly resulted in a closer look at their host galaxies. The first analyses of these host galaxies were carried out using ground based telescopes (see Abraham et al. 1991; Falomo 1996; Wurtz et al. 1996; Falomo & Kotilainen 1999; Heidt et al. 1999) and indicated that these host galaxies were massive, red, elliptical galaxies with a mean magnitude of $M_R = -22.9 \pm 0.5$. Follow up studies using the Hubble Space Telescope (HST) and the

Wide Field Planetary Camera 2 (WFPC2, see Falomo et al. 1997; Urry et al. 1999, Urry et al. 2000; Scarpa et al. 2000a, Scarpa et al. 2000b; Falomo et al. 2000; O'Dowd & Urry 2005) included more objects to a greater detail and not only confirmed the previous findings but also narrowed down the range of luminosities the host galaxies appeared to have. This made them well suited as standard candles since their absolute magnitude could be assumed once a BL Lac was discovered and its host galaxy had a measurable apparent magnitude (see Scarpa et al. 2000b; Urry et al. 2000; Sbarufatti et al. 2005). Due to the large amount of flux from the nucleus of these galaxies such methods need a good enough angular resolution to model their radial light curve which is generally not available for BL Lac objects at higher redshifts or for many objects in SDSS. Plotkin et al. (2008) and Plotkin et al. (2010) has however shown that it is possible to use simple models to separate the flux contributions of the nucleus and the host galaxy and therefore make it possible to use BL Lacs without good angular resolution measurements as standard candles. Unfortunately it is not possible to avoid creating additional scatter beyond the $M_R = -22.9 \pm 0.5$ in the Cousins R band (Sbarufatti et al. 2005) that the host galaxies naturally have, but it does open new avenues of BL Lac research at higher redshifts.

It is also still precise enough to use as distance measurement where the host galaxies are assumed to have $M_R = -22.9 \pm 0.5$. While this value has been obtained purely from observations there are some explanations for the value (see Abraham et al. 1991; Falomo 1996; Wurtz et al. 1996; Falomo & Kotilainen 1999; Heidt et al. 1999) based on them being giant red ellipticals with massive black holes. Measurements of very radio luminous galaxies from the 3CRR sample (Laing et al. 1983) also show galaxies following a tight correlation in the Counsins K band (Jarvis et al. (2001)). Willott et al. (2003) confirms this finding using the 7C Redshift Survey (7CRS; (Willott et al., 1998)). For more directly applicable findings Dunlop et al. (2003) and Zheng et al. (2020) looks directly at host galaxies of quasars and find a similarly tight correlation once passive evolution is accounted for.

In this paper we search for BL Lac candidates in data from the Baryon Oscillation Spectroscopic Survey (BOSS, Dawson et al. 2012), an SDSS project. BOSS targets distant QSOs and LRGs which we then analyse using the method described by Plotkin et al. (2010)

and attempt to measure the distance to these objects as a test to see how far host galaxy measurements can be used as standard candles. These tests are crucial in understanding objects like BL Lacs and BOSS data is particularly of interest since we expect BOSS target selection to select several BL Lacs in a redshift regime where optical methods are not usually used. Due to this it is also done as a limit test to see if extra steps are needed to remove false positives as well as to highlight more objects which look like BL Lac objects in the optical spectrum but lack radio and X-ray emission.

In Section 3.3 we explain what data we are using and why we are taking that specific data. In Section 3.4 we go over our test for selecting BL Lacs and how it compares to Plotkin et al. (2010). For Section 3.5 we use the data we get from the previous section to test our method as we compare our measured redshift from host galaxies to a spectroscopic redshift. In Section 3.6 we present the new objects we find from looking at the BOSS catalogue and quickly discuss the limits that are now becoming apparent, we discuss these results in Section 3.7. We look at the limits of the method, and finally state our conclusions in Section 3.8. Throughout this work we use ΛCDM cosmology in which $\Omega_M = 0.3$, $\Omega_\Lambda = 0.7$, and $H_0 = 70\mathrm{km\ s^{-1}Mpc^{-1}}$. While we do call all our final objects BL Lacs care should be taken by future authors to note that a different approach might not rediscover the same objects and that better measurements might reveal an object to not be a BL Lac especially when looking at objects at higher redshifts where the signal to noise is lower.

3.3   Data sources

For testing the method we use data from three different data releases of SDSS. The MPA-JHU (Brinchmann et al. 2004, Kauffmann et al. 2003; Tremonti et al. 2004 [1]) catalogue for SDSS data release 8 (DR8) is used to test data flagged as galaxies while spectra flagged as stars in SDSS data release 12 (DR12) is used and finally we use data release 15 (DR 15) for a remainder group to get better coverage of the objects Plotkin et al. (2010) reports. The reason we are using different data releases is due to how much data is available and its similarity to SDSS data release 7 (DR 7) that Plotkin et al. (2010) used. We use Plotkin et al. (2010) as

---

[1]https://www.sdss.org/dr12/spectro/galaxy_mpajhu/

a comparison since we loosely follow his method of detecting BL Lacs as well as analysing their host galaxies. We detail our whole methods as well as where we differ from Plotkin et al. (2010) in 3.4. In the case of our objects flagged as galaxy data we want to avoid manually checking spectra as Plotkin et al. (2010) did since MPA-JHU has all the necessary data, such as line equivalent widths (EQW), photometric data such as colour and band flux, as well as the raw spectrum, and the data being recorded are roughly the same time - the main difference between the DR7 catalogue and our data being that MPA-JHU has more objects. Although the pipeline for DR 8 has been updated since DR 7 this was done to improve subtraction of bright objects, recalibrated using the 'ubercalibration' method of Padmanabhan et al. (2008), this should not be a problem since this will mostly result in less noisy data which should not cause us to remove actual BL Lacs Plotkin et al. (2010) found. For the stellar data we use DR12 since some properties of the objects have not been calculated in previous data releases. DR12 has more objects flagged as stars than DR7 due to the Apache Point Observatory Galactic Evolution Experiment (APOGEE, Zasowski et al. 2013) as well as the Multi-object APO Radial Velocity Exoplanets Large-area Survey (MARVELS, Paegert et al. 2015). These do not cause a problem since almost all of these objects do not match our criteria for BL Lacs meaning eliminating the last few objects can be done by a few simple tests as detailed in chapter 3.4.

Compared to Plotkin et al. (2010) our data from DR8 and DR12 fail to recover about 600 objects found by Plotkin et al. (2010). While this is most of the objects Plotkin et al. (2010) the discrepancy is due to the objects failing tests as we show in 3.4. Most of these missed objects have not been classified and a few of them are classified as QSOs. We select the missing objects from SDSS DR15 based on position and redshift and include them in our test data to see if we can recover the results Plotkin et al. (2010) using newer data or if the better data indicates that they might be false positives in sample used by Plotkin et al. (2010). We use DR15 for these objects to get the most up to date data possible. The pipeline for DR 15 has not been updated since DR 12 but some objects have been covered by new surveys and will therefore have better data. In the future we will refer to these samples as 'galaxy sample' for the DR8's MPA-JHU, 'quasi stellar sample' for the DR12 data and 'extra sample' for the

sample based on the data in Plotkin et al. (2010).

Having optically selected our test sample, we check for radio or X-ray detections aligning with our objects. We do this by using the Million Optical/Radio/X-Ray Associations Catalog (MORX, Flesch 2016) and comparing their results. In this catalogue, the authors assemble radio and X-ray detections from 8 different catalogues, totalling 1,176,782 objects, and where possible associate them with the closest optical detection in SDSS. Compared to just checking for radio or X-ray emissions at the point of the object this removes false positives where a nearby luminous objects or a large objects with sufficiently high radio or X-ray emission would result in positives if we just checked the background. There will still be some false positives in our results in cases where the radio or X-ray detection has a low likelihood of being associated with the optical object the MORX catalogue has associated it with. In our sample we find that about 77% of of the objects have above a 90% likelihood of being correctly associated. These likelihoods are based on the density of optical objects in the area of the radio source as well as colour and PSF type as explained in (see Flesch 2016) and we have presented one of these matches in Fig. 3.3. Since MORX is created using a few different catalogues there is going to be different limits for each of the catalogues. Radio sources in MORX are compiled from NRAO VLA Sky Survey (NVSS, Condon et al. 1998) and Sydney University Molonglo Sky Survey catalogue (SUMSS, Murphy et al. 2007) which has a completeness limit of 2.5 mJy looking at 1.4 GHz and 843 MHz respectively as well as FIRST (White et al. 1997) which has a completeness limit of 1 mJy looking at 1.4 GHz. The radio surveys are not full sky but are chosen so that they cover approximately the same area as SDSS. Since we only look at SDSS data all our objects should be covered by FIRST or, to a lesser degree, one of the other surveys and as we shall see in section 3.4 we make a cut based on FIRST completeness limit when regarding which objects are radio loud and which objects are not. We finally use our method to go through SDSS DR15 BOSS data to check if there are any BL Lac candidates there. We use this data since it has not been fully explored in regards to BL Lacs, and part of the aim of this work is to find new BL Lac candidates in this more recent data release.
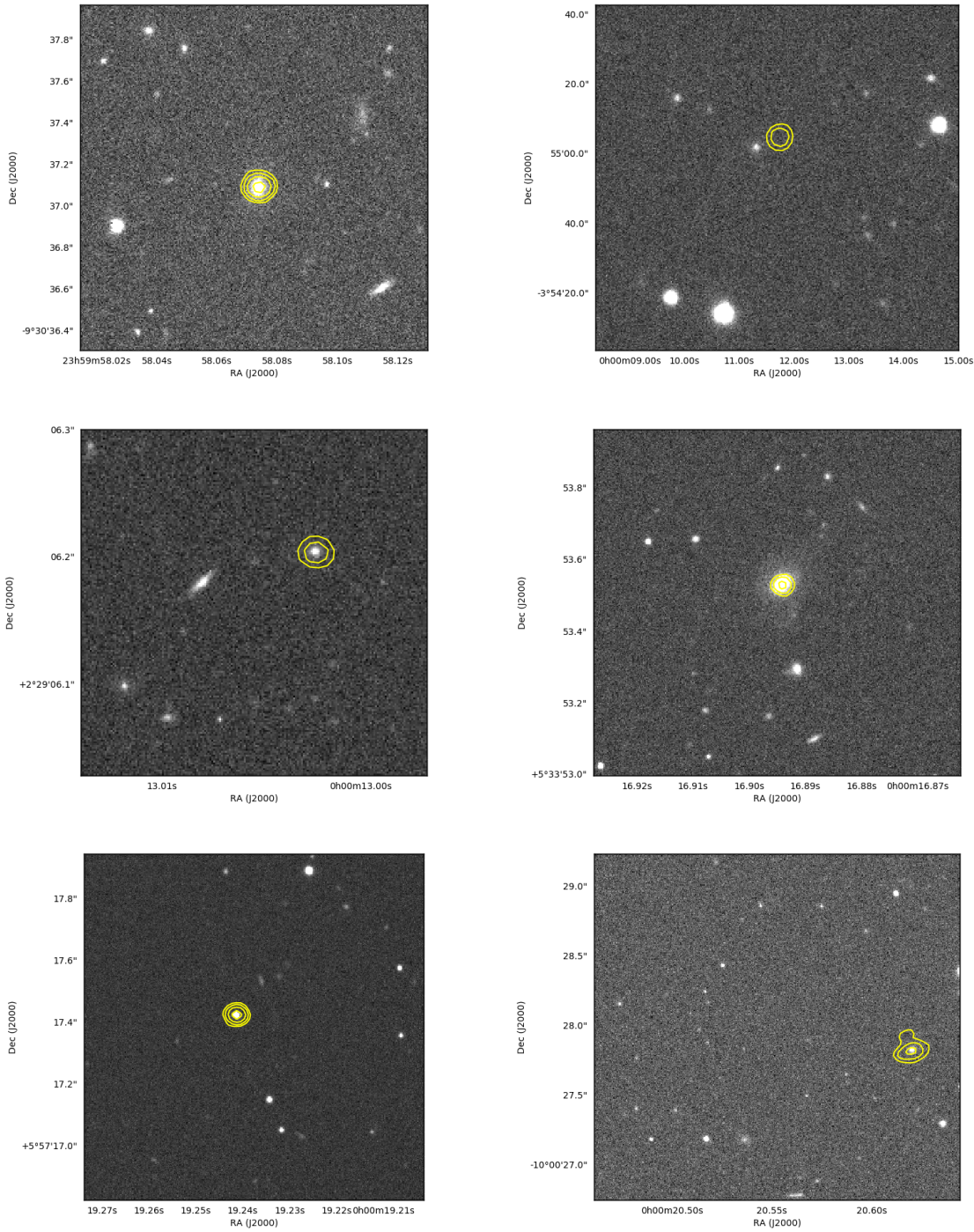
Figure 3.3:   Plots of SDSS J000001.57-092940.2 (top left), J000013.71-035439.6 (top right), J000016.10+022954.8 (middle left), J000021.72+053504.6 (middle right), J000024.70+055824.6 (bottom left), and J000025.55-095753.0 (bottom right) along with the radio contours in the areas observed by FIRST. The confidence of these are 99.7%, 99.8%, 99.7%, 99.8%, 99.8%, and 99.4% match in the MORX database and shows some of the typical matches MORX makes between radio signatures of objects observed by optical telescopes which in general are very clearly correlated.

3.4   BL Lac selection

In order to find BL Lacs we look at the spectra of hundreds of thousands of galaxies to determine if they are possible candidates. We do this since BL Lacs are often misidentified or not identified at all due to their odd spectra as described in 3.2. The objects we are looking for have spectra with high signal to noise, so we can confirm if they contain few artefacts from noise and have spectra that contains few features, in line with what we expect from BL Lac objects. We present a flowchart in Fig. 3.4 that goes over the first steps of the process and the rest of this chapter further details the complete method along with similar flowcharts which go over the later steps.

3.4.1   Signal to noise test

We use magnitudes from photometry to test for a high signal to noise since if large number of photons are detected from the source it should translate into a high S/N ratio (see Plotkin et al. 2010). Following the estimate made by Plotkin et al. (2010) we use minimum 'cmodel' (see Abazajian et al. 2004) band magnitudes of $g < 20.5$, $r < 20.3$, and $i < 19.6$ which removes about 7.5% of our galaxy sample, 6.9% of our star sample and 1% of our extra sample. We then remove a further 5% of each sample by also requiring that they have more than a S/N ratio of 6 per point in the spectra throughout the bandwidth of at least one of the filters. In Plotkin et al. (2010) they cut about 11.5% using this method. The small difference is likely due to differences in the data releases used additionally we use entire pass bands whereas they use S/N of smaller regions with a width of $\Delta\lambda = 500$ Å and require $S/N > 100$ in at least one of those regions. This test is done to remove objects with noise which could hide emission lines to the point where later tests would not remove the object. This means we might remove actual BL Lac objects but the alternative is including false positives.

3.4.2   Removing well classified objects

BL Lacs spectral characteristics are caused by non-thermal processes and as such are distinctly different from other objects. We therefore remove any objects which SDSS has classified as
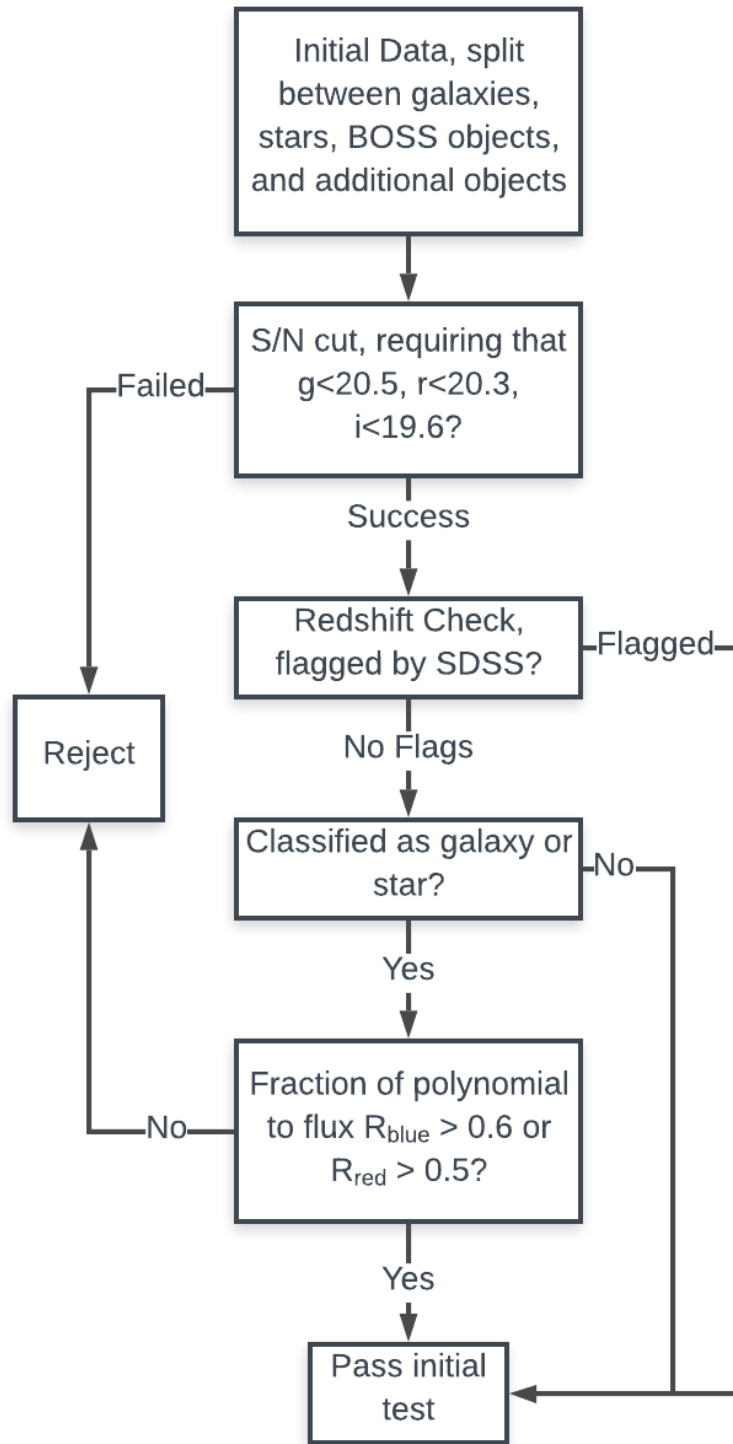
Figure 3.4: Flowchart describing the initial tests we use on our data. We do not make a classification test if the redshift has been poorly determined as the classification then has a higher probability of being wrong. We also only perform a polynomial test if the classification test indicates a type of object we are not looking for.
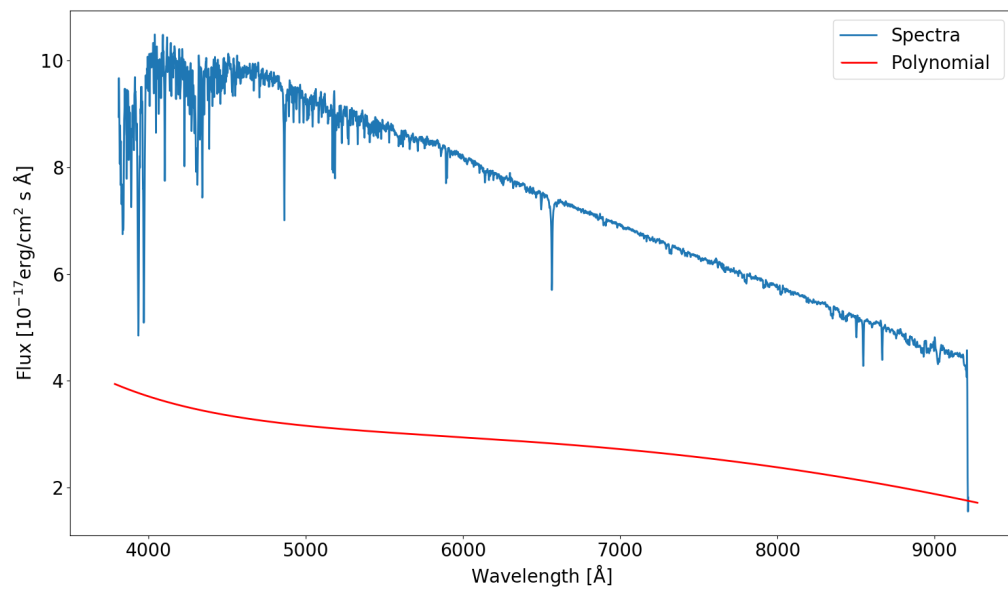
Figure 3.5: Spectra rejected due to a small polynomial accounting for more than 60% of the spectra as explained in Section 3.4.2. The polynomial shown in the plot is about 40% of the modelled flux which is less than what we expect for a BL Lac object.

another type of object to a high degree of confidence. These objects are typically galaxies or stars which are well modelled by one of the templates used by SDSS and as such are likely not a BL Lac. We test for a high degree of confidence as follows. Objects with a redshift flag are considered to be poorly measured by default and pass the test. The same goes for objects not classified as stars or galaxies. The remaining objects are passed if more than half of the SDSS model flux is due to the polynomial SDSS adds when generating its model flux of the fit with the rest being a stellar or galaxy template to fit the spectrum. For our case we use the spectrum in the wavelength ranges 3800-4200 Å and 8800-9200 Å and if the polynomial fit constitutes more than 60% of the flux for the first set of wavelengths and 50% of the flux for the latter set we study the object further (see Fig. 3.5). This should remove all objects with spectra well fitted by star and galaxy model spectra while not removing BL Lacs as their spectral characteristics are caused by non-thermal processes and therefore require significant contributions from the polynomial added to the templates to get a good fit of the observed data. We also remove any objects for that have a redshift measurement of $z <= 0$ as such objects are extremely likely to be stars even if they passes the polynomial test.

3.4.3 Optical spectra test

To test if the spectrum of a given object is similar to the spectrum we would expect of a BL Lac we start by checking the D4000 break. Plotkin et al. (2010) defines a value C such that

$$C \equiv 0.14 + 0.86 \left(\frac{\langle f_{\lambda,r} \rangle - \langle f_{\lambda,b} \rangle}{\langle f_{\lambda,r} \rangle} \right).$$

Here $\langle f_{\lambda,r} \rangle$ refer to the average flux per Å in the region 4050 Å to 4200 Å and $\langle f_{\lambda,b} \rangle$ refer to the same calculation over the range 3800 Å to 3950 Å. If a given spectrum has a break larger than $C = 0.4$ we remove that candidate as such objects are unlikely to be BL Lacs and instead are likely galaxies or quasars since lower C directly correlates to larger jet power and radio core dominance which both of which are correlated to the orientation of the galaxy (see Landt et al. 2002, Fig. 3.7 and Fig. 3.8 for an example in our data). Since we expect BL Lac objects to have jets aligned with our line of sight any objects with a high C value, and therefore not facing us, is unlikely to be a BL Lacac object. For any spectra passing this test, we examine each of their emission lines individually, and spectra with any emission line with
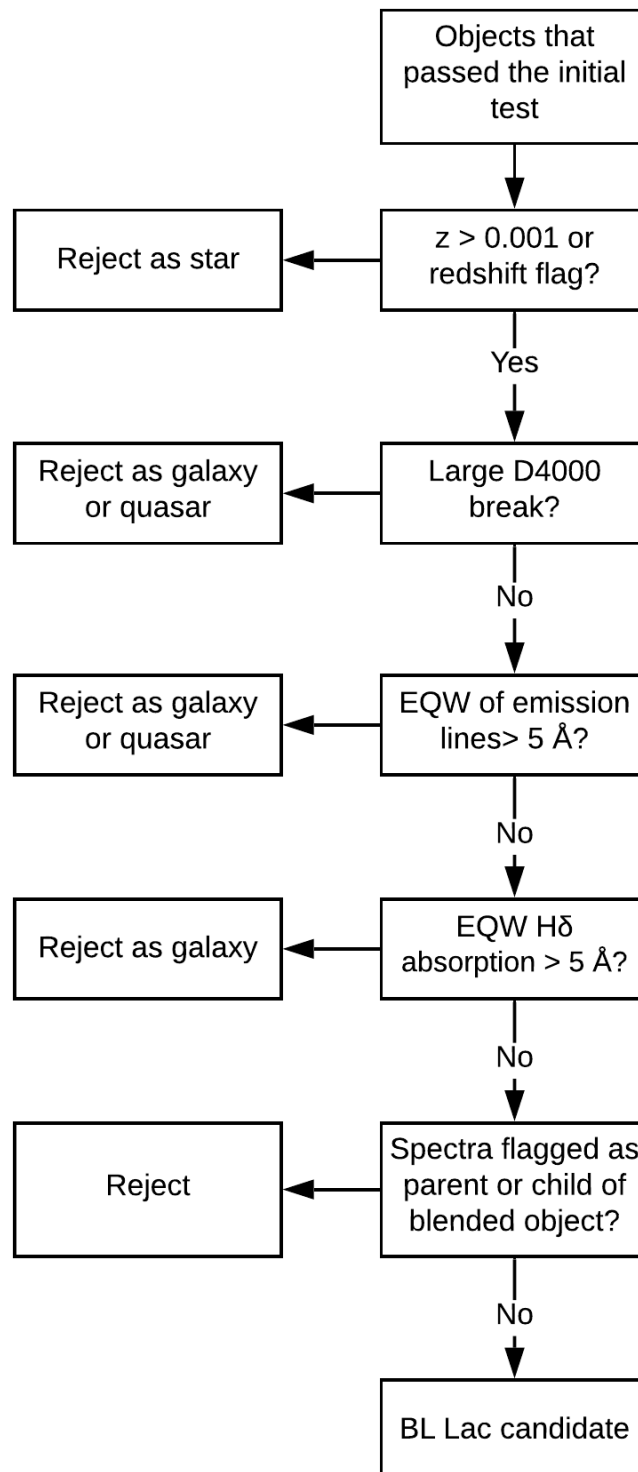
Figure 3.6: Second set of tests we perform on the data. This is mainly focused on spectroscopic tests such as emission lines, absorption lines as well as removing blended objects.
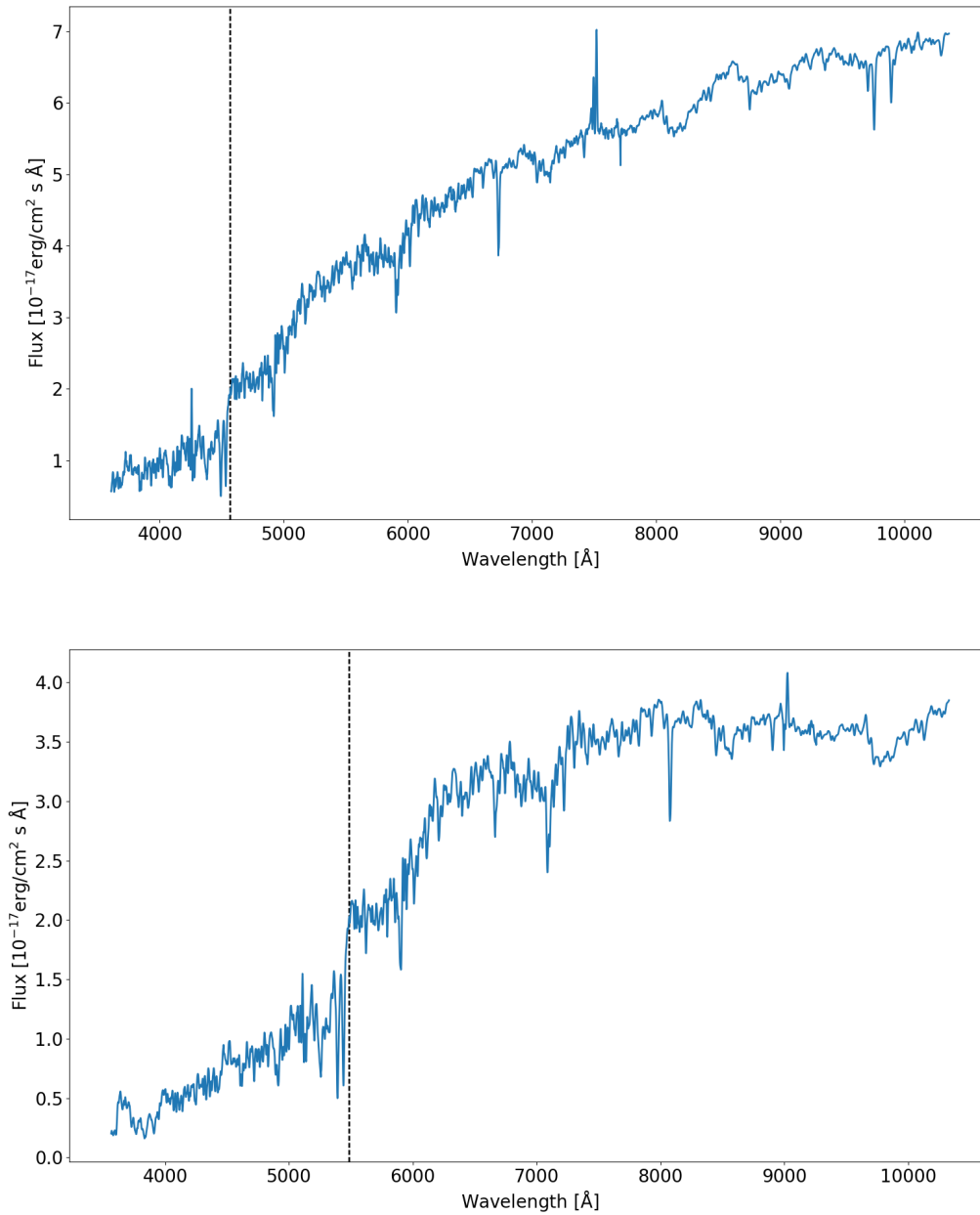
Figure 3.7: Both spectra are rejected due to a large $D4000$ which is located at the vertical dashed line. Top spectrum has a C value of 0.404 and additionally has a few prominent absorption and emission lines which are not marked but would also lead to a rejection of the spectra. Bottom spectrum has a C value of 0.474 but is otherwise relatively featureless outside of the absorption around 7100 Å as well as several very thin absorption lines.
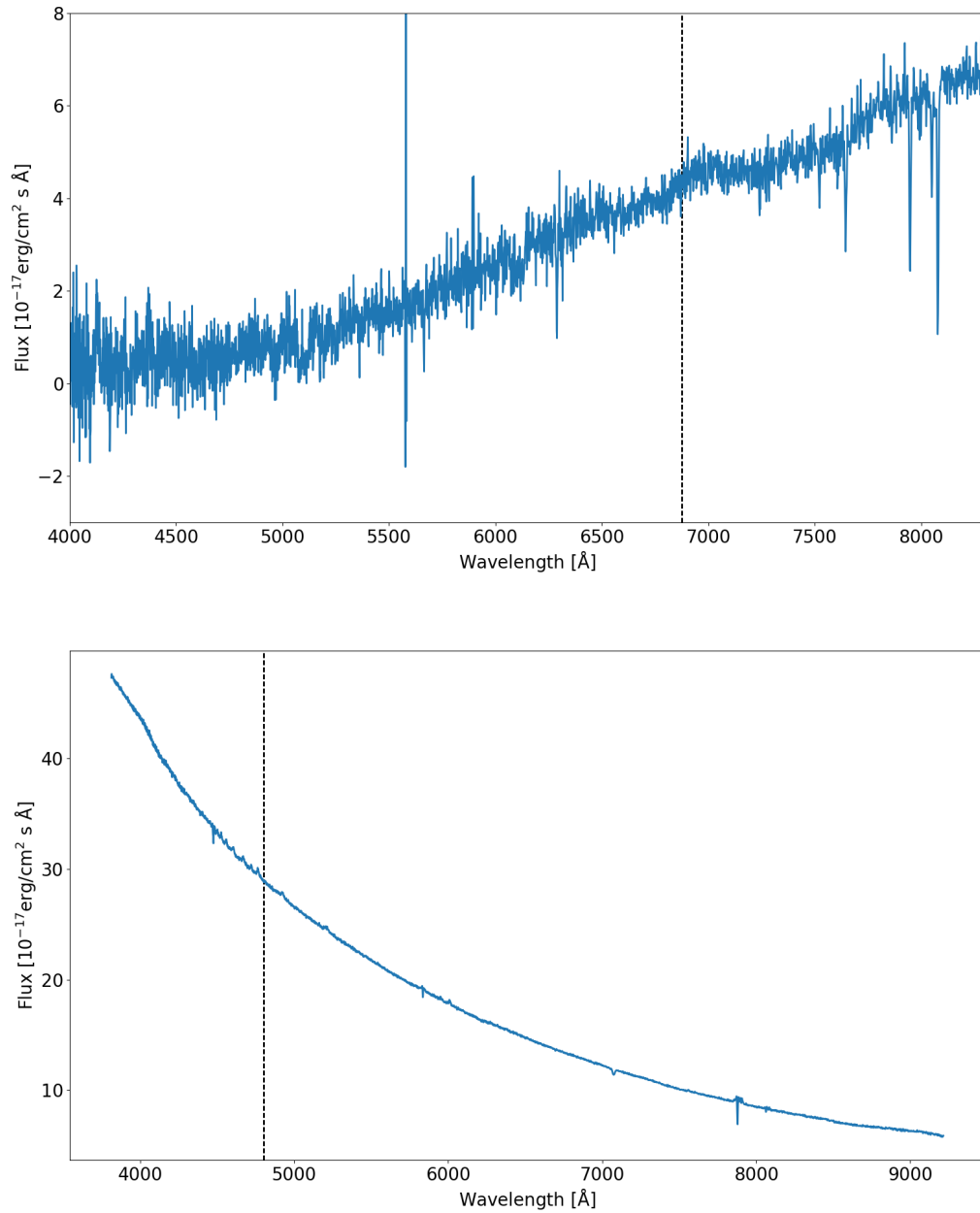
Figure 3.8: Both spectra are accepted in the $D4000$ test. The vertical dashed line represents 4000 Å at restframe of the object. Top spectrum has a C value of 0.315 and has a generally low flux. Bottom spectrum has a C value of 0.001 but is otherwise very featureless with the possible exception of the absorption line around 7900 Å although that is thin enough to likely be an artefact.

an equivalent width more than 5 Å in emission are removed since such emission lines are a result of excited atoms which we do not expect to see since the jet's emission that has been created by Inverse Compton scattering is the dominant factor in their specta which in turn causes BL Lacs to have almost featureless spectra. Spectra which have larger emission lines are therefore likely either galaxies or quasars. We use 21 different emission and absorption lines for the EQW test as presented in table 3.1 (see Fig. 3.9 for an example).

We also require that Hδ absorption has EQW $<$ 5Å is detected so as to rule out any galaxies that have recently undergone star formation but where the emission lines have now disappeared to remove E+A galaxies (see Wilkinson et al. 2017, see Fig. 3.10 for an example) and is also likely to remove galaxies with stellar populations 1-2 million years in range as the line is sensitive to A stars (Cananzi et al. (1993)). While we could also test for Hγ absorption it is unlikely to produce results considerably different from Hδ absorption as those lines are typically correlated. Any spectra that pass these tests are included as BL Lac candidates and undergo tests that are not based on the optical spectrum (see Fig 3.11 for an example of a spectra that passes the tests).

3.4.4   Additional, multi-wavelength testing

We also check if we can match any objects to X-ray and radio sources since the mechanism that creates the jet also produces a radio signal. We do this by using MORX that takes each radio and X-ray detection in their catalogue and linked it to the most likely optical object, if they can find one. We present a histogram of offsets in MORX as well as our final sample in Fig. 3.12. We cross-match our objects with their optical detections and if we are successful in finding a match we include it as a BL Lac candidate provided that the object appears as a point source in its radio detection. If we are unsuccessful we use two different colour tests depending on if their redshift is flagged in SDSS in any way. If it is flagged we test if it might still be a white dwarf star by removing all objects where $g - r < 0.35$ and $r - i < 0.13$ as per Plotkin et al. (2010) or if their proper motion is $\mu > 30$ mas/yr. If their redshift is known we reject them as Luminous Red Galaxies (LRG) if $g - r > 1.4$ also as per Plotkin et al. (2010). If the objects pass these test we include them as BL Lac candidates. In Fig. 3.14 we show a

Line name	Central wavelength	Line name	Central wavelength
Ly α	1215 Å	[OIII]	4959 Å
C IV	1549 Å	[OIII]	5007 Å
C III]	1908 Å	HE I	5876 Å
Mg II]	2799 Å	[OI]	6300 Å
[OII]	3726 Å	[NII]	6548 Å
[OII]	3729 Å	Hα	6565 Å
[NEIII]	3869 Å	[NII]	6584 Å
Hδ	4101 Å	[SII]	6717 Å
Hγ	4340 Å	[SII]	6731 Å
[OIII]	4363 Å	[ARIII]	7135 Å
Hβ	4861 Å		

Table 3.1: List of lines we use to test for emission features in our spectra.
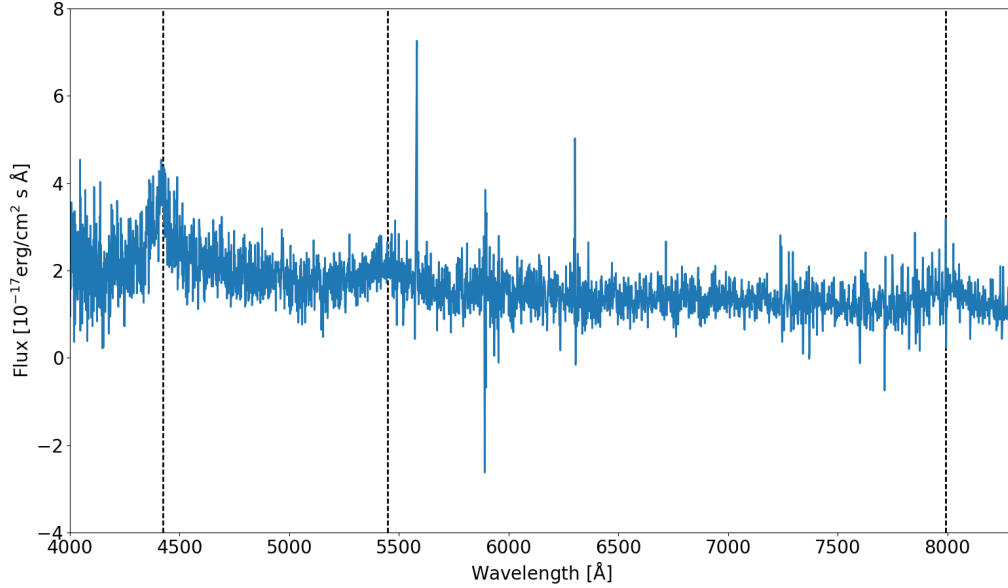
Figure 3.9: Spectrum is rejected due to emission lines C_{IV} at 1549 Å; C_{III} at 1908 Å; and Mg_{II} at 2799 Å which are all represented by vertical dashed lines. There are a few other spikes in flux but these are likely artefacts from the measurement rather than actual emission since their equivalent width is small.
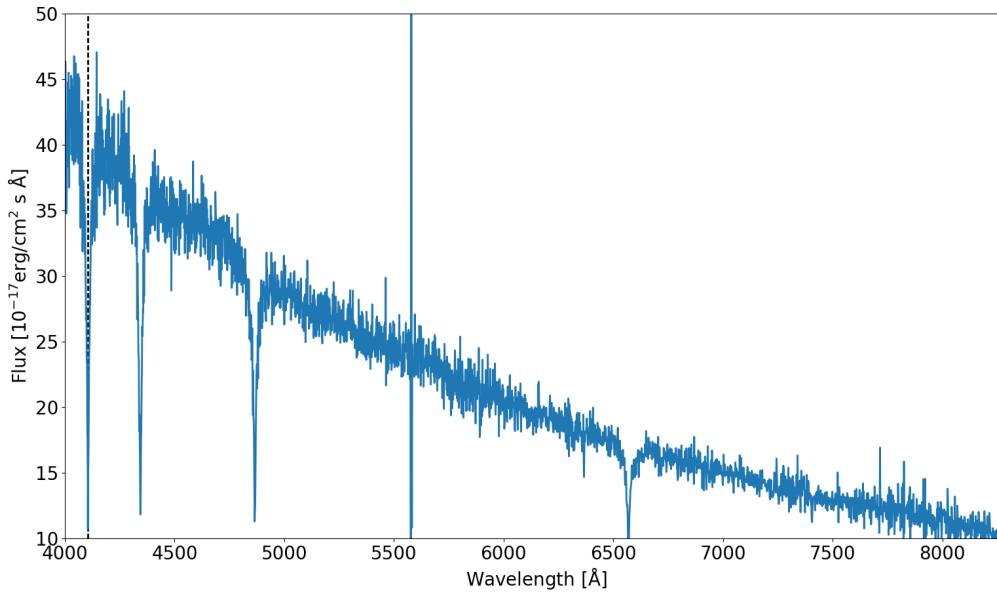
Figure 3.10: Clear absorption in the H_δ line along with H_γ; H_β; and H_α causing the spectra to be rejected by our method. We have here highlighted H_δ since that is the line our test uses. There also seem to be a large emission line at 5577 Å, which is likely an artefact.
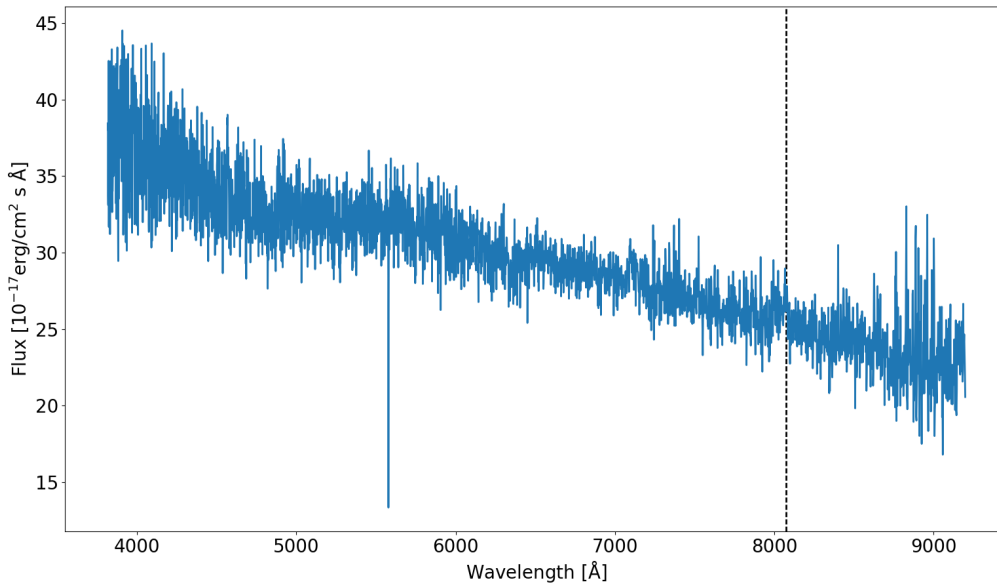
Figure 3.11: Spectra passes our test but with a few notes: There is a small N_{II} line at 6583 Å represented by the vertical dashed line but the EQW is less than 5 Å so we do not reject it due to this; another note is the amount of noise in the spectra. We still accept this due to the large signal of the spectra, causing an acceptable S/N ratio.
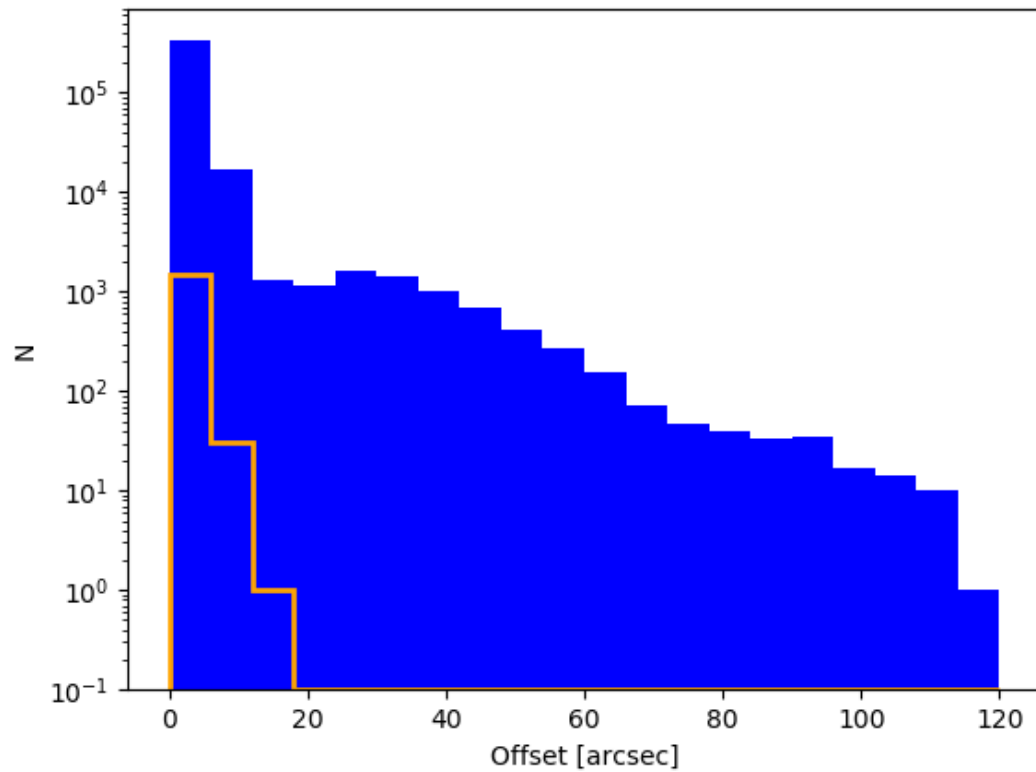
Figure 3.12: Histogram of offsets between radio source center and optical source center in the MORX catalogue. The entire catalogue is presented in blue while our data is presented as an orange outline since our data is only a subset of the entire catalogue.
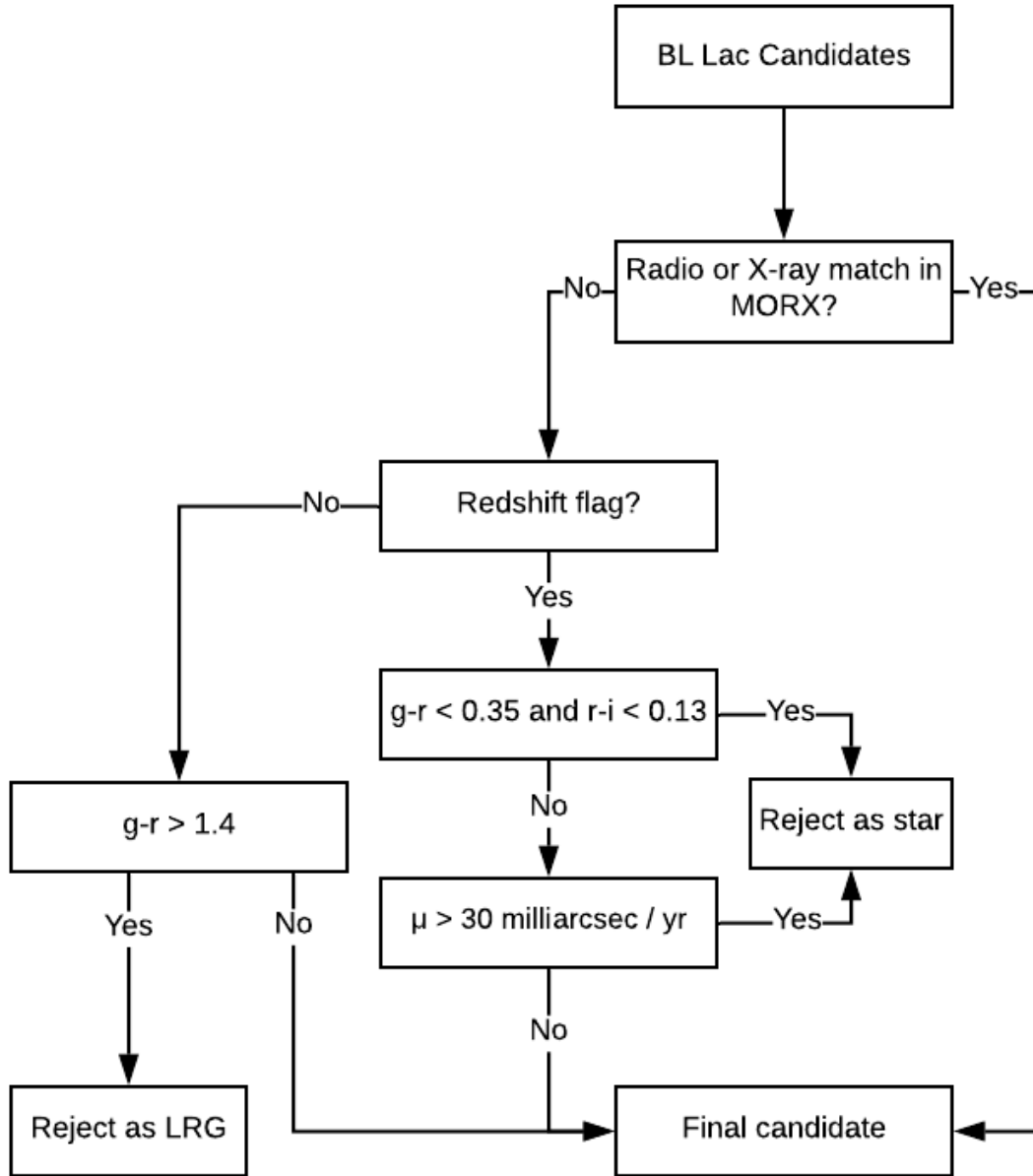
Figure 3.13: Final tests we apply to the data. If the objects are radio loud they automatically pass these tests otherwise remove or keep them based on a colour test as seen in 3.14. We apply different colour tests depending on if the redshift is well determined since it is generally possible to determine redshift of LRGs
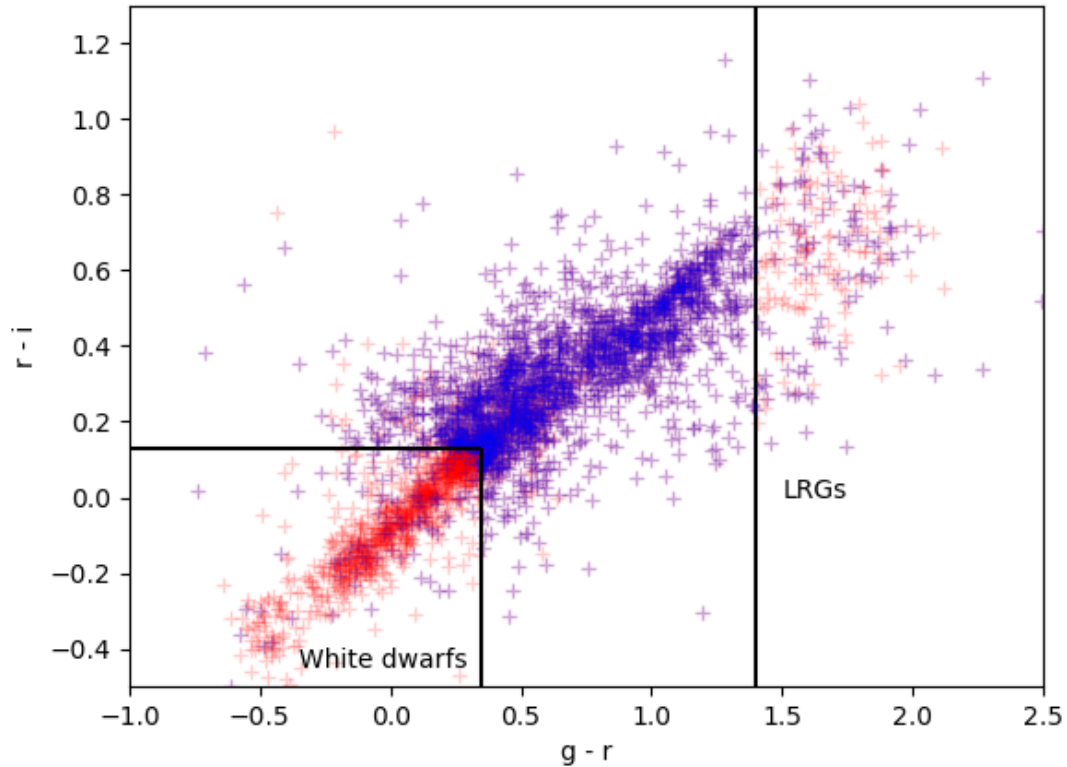
Figure 3.14: Plot of the colours of all our BL Lac candidates. We have here added transparancy to the points for a better visualization of densities of points. Objects marked in blue have radio or X-ray sources associated with them and are not rejected based on our colour test since our other tests should have already removed non BL Lac objects with radio or X-ray signature; objects marked in red have no radio or X-ray sources associated with them and get removed if $g - r < 0.35$ and $r - i < 0.13$ or $g - r > 1.4$ since they are likely white dwarfs or LRGs.

plot of all our candidate objects in $g - r, r - i$ space where it can clearly be seen that there are only a few radio loud objects that would be cut if we apply the colour tests to them but since the previous tests have already eliminated objects like micro quasars and X-ray binaries we expect these radio loud objects to be BL Lacs rather than any other type of object.

3.4.5   Comparison with Plotkin et al. (2010)

While our method is based on the Plotkin et al. (2010) paper we have made some changes to the method.

1. Instead of directly measuring a S/N from small spectral regimes within each pass band we require high flux values in entire flux bands.

2. We eliminate objects as stars if they have z < 0.001 instead of z=0.

3. We check 21 different emission lines, whereas Plotkin et al. (2010) uses 'standard emission features' and mentions 6 specific ones.

4. Plotkin et al. (2008) checks for blended spectra as well as blue low surface brightness galaxies by eye whereas we rely on the objects being flagged by the SDSS routine, which uses simple model fits to check for blended objects, due to needing a fully automated program.

5. Plotkin et al. (2010) checks for background radio or X-ray emission exceeding a certain value at the optical location of his objects whereas we use the MORX catalogue to link radio and X-ray sources to optical objects and checking for matches between those objects and our candidates.

In Plotkin et al. (2010) they report 723 BL Lac candidates of which 637 of them are radio loud. We do not consider the radio quiet ones since those objects are not as well understood theoretically and we want our test group to be as sound as possible. Of the radio loud BL Lacs we confirm 122 of them and reject the remaining 80.8% of the objects. The rejections are mostly due to large EQW of lines, objects appearing extended in radio, as well as poor

S/N ratio of the bands and a few of them are due to the D_{4000} break. This difference is likely due to a combination of us working with newer data (Plotkin et al. 2010 using DR7 versus us using DR8 or newer depending on object in question) as well as using a more aggressive S/N ratio cut and therefore we reject most of the objects they previously found even if we find more in total due to the larger amount of data we are using. Compared to Plotkin et al. 2010 we find a much larger ratio of radio quiet BL Lac candidates compared to radio loud BL Lacs. This is likely due to our test sample including more objects, many of which are at higher redshifts than the sample of Plotkin et al. 2010. Our methods are also slightly different but should not cause a difference of this magnitude. This discrepancy does however suggest that the reliability of this method is somewhat compromised when looking at radio quiet objects and highlights a need to also look for radio loudness when using this method. For the rest of this chapter we will however continue looking at the radio quiet sample as well to further investigate this sample and see how it compares to the radio loud sample. An overview of the details is presented in Table 3.2.

This should not be a surprise and since we use newer data and use MORX for radio pairings instead of background signals we should get better results. We still compare our results to Plotkin et al. (2010) since we are likely to find many of the same objects. In total we find 385 radio loud BL Lac objects as well as 17,198 weak-featured radio quiet objects in our test data when using a radio flux cut-off of 2 mJy in line with the completeness of the FIRST survey.

3.5   Redshift estimation

Although it is part of the goal of this paper to use the method on BOSS data this chapter only uses non BOSS data as we want to calibrate and test our method with data similar to Plotkin et al. (2010). To use a BL Lac as a standard candle it is necessary to obtain the absolute magnitude of the host galaxy. We do this by fitting the measured spectrum with an assumed AGN spectrum and a template elliptical spectrum which we describe later in the section. After this we subtract the AGN fitted flux from the measured flux and measure the resulting flux.

Number of objects found in each sample		
Survey	Radio-Loud	Radio-Quiet
Plotkin et al. (2010)	637	87
Our test sample	385	17,198
Boss data	4,216	41,835

Table 3.2: Table listing the amount of objects from the different samples we have used as well as the number of objects Plotkin et al. 2010 finds.

3.5.1   Spectral fitting

The spectrum from a given BL Lac will likely have two dominant components: one from the AGN, which usually contributes the majority of the flux and one from the host galaxy which typically produces significantly less of the total flux. The rest is then sourced from foreground or background objects which produce a negligible amount of flux when compared to the object itself (Plotkin et al. 2010). In some cases the AGN produces a larger proportion of the flux. In than that case we still do the same procedure but we are unlikely to get accurate results for such objects.

The easiest component of the system to model is the AGN part which will have a roughly polynomial shape which we approximate in the form of

$$f_\lambda = f_{\lambda_0} \left(\frac{\lambda}{\lambda_0} \right)^{-\alpha} \tag{3.1}$$

where λ_0 is a reference wavelength, f_{λ_0} is the AGN flux at λ_0 and α is spectral index of the AGN in the optical part of the spectrum. To fit the observed spectra we still need to model the contribution from the host galaxy. We use the model of an elliptical galaxy from Mannucci et al. 2001 to get a rough shape of the galaxy's spectrum, assuming it is a normal elliptical galaxy (see Urry et al. 2000), which we then redshift and multiply by free parameter for the purpose of fitting. Our complete fit then takes the form of

$$f_\lambda = n f_{\text{model}} (\lambda, z) + f_{\lambda_0} \left(\frac{\lambda}{\lambda_0} \right)^{-\alpha} \tag{3.2}$$

where n is a constant multiplied to the galaxy model spectrum and z is the redshift of the object, and f_{model} is the best fitting model in the SDSS database after the polynomial has been aplied. We use n, f_{λ_0}, and α as free parameters. Fig. 3.15 presents an example of one of these fits.

Due to using a single galaxy spectrum model, we do not expect it to line up with whatever weak emission or absorption lines there are in the real spectrum, but since we are not measuring those contributions but rather the a band magnitude of the galaxy we only need to get the correct shape and size of the galaxy's contribution. Once we have the fit we subtract just the AGN part of it from the observed spectrum and measure the flux from the resulting spectrum.
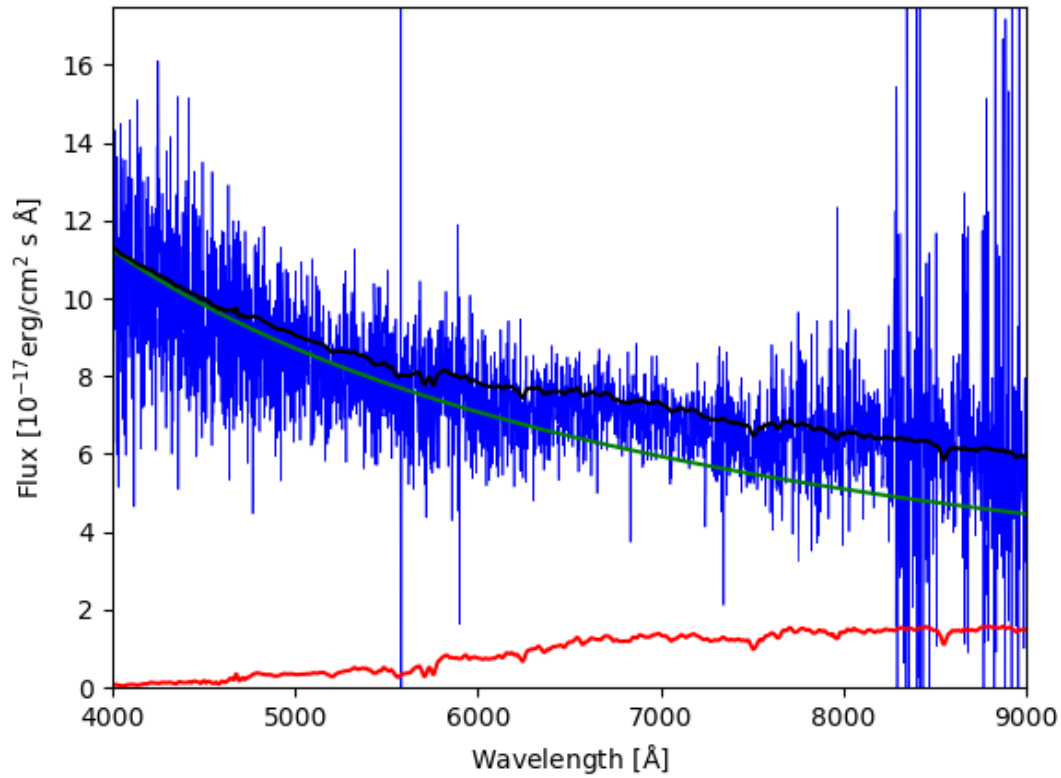
Figure 3.15: Flux of SDSS J111717.53+000633.6 in blue. We have marked up each component of our fit in green for the AGN part and red for the galactic part which is a about a factor of 9 dimmer than the AGN part when averaged over the entire part spectra that is shown here. The complete fit is marked in black and closely follows the spectra of the object and obtains a $R^2 = 0.997$ when compared to the SDSS best fit of the raw spectra.

3.5.2 Aperture correction

Since the galaxies we are working on have a radius of ~ 10 kpc (Urry et al. 2000) a significant number of them will not fall within the optical fiber of the SDSS telescope (3" diameter). For the sample we compare with Plotkin et al. (2010) about 93% of the objects will be too close to fit the 20 kpc diameter of the galaxy within a single fiber as that is achieved at $z \approx 0.6$. This results in some of the light of the galaxy not being included in the observation and makes the object appear dimmer than it actually is. We correct for this by assuming the host galaxy has a de Vaucouleurs profile (de Vaucouleurs 1948) and calculate the amount of unobserved to observed flux ratio such a profile would have at a given redshift if we had used an aperture of infinite size. We then correct the magnitude accordingly to include flux from the entire galaxy.

3.5.3 k+e correction

Since we are trying to get the absolute magnitude of the galaxies we need to take into account both the k-correction and evolution correction of the galaxies we are measuring. The k-correction is applied since we want to measure the same rest frame wavelengths of each galaxy however since we will often not have measured the entire spectrum we instead model how the magnitude a typical galaxy at the rest frame wavelengths we measure will be different from the magnitude at the rest frame wavelengths we want to measure. The other large corrections we apply is based on the evolution of the galaxy and our own galactic extinction. The former is due to the fact that galaxies change color with time as they evolve and change their stellar and chemical makeup (Bruzual & Charlot 2003; chapter 2) whereas the latter is due to our own galaxy's extinction of the incoming light (Marshall et al. 2006).

To correct for evolution and redshift of the host galaxies and BL Lacs we use a Salpeter (1955) initial mass function (IMF) which we create using the method presented in Bruzual & Charlot (2003). We assume that since host galaxies for BL Lacs are large, red, ellipticals a simple stellar population with an age of 12 Gyr at $z = 0$ and a metallicity of $Z = 0.008$ approximates them well (Thomas et al. 2005). While a more precise k+e correction could be achieved by using multiple simple stellar populations (SSP's) the change in the correction is
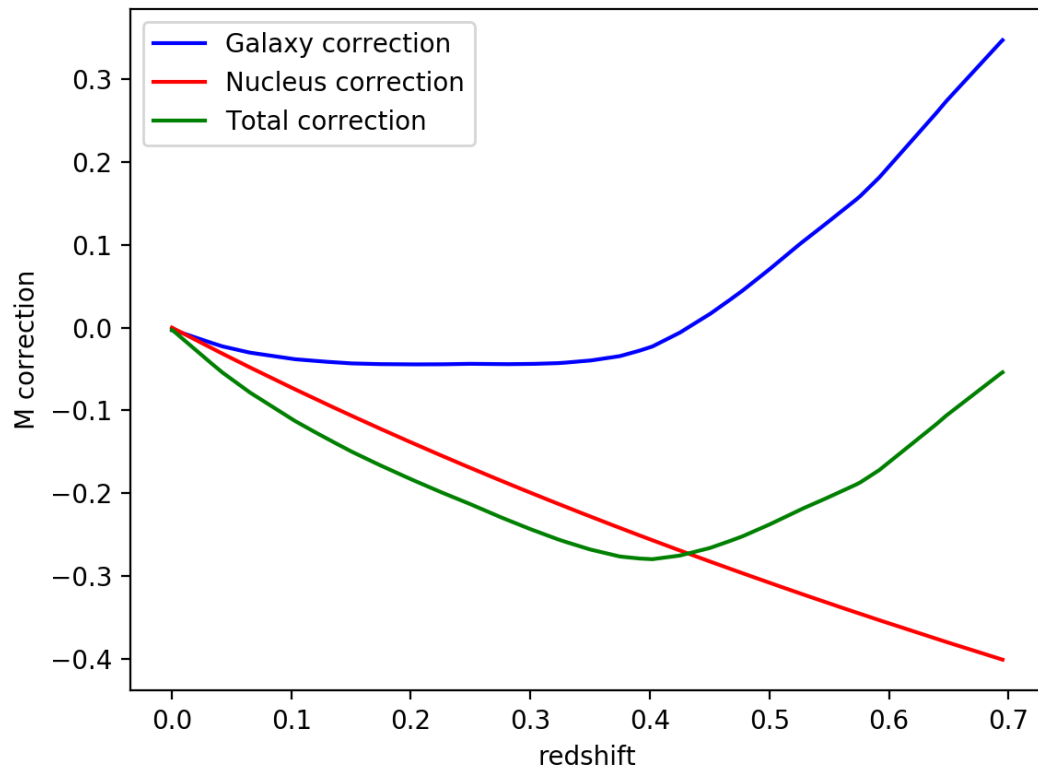
Figure 3.16: Corrections we apply to our objects based on redshift. Blue represents the correction applied due to the k+e correction of the galaxy, red is the correction from the nucleus assuming it has a spectrum where $F(\lambda) \propto \lambda^{-0.7}$. Green is the total correction applied to the extended object. We have invenstigated the error on these measurements and based on Bruzual & Charlot (2003) and Roche et al. (2009) the errors do not effect the final results presented in this thesis as they are far too small.

relatively small. By making these assumptions we get a k+e correction as shown in Fig. 3.16. For the AGN component of the BL Lacs we assume a profile as we described in 3.1. This profile results in an additional k correction of $-1.75\log(1 + z)$ as seen in Fig. 3.16. Since we are measuring both the nucleus and host galaxy we apply both k-corrections as well as the e-correction for the galaxy when calculating the absolute magnitude for the entire system. We do not apply an e-correction to the nucleus as that part is unlikely to have changed magnitude or colour with age.

3.5.4 Host galaxy measurement

By using the α and f_λ measured in Eq. 3.1 we can get a rough estimate of the spectral flux density of the nucleus. Using this we calculate the flux density of the galaxy as

$$f_{\nu,\mathrm{hg}}(z) = \frac{\lambda_{\mathrm{eff},R}^2}{c} A(z) \cdot (f_{\lambda,\mathrm{total}}(\lambda_{\mathrm{eff},R}) - f_{\lambda 6165}(1.067)^{-\alpha_\lambda}) \tag{3.3}$$

where $A(z)$ is the aperture correction, $f_{\lambda,\mathrm{total}}$ is the spectrum and 1.067 is a correction that transform our nucleus measurement at 6165 Å to the effective wavelength of the Cousins R band. We effectively measure the flux of the host galaxy as the difference between the nucleus component we measured in 3.1 and the spectrum. While there is a redshift component in Eq. 3.3, it is only weakly from aperture and the α and f_λ measurement, while it is dependent on redshift it is mostly to get a decent template for the host galaxy. As such Eq. 3.3 varies only weakly with redshift and mostly varies with the measured flux from the galaxies as well as the flux distance measurement when converting from observed magnitude to absolute magnitude. It should be noted that while we are measuring a band magnitude, the Cousins R band, we are doing so through spectroscopy rather than photometry. We use the Cousins R band rather than the SDSS r band for easier comparison with other works that also stick to Cousins R band magnitudes.

We use an initial guess and calculate an absolute magnitude of the galaxies using

$$M_R = m_R + k + e(z) + 5 - 5\log(d(z)). \tag{3.4}$$

where $k + e(z)$ are the k and evolution corrections, $d(z)$ is the luminosity distance and M_R is the absolute magnitude. This is then fitted until the redshift provides an absolute magnitude
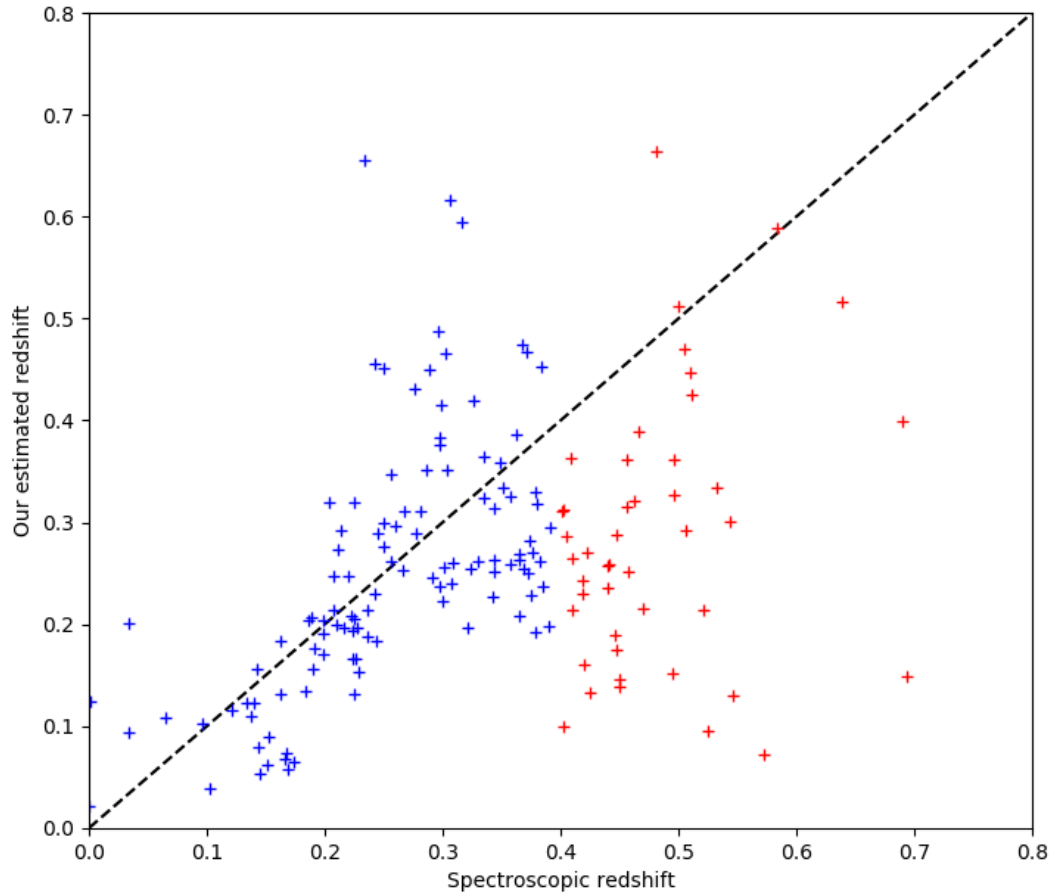
Figure 3.17: This plot is our measured redshift against the redshift measured by SDSS. While we generally get good predictions at lower redshifts they do seem to deteriorate at higher redshifts. This is likely due to the galaxies being dimmer and therefore even a small uncertainty in magnitude can have a large impact on the measurement. This in general seem to happen at around $z = 0.4$, above which the standard deviation of the measurement seems to be too high to use properly. The dashed line represents a 1 to 1 match between our redshift and spectroscopic SDSS redshift.
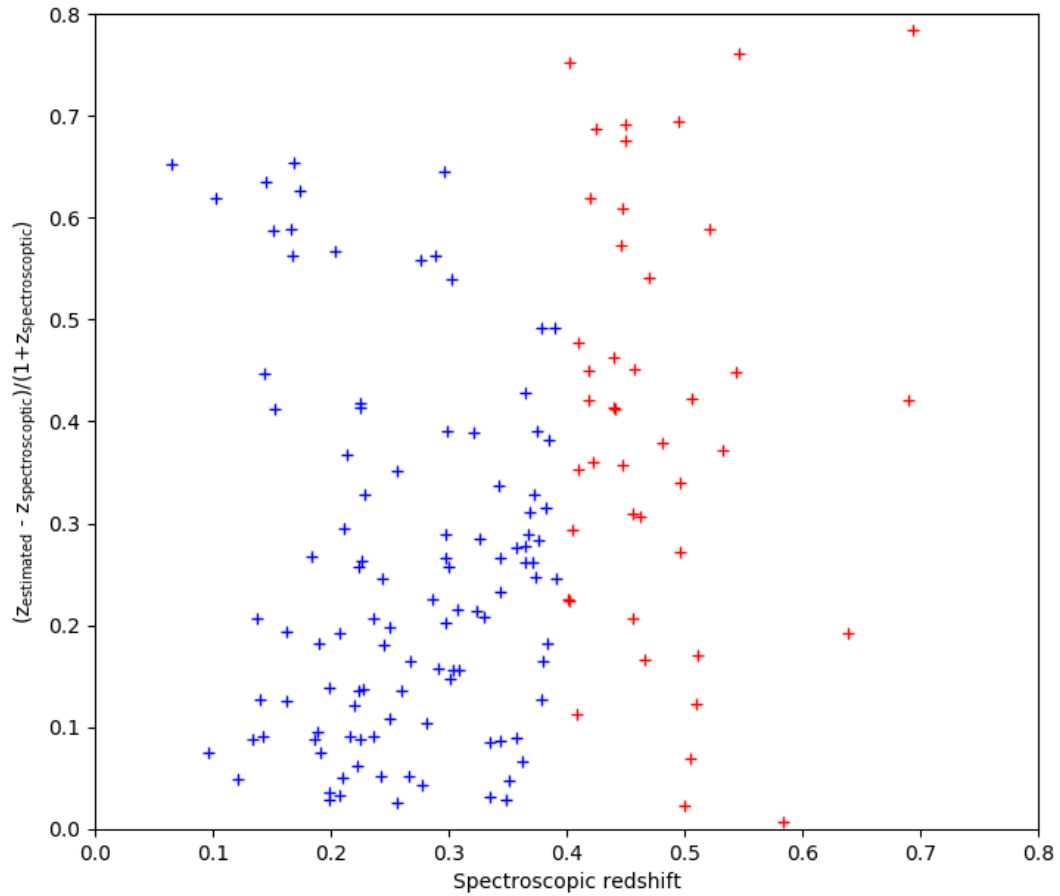
Figure 3.18: Plot of the normalized deviation of our measurements from the spectroscopic redshift. Similar to what is mentioned in figure 3.17 it is much clearer here where the deviation in distance measurement starts going wrong.

of close to the one we used to calculate the k- and e-corrections. For the galaxies with a known redshift we calculate the absolute magnitude without using the spectroscopically measured redshift but instead assume an absolute magnitude of -22.9 and through that we find a redshift for our objects which can be compared to the spectroscopic redshift as seen in Fig. 3.17 and Fig. 3.18. We do not assume any knowledge of average redshifts for BL Lac host galaxies and use the average absolute magnitude found in this sample when calculating redshift. There does seem to be a deterioration at redshifts larger than $z \approx 0.4$. This is unlike the results that Plotkin et al. (2010) represents which only slightly deteriorate, although in the same manner of favouring lower redshift estimations, and while we do use a different method to apply k and e correction neither of those should have as large an effect as seen here. As such we conclude the difference is likely due to differences in how the fit was done and its accuracy at higher redshifts.

3.5.5   Method test

We expect the absolute magnitudes to have a roughly Gaussian distributions with an average and standard deviation of $M_R = -22.9 \pm 0.5$ based measurements by Sbarufatti et al. (2005). In our test sample we find $M_R = -22.7 \pm 0.7$, as seen in Fig. 3.19 which is slightly lower and with slightly higher dispersion than what we expected but still statistically the same as Sbarufatti et al. (2005). We believe this is due to the difference in method between what we and Sbarufatti et al. (2005) do and since Plotkin et al. (2010) do not quote their absolute magnitude statistics we cannot directly compare our method to theirs. Note also that the difference between our results and those of Sbarufatti et al. (2005) are statistically insigni-ficant and we do also retrieve a Gaussian shape where a Shapiro-Wilk test to check for the similarity between our data and a Gaussian distribution yields a p-value of ≈ 0.99. Since we do not go to redshifts higher than about $z = 0.8$ in this calibration it is uncertain based on this data if this method is usable at higher redshifts and we arguably only have a good fit for $z < 0.4$.
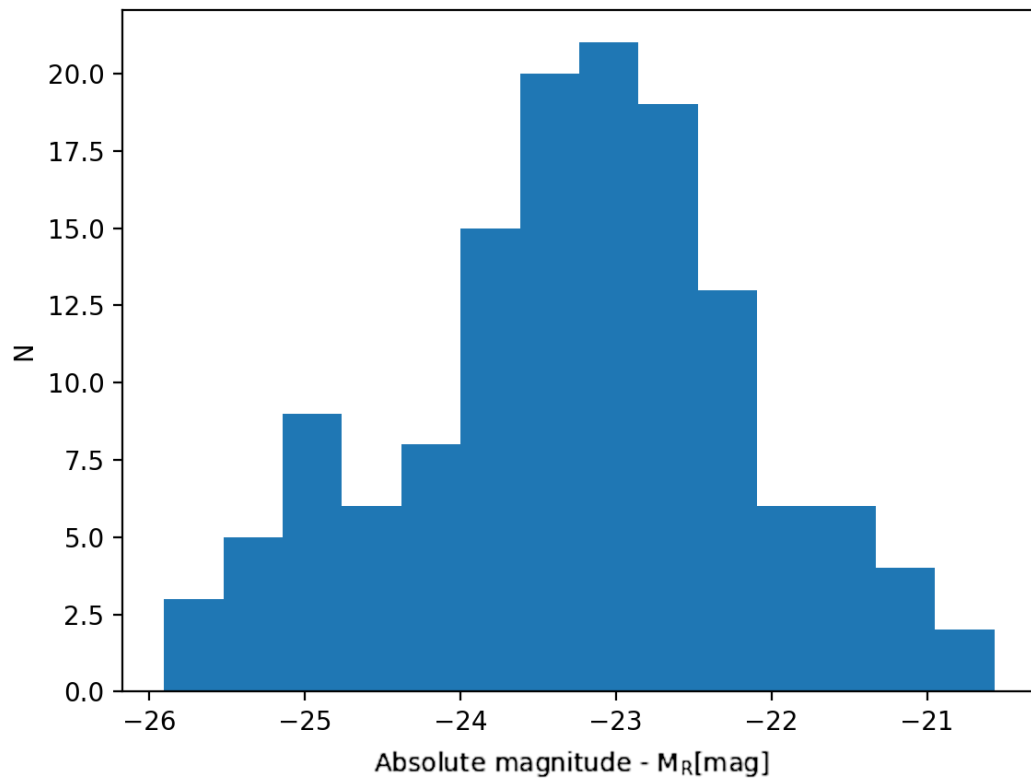
Figure 3.19: Our measured absolute magnitudes in the cousins R band, showing a Gaussian distribution. There do seem to be slightly too many objects at very bright magnitudes but the Shapiro-Wilk test provides a very high *p*-value suggesting that this is likely just a statistical coincidence.

3.6   Application to BOSS data

We apply the method to the data collected in the BOSS survey as this survey is of particular interest due to its observation of a high number of high redshift objects, including many confirmed quasars (Pâris et al. 2012; Ross et al. 2012). We apply the same method as outlined above and in doing so find 46,051 objects of which 41,835 of them have no confirmed radio or X-ray signature. Some of this might be due a lack of measurements for such signatures at the position with sufficiently sensitive surveys, but there will likely be significant number of them with neither radio nor X-ray similar to what we are seeing with the test data. Plotkin et al. (2010) does hint that there might be more of such objects at higher redshift which could contribute to explaining why we are detecting this many of them but without further radio and X-ray surveys with higher sensitivity it is hard to say anything for certain.

3.6.1   Magnitude measurement

Approximately 22% of objects show no significant signs of a host galaxy due to the large distances we are working with. For the remainder we measure their magnitude and compare that to typical value of the average we found in our test sample of $M_R = -22.7$ as seen in Fig. 3.20. For low redshifts this does seem to retrieve a close to correct measurement with some scatter similar to our results presented in section 3.5. For the higher redshift above $z = 0.4$ the scatter is slightly higher and the objects seem to be brighter than the data that Plotkin et al. (2010) presented which is likely due to a selection bias in the BOSS targeting that favours bright objects, although this does not have a large effect at low redshift. The scatter at large redshifts is likely due to a couple of factors both based on radio loudness as well as completeness limits. We will discuss why we are seeing this in the discussion Section 3.7.3.

In upper plot of Fig. 3.20 we have plotted the absolute magnitudes of the host galaxies before k- and e-corrections. We have not applied those corrections to this plot since the e-correction based on our SSP is inaccurate at redshifts $z > 1.5$, as we explain in the discussion (3.7.3). The radio loud objects in the BOSS data have an absolute magnitude of
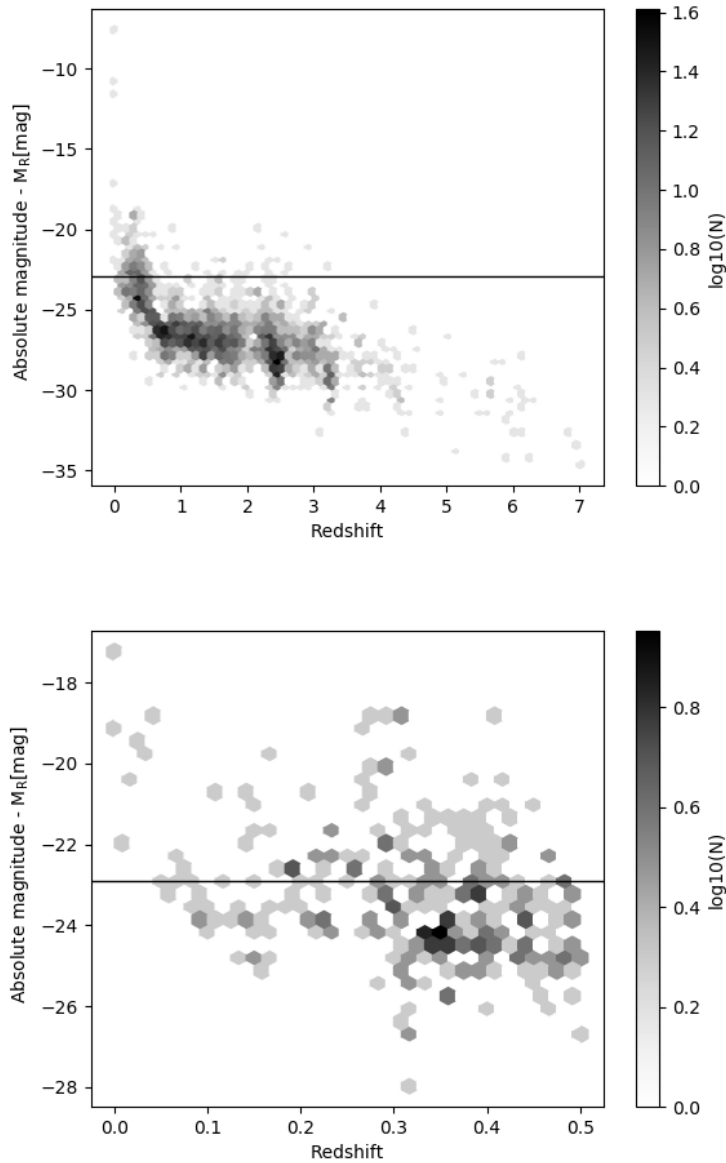
Figure 3.20: The BL Lac candidates we have found in BOSS using our method. The horizontal line in both the figures represents the typical BL Lac value of -22.9. The top figure is over the entire redshift range for our radio-loud objects. We see a clear drop in M_R at around $z = 0.4$ which is likely due to selection bias in the BOSS that favours brighter objects Ahn et al. (2012). We also see a trend towards brighter objects at higher redshifts due to incompleteness as it is difficult to observe dim objects at high redshift. The bottom figure is a zoom in on the $z < 0.5$ part of the top figure. Here our sample resembles a typical reported BL Lac sample, although slightly brighter.
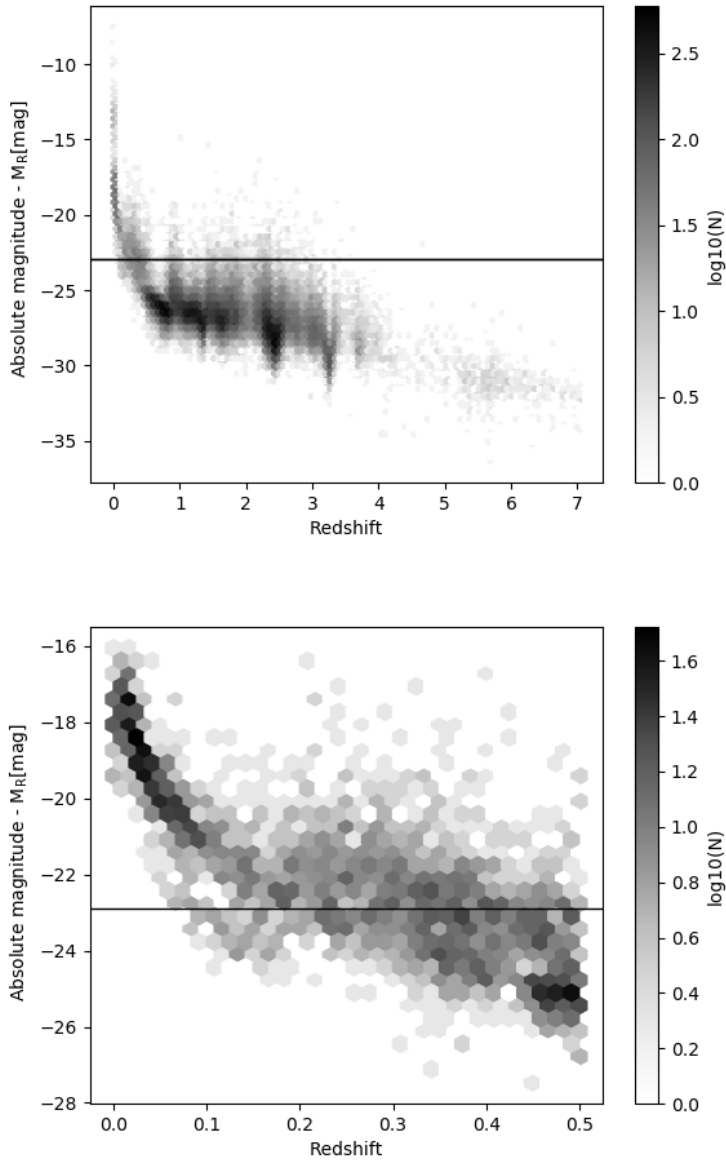
Figure 3.21: The figures are the same as figures from Fig 3.20 but for the radio-quiet sample. The horizontal line in both the figures represents the typical BL Lac value of -22.9. This samples both contain far more objects than the radio loud sample and the tail end towards dimmer objects at very low redshift is very obvious here. This is likely due to these objects not being true BL Lacs but rather false positives.

$M_R = -23.0 \pm 0.9$, consistent with the frequently used $M_R = -22.9 \pm 0.5$. It should however be noted that the BL Lacs we have found with X-ray or radio signatures seem to be brighter by $\smile$ 0.6 magnitudes on average compared to the objects for which we have found no X-ray or radio signatures. We have plotted both the samples in Fig. 3.20 as can be clearly seen there are a significant amount of objects without X-ray or radio signatures towards dimmer magnitudes although there still seem to be a large concentration slightly below $M_R = -22.6$ magnitudes further calling in to question the true nature of radio and X-ray quiet BL Lac possibly hinting at them being another type of object rather than a rare type of BL Lac.

3.7   Results and discussion

We find a large number of new BL Lac candidates by relying primarily on optical data with radio confirmation and create a fully automated system for picking them out. Based on comparison between redshift data and our own distance measurements there are fewer than 5 false positives however these could also be abnormal BL Lacs. That being said the dispersion in absolute magnitudes for BL Lac host galaxies is not due to measurement errors but rather due to those galaxies being different from each other even in the radio loud population, which according to our test data is the most well behaved sample, having an average absolute magnitude of about $M_R = -23.0$. This means that while we are seeing BL Lacs at higher redshift, measurements of single objects cannot be used to measure distance at high redshift due to completeness issues and these objects likely being significantly different at those redshifts.

3.7.1   Observational statistics

Similar to our non BOSS data we also do a Shapiro-Wilk test for our BOSS data as an extra check that they are behaving like BL Lacs and forming a Gaussian distribution for their absolute magnitudes in the cousins R band. Based on this test our X-ray or radio loud population (shown in Fig. 3.22) has a p-value of ≈ 0.15 which is well above the normally used p-value of 0.05 indicating that it is likely a Gaussian distribution in line with what other research has found. This indicates that our population is unlikely to be noise and is not
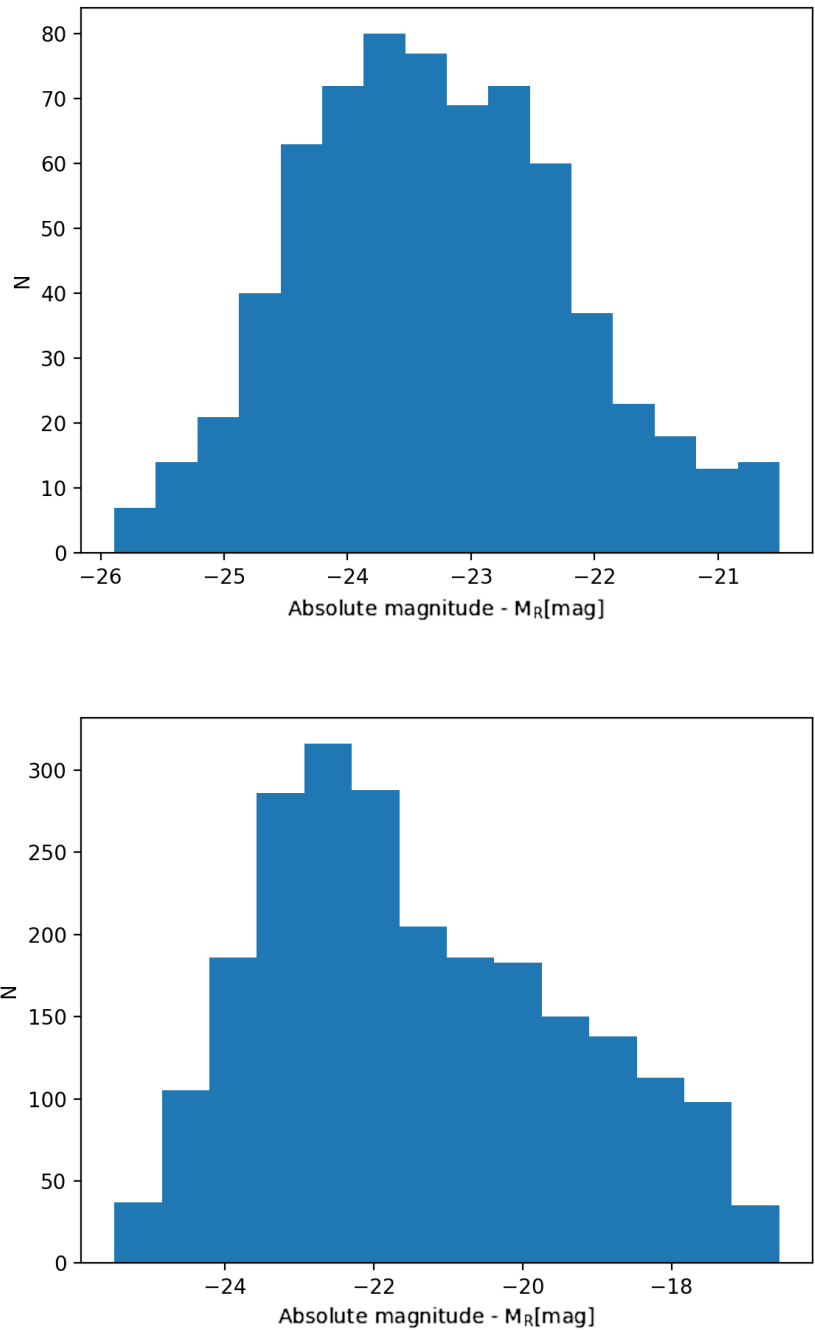
Figure 3.22: Histograms showing the absolute magnitudes in the cousins R band of each of our samples for $z < 0.4$ where we can be confident there is no bias. Top figure represents the radio loud sample and is shapes fairly similarly to a Gaussian distribution with a p-value of 0.99. Bottom figure represents the radio quiet sample and is shaped like a Gaussian but has a tail towards dimmer objects causing a smaller p-value of 0.98 for the Shapiro-Wilk test.

dominated by false positives.

For the radio quiet population we see an average magnitude of $M_R = -22.4 \pm 1.0$ which is below the average for the radio loud population, although still within 0.4σ. The Shapiro-Wilk test for this population results in a p-value of ≈ 0.05. Considering the number of objects in this sample (117,212) the p-value is likely to be lower when compared to the smaller number of objects in our radio loud sample or in our test sample and based on the shape of the distribution as seen in Fig. (3.20) a large amount of this is due to the tail end towards dimmer galaxies containing significantly more objects than we would expect. This result suggests the presence of false positives that we have not been able to remove. Based on 3.20 these objects should be fairly dim, with few or small features and no radio or X-ray emission as the data points towards that BL Lacs should always have a radio signature at some level.

We finally compare the radio quiet and the radio loud populations to each other. The Shapiro-Wilk test based on this results in a p-value of $2.7 \cdot 10^{-13}$ which clearly indicates that the two populations are not similar and likely stem from different sources. Even taking the dim tail of the radio quiet population into account does not explain this p-value and as such the differences are likely due to physical differences between the populations. The radio quiet objects could be similar to BL Lacs or another stage of them that current models do not predict well. They are likely to still be some type of galaxy with an active nucleus as it does seem there is significant radiation coming from them but the host galaxies are significantly dimmer and the nucleus is radio quiet, both of which are not normally seen in BL Lacs.

It is likely that at least a few objects has been classified as radio loud while being radio quiet objects due to incorrect association in the MORX catalogue. This number is unlikely to be statistically significant enough to change our results but a cleaner association might yield even more clear evidence that the two populations are different objects. According to MORX about 77% of our objects have 90% or better likelihood of being correctly associated, with 93% of our objects have a likelihood of above 70% as seen in Fig. 3.23. These likelihoods are based on the density of optical objects in the area of the radio source and distance to the radio source from the optical objects as explained in Flesch (2016). While those numbers are not optimal, if we restrict our radio loud sample to only include objects with above 90% likelihood
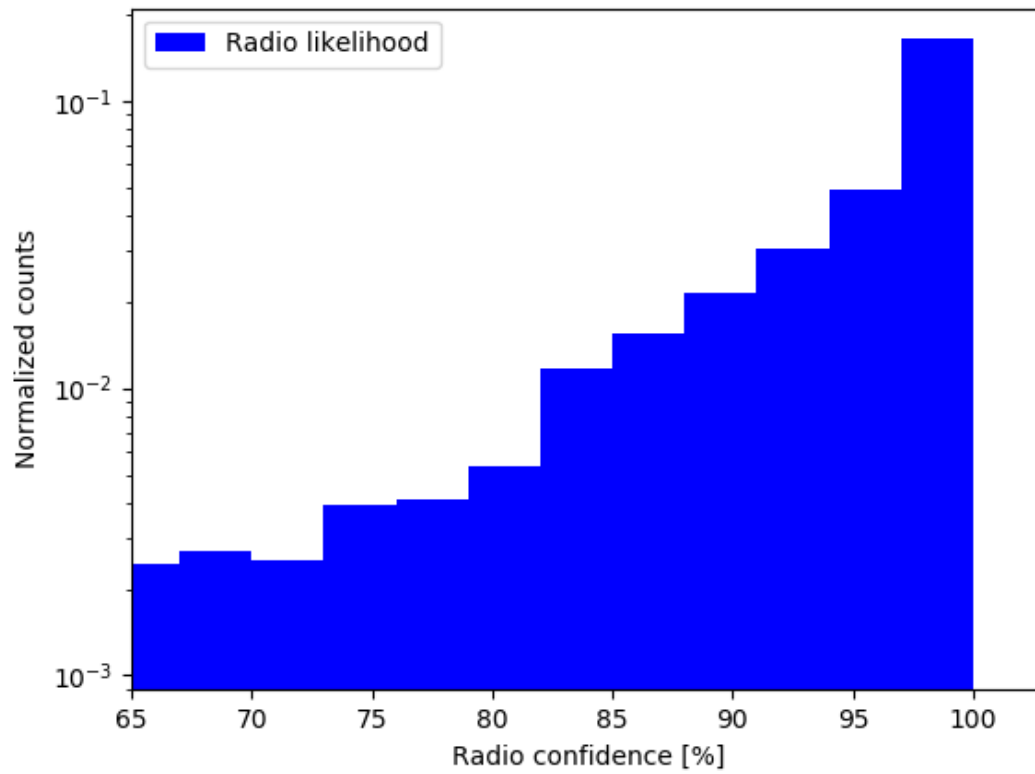
Figure 3.23: Histogram showing the spread of likelihoods of our radio associations. They begin rising at about 80% with 77% of the objects lying above 9% confidence.
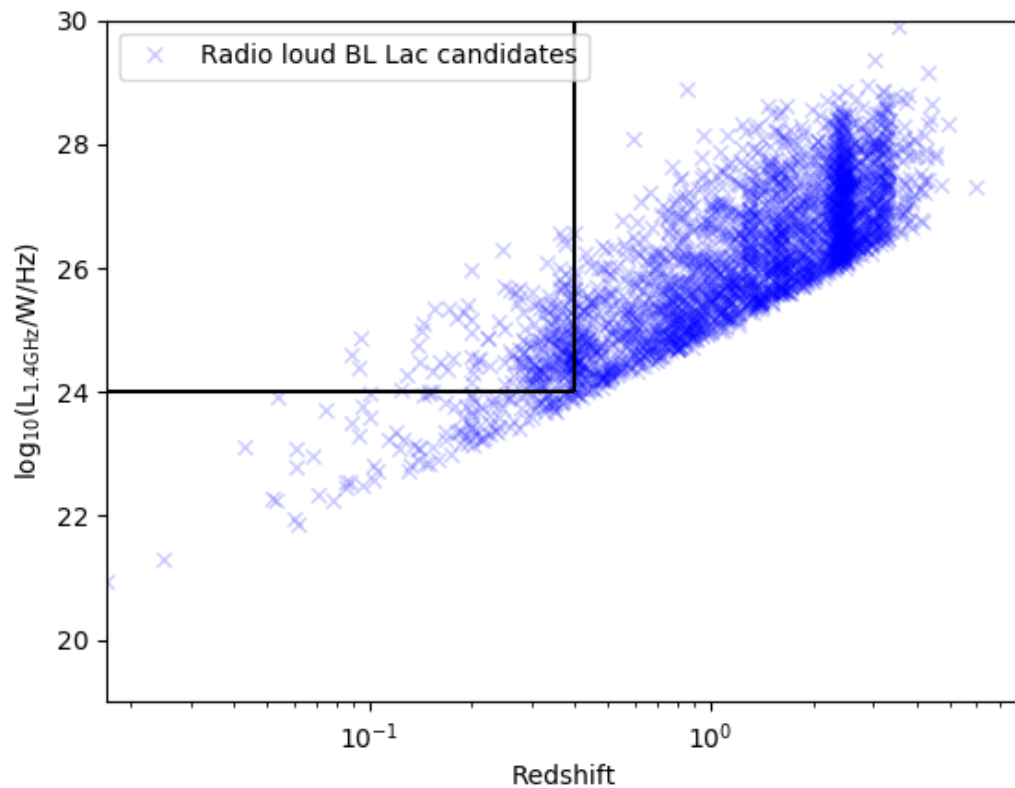
Figure 3.24: Graph of radio luminosities against redshift where we have added transparancy to the points for a better visualization of densities of points. The data shows a very clear Malmquist bias. We have marked the objects we use to test if this affects our results in any way in the top left corner. The lines are drawn at z=0.4 and luminosity = 10^{24}W/Hz.

but this does not change the mean or the standard deviation of the results significantly.

Another source of bias could come from completeness of our radio sources. We have plotted our radio sources against redshift in Fig. 3.24 where we clearly see a Malmquist bias. If we correct for completeness of radio sources due to Malmquist bias by using only radio sources below $z < 0.4$ and peak luminosities above 10^{24}W/Hz we see a magnitude change of about 0.1 down to a magnitude of -22.9 as well as a slight increase in standard deviation which suggests that including objects with low radio luminosity does not affect the results in a major way.

3.7.2   Observational limits from BOSS data

While some parts of the method are not applicable at higher redshift ranges due to us not looking at near infra red data we still try to measure these objects. We also do not detect the host galaxies in about 8.8% of objects below $z = 1$ due to the host galaxy being dim relative to the nucleus. We do not detect many BL Lacs at high redshift unless their absolute magnitudes are well beyond the average and it will be hard to work statistically on high redshift BL Lacs until we have detailed simulations that are in agreement with observations for comparison with our results.

Another limit of our method comes from the e-correction which we derive based on a SSP which is likely a good approximation up to about $z \approx 1.5$ but beyond this our specific model predicts a large change in the correction as it gets closer to the initial time of the SSP. This could be slightly mitigated by choosing an older SSP but it would still have the same problem at a higher redshift and would likely not be fitting the lower end as well. We also expect to see some false positives at high redshift due to difficulty in detecting weak lines which would have been detected at lower redshift, but would have caused the object to fail our test had they been detected.

3.7.3   Statistically based limitations

We see a sudden shift downwards at about $z \sim 0.4$ as seen in Fig. 3.20. This is likely due to selection bias in the BOSS survey where they have followed up in interesting objects discovered by previous surveys but due to how their targets were selected there is a an increased amount of bright objects starting from $z \sim 0.4$. The distance to the objects catches slightly up to this bias causing for a somewhat constant, although very noisy, average magnitude until $z \sim 1.3$ above which completeness becomes an issue despite BOSS selecting for bright objects.

We also see an increase in objects where we do not detect any flux from the host galaxy at $z > 1.0$. This increase is a factor of ~ 5 between relative number of such objects above and below $z = 1.0$. This increase does have an effect statistically as $\sim 45\%$ of objects $z > 1.0$ has no detected host galaxy flux contribution whereas it is only $\sim 8.8\%$ of objects below that redshift. As we mention above this effect is likely a completeness issue, mainly resulting from the host galaxies having a very faint apparent magnitude.

3.8   Conclusions

Based on our results we have created a fully automated method to select BL Lacs from the large samples of data and have succeeded at confirming previously found BL Lacs as well as a set of new BL Lac objects in the BOSS survey. While we do detect several BL Lac at higher redshifts BOSS target selection makes it difficult to say much about them with confidence due to completeness issues although we do find some noteworthy BL Lacs whose host galaxies have extremely high magnitude and while a k+e correction could correct for it, it is unlikely that such corrections can account for all of it. While we observe increasingly more high magnitude host galaxies at higher redshift it is hard to say anything for certain since BOSS target selection already skews the results at around $z = 0.4$ resulting in a completeness limit for this paper of $z = 0.4$. The results, however, indicate that the limit for the method could potentially be much higher in the future when better data has been obtained. We also test for differences in radio quiet and radio loud objects and find that the populations we have found

are likely too different to be the same type of object thus hinting at previously observed 'radio quiet BL Lac' to actually be another object altogether.

Acknowledgements

---

[2] http://www.astropy.org

Astronomy ([Astropy Collaboration et al., 2013](), [2018]())

This research has made use of the VizieR catalogue access tool, CDS, Strasbourg, France ([Ochsenbein]() ([1996]())). The original description of the VizieR service was published in 2000, A& AS 143, 23

The research uses the NVSS and FIRST radio surveys, carried out using the National Radio Astronomy Observatory Very Large Array: NRAO is operated by Associated Universities Inc., under co-operative agreement with the National Science Foundation

4. Comparisons of the two methods

It is common sense to take a method and try it. If it fails, admit it frankly and try another. But above all, try something.

– Franklin D. Roosevelt, *Oglethorpe University Commencement Address (1932)*

4.1 Prologue

Numerous methods of distance measurement have been developed and refined with many of them either relying on each other or using each other as tests to check for reliability of calibration and training. The following chapter is comparison of the methods presented in this thesis as well as a method developed by an independent astronomer using Bayesian probability and photometric data to calculate the redshifts of galaxies. By doing this we hope to get insight into the reliability and accuracy of the methods presented in the thesis and show an example of how they can be used in the grander scheme to further research of other methods. This chapter has not been published. We will consider incorporating some of this in to a publication with the prior chapter, or as an RNAAS note.

4.2 Introduction

The cosmological distance ladder is one of the most fundamental tools in modern astronomy. On account of this work is continuously being done to improve our understanding of every step of the distance ladder since later steps of it depend directly on previous steps. In recent years the distance ladder has however become somewhat of a 'distance tree' where several different distance measurements can be based on the same previous step and lead of into even more different measurements. This is largely the result of different measurements being optimal in specific situations even at the same redshift range. In this work we will be comparing two different branches of this distance tree as a check to see if they give approximately the same result. One of the branches is based on star formation rate while the other is produced

based on the total luminosity of a certain subtype of galaxies, namely galaxies containing BL Lacertae (BL Lac) objects.

As shown in chapter 2 star formation rate can be directly related to distance through measuring the main and quenched sequence of galaxies. These sequences have been observed at a wide range of redshifts (e.g., Guzmán et al. 1997; Bell et al. 2005; Reddy et al. 2006; Salim et al. 2007; Daddi et al. 2007; Noeske et al. 2007b; Elbaz et al. 2007; Rodighiero et al. 2011; Wuyts et al. 2011; Salmi et al. 2012; Whitaker et al. 2012; Guo et al. 2013; Guo et al. 2015; Pannella et al. 2015; amongst others) and has received attention by simulators in recent years (e.g., Sparre et al. 2016; Obreja et al. 2014; Dutton et al. 2010; Bouche et al. 2010).

Chapter 2 uses the fact that star formation rate (SFR) changes with redshift and that this change can be observed from the main and quenched sequences (Zamojski et al. 2007). It appears that this is caused by galaxies with less mass having their major star formation episodes later. This means that there are mainly low mass galaxies still in their main sequence at lower redshift as the majority of high mass galaxies have already had their major star formation episodes. While this method is not as precise as other methods on the distance ladder it is useful as a cheap way to check the distance to galaxies as it only requires photometric measurements rather than more time and money consuming spectroscopic measurements.

The other type of objects used in this work, BL Lacs, are a subtype of blazar. As mentioned in chapter 3 host galaxies of BL Lacs are typically red ellipticals which have approximately the same luminosity (Falomo 1996; Falomo & Kotilainen 1999; Sbarufatti et al. 2005). Using this property and correcting for distance and matter between us and the BL Lac we can use the absolute magnitude to find the distance to the BL Lacs.

Considering how widely different both methods are in both application as well as requirements it therefore becomes an interesting test on both of them to compare them to each other. The main problem in this comparison lies in finding objects that satisfy both the methods limitations. While we find quite a few BL Lac objects in 3 most of these are beyond the redshift range where the method outlined in chapter 2 works. Similarly that method also requires a larger group of galaxies close to the BL Lac meaning that even among the BL Lacs in the correct redshift range we are unlikely to be able to get results for all of them.

Lastly we want to test both methods against a few independent photometric redshifts. We do this as a test to our own method partly to see if we have any biases which might be easier to see when comparing our results with photometric redshift methods than when comparing with spectroscopic redshift but also to see how well our methods hold up to other photometric redshift methods. For this purpose the main method we have chosen is a Bayesian Photometric Redshift (BPZ) estimation method described in Benítez (2000). This method compared the colours of an object to template data base and using this database tries to create a probability space of redshifts. It then weights this probability space against the maximum likelihood redshift obtained by direct comparison with its training set templates thus creating a Bayesian redshift estimation (see Benítez (2000) for a more in depth explanation). Since the BPZ method is difficult to use for directly comparing the SFR method we also use Tully-Fisher Relaelation for a comparison for that method (see Tully et al. 1975).

In section 4.3 we will be going over the data sets used for both methods and describe which parts we use for what; in section 4.4 we will give a description of both the methods used; in section 4.5 we will present our results based on the comparison between the methods as well as a comparison with an independent method for measuring photometric redshifts; finally in section 4.6 we will discuss and evaluate these results.

4.3   Data

Since we are comparing two different methods which uses different types of data we will in this work use several different catalogues with some just being older versions than the others. Here we will summarize what data is used and what it is used for but for a full explanation see chapter 2 and chapter 3.

4.3.1   Star formation data

To obtain a general relationship between redshift and the SFR-$M_\star$ plane we make use of the Sloan Digital Sky Survey (SDSS) data release 8 (DR8), as it is the latest available data release in which masses and SFR have been calculated homogeneously (Brinchmann et al. 2004 and Kauffmann et al. 2004). For this data we require that it is complete in the star formation rate

limit as well as the stellar mass limit to ensure that we are not getting biased results.

The sample of clusters used in this work is selected from the X-Ray Clusters Database. We only use clusters with luminosity $L_X > 0.3 \times 10^{44}$erg/s and with redshift smaller than $z = 0.20$. Additionally we use Base de Données Amas de Galaxies X (BAX) to identify the rough X-ray centre of the galaxy cluster centre and therefore the corresponding galaxies in SDSS DR8 that are potentially part of the cluster.

4.3.2   BL Lac data

To find BL Lacs we search 3 different data sets. The MPA-JHU Brinchmann et al. (2004) [1] catalogue for SDSS data release 8 (DR8) is used to test data flagged as galaxies while spectra flagged as stars in SDSS data release 12 (DR12) is used. We use different data releases since we want to do a sanity test against Plotkin et al. (2010) which is the original method that 3 follows. To follow up on this sanity check we finally include some objects from SDSS DR 15 which positionally and redshift wise match Plotkin et al. (2010) to test if our initial selection did not include them or because they were not grandfathered properly from SDSS DR7 which Plotkin et al. (2010) uses.

We also make use of the Million Optical/Radio/X-Ray Associations Catalog (MORX, Flesch 2016) when comparing our optically selected objects with radio and X-ray detections. This catalogue is assembled from 8 different catalogues and contains a total of 1,176,782 objects where each objects has been matched to a nearby radio source. Since BL Lac objects are likely to have associated radio sources we use these as an additional test for our BL Lac candidates as done in chapter 3. Following chapter 3 we also check SDSS DR15 BOSS data to check for any BL Lac objects to use for the comparison. All the objects used are reported in chapter 3.

4.3.3   Bayesian Photometric Redshifts

We use SDSS DR15 to get the apparent magnitudes of each of the objects identified as a BL Lac object. This data is used in a Bayesian Photometric Redshift which works independently

---

[1]https://www.sdss.org/dr12/spectro/galaxy_mpajhu/

from the other two methods. We use DR15 to get the newest data available and therefore hopefully the best results.

4.3.4   Tully-Fisher distances

For Tully-Fisher distances we use an already existing catalogue of Tully-Fisher distances. We use Sorce et al. (2014) which relies on data from Cosmicflows (see Tully & Courtois 2012) to measure the Tully-Fisher relation of 1935 galaxies. Of these galaxies we find 5 of them that are close to the center of one of the analysed clusters presented in chapter 2.

4.4   Method

Since the two methods we are comparing are not made to measure distance at the same redshift region we first start by searching for BL Lacs and then testing if there is a well observed cluster near one of those BL Lacs as well as if the cluster has enough members to do a full test by applying the same limits as in chapter 2. We use the method outlined in Diaferio (1999) to identify if galaxies and substructures are part of the clusters. In total we find 47 clusters that have enough galaxies to use in the method outlined in chapter 2 and that overlaps with clusters where a BL Lac has been found as discussed in below. Let us first go over each of the methods to understand what we do to achieve this.

4.4.1   Ridge detection

Following the method outlined in chapter 2, hereafter referred to as the 'SFR method', we start by finding an inclination of the star forming and quenched ridges in the SFR-$M_\star$ plane. This is done to improve accuracy of later steps and to keep measurements of the ridge SFR consistent. After this we follow chapter 2 and fit the ridges for each of our target objects. We expect these regions to contain most of the objects and thus use the highest density of galaxies as an initial guess which happens to be close to the correct guess for most clusters. The rest of the galaxies are generally located in the "green valley" between the star forming and the quenched ridge. These galaxies are likely in transition from being star forming to being quenched. We follow chapter 2 and fit densities in a line perpendicular to the ridges. Since

the main features of such lines of densities will be ridges and these ridges will approximately form Gaussian curves we can safely assume that the largest Gaussian we can fit to the density line is going to be one of the ridges and that the second largest is either going to be noise or the other ridge. By removing all the Gaussian fits that are in the noise we end up with a series of Gaussians indicating the center of ridge along the line perpendicular to the ridge. We can then correlate that point along the line to a point in the SFR-$M_\star$ plane and by repeating this method for several different lines we end up with a string of points indicating the ridge in the SFR-$M_\star$ plane. For most of our clusters this method finds several points for both of the ridges.

Once we have found these points we fit with to a standardized line as described in chapter 2 to get a measurement of the ridge SFR. These measurements are then compared to a list of measurements of redshift bins. These bins are effectively taking a small band of redshift (e.g. z=0.105 to z=0.110) and getting a similar measurement for those. Since these bins contain more galaxies than an individual cluster will those measurements will be more precise and can be directly correlated to redshift. By then comparing our results from clusters to these redshift bins we get a measurement of redshift for the cluster.

4.4.2   BL Lac detections

Similarly to the method outlined in chapter 3 we start by searching for BL Lacs. This is done by checking for features in the spectra of the objects we have included in our data. We closely follow the steps taken in chapter 3 with the sole exception being that we also require the objects to be close to, or part of, a galaxy cluster large enough that the method outlined in chapter 2 can be used to get an indirect redshift measurement as well. This method first tests the potential BL Lac object for high enough magnitude that the rest of the measurements can be made while not just being drowned in noise. After this it tests the classification of the object automatically passing it on if it has not been identified well and testing objects which have been identified but possibly misidentified due to SDSS not testing specifically for BL Lac objects in their pipeline. After this their spectrum is tested for any features such as the D4000 line, various emission lines as well as absorption of the Hδ line. Finally the objects

are tested for radio and X-ray signals. In 3 the radio loud objects are better behaved with some of the radio quiet objects having considerably different magnitudes and we therefore do not include them in this chapter as they will in general not make a very good comparison.

To then get a measure of redshift they have to find the absolute magnitude of the galaxy. These host galaxies should have an absolute magnitude of $M_R \approx -22.9 \pm 0.5$ based on measurements of other host galaxies of BL Lac objects (see Sbarufatti et al. 2005). This is done by separating the flux contributions from the nucleus and the host galaxy and then keeping the host galaxy part for further measurement. Since the nucleus is much easier to create a model of compared to the nucleus we do this by just creating a rough estimate of the host galaxy contribution and a much better estimate of the nucleus. We then subtract the nucleus flux from the entire spectrum and assume that the remainder is the flux of the host galaxy. While this is unlikely to create precise measurement it is good enough for measuring the host galaxy flux since the upper and lower bounds for the absolute magnitudes of these galaxies are not too tight. Now that we are left with the apparent magnitude of host galaxy we need to make several corrections to account for extinction as well as the distance to the object. We do this by using the method outlined in Bruzual & Charlot (2003) where we assume that an SSP can be a good approximation since the host galaxies in general are old, red, giant ellipticals. By then using the code presented in Bruzual & Charlot (2003) we get a k and e correction to our apparent magnitudes. These corrections are needed to correct for the redshifting of the spectra since we want to measure on the rest frame spectra in the case of k correction while the e correction corrects for the natural evolution of the galaxies they experience over time due to increasing amounts of metals and evolving stellar compositions.

4.4.3   Bayesian Photometric Redshifts

Lastly we use a code based on the BPZ method (see Benítez (2000); Benítez et al. (2004); as well as https://www.stsci.edu/ dcoe/BPZ/). While we do obtain and run the code ourselves we use a code which has already been trained on a training set as presented in Benítez (2000) and Benítez et al. (2004). This means that it has trained on a database which is not related

to our data more than coincidental overlap which it then creates its probability distribution based on. The database is build on template spectra from Coleman et al. (1980), Kinney et al. (1996) and two single stellar populations from Bruzual & Charlot (2003) as shown in Fig. 4.1 and Fig. 4.2.

The BPZ code uses, as its name suggests, Bayesian likelihood to estimate a redshift. As shown in Benítez (2000) Bayesian redshift estimation compares favourably to maximum likelihood estimations which are calculated by taking the apparent magnitudes of the object provided to it and then finding the best match with a single template and redshift. Instead the code we use also takes into account the likelihood of finding a given type of galaxy at a given redshift with the magnitude provided to create a prior. This probability can be written down as

$$p(z \mid C, m_0, I) = \frac{p(z \mid m_0, I)p(C \mid z)}{p(C)}$$

where C are the colour magnitudes, m_0 is the apparent magnitude of the object, z is redshift, I is the prior information meaning that $p(z \mid C, m_0, I)$ is the total probability of any given redshift, $p(z \mid m_0, I)$ is the prior, $p(C \mid z)$ is the likelihood of the observed colours magnitudes at a given redshift and $p(C)$ is a normalization factor. Note here that without the $p(z \mid C, m_0, I)$ term this equation becomes equal to the maximum likelihood method. Let us illustrate this with an example.

If the colour magnitudes would point to a spiral galaxy at a redshift of $z = 3$ which is contrary to our prior that says this is an extremely unlikely, but not impossible, redshift to find a spiral galaxy at then the method weights this result very poorly, but not impossible, based on that prior. If however the estimate would suggest a lower redshift of $z = 0.2$ for the spiral galaxy then the prior would not interfere with that and might even weight it higher than other redshift and morphology estimates since the prior shows that this is a likely redshift for a spiral galaxy to be located at. In the case of the code we are using the prior is formulated as

$$n(z, m_0, T) \propto \frac{dV(z)}{dz}\phi_T(m_0) \tag{4.1}$$

where $V(z)$ is the comoving volume as a function of redshift, which itself depends on Ω_0, Λ_0 and H_0, and ϕ_T is the Schechter luminosity function (see Schechter 1976) for each of the
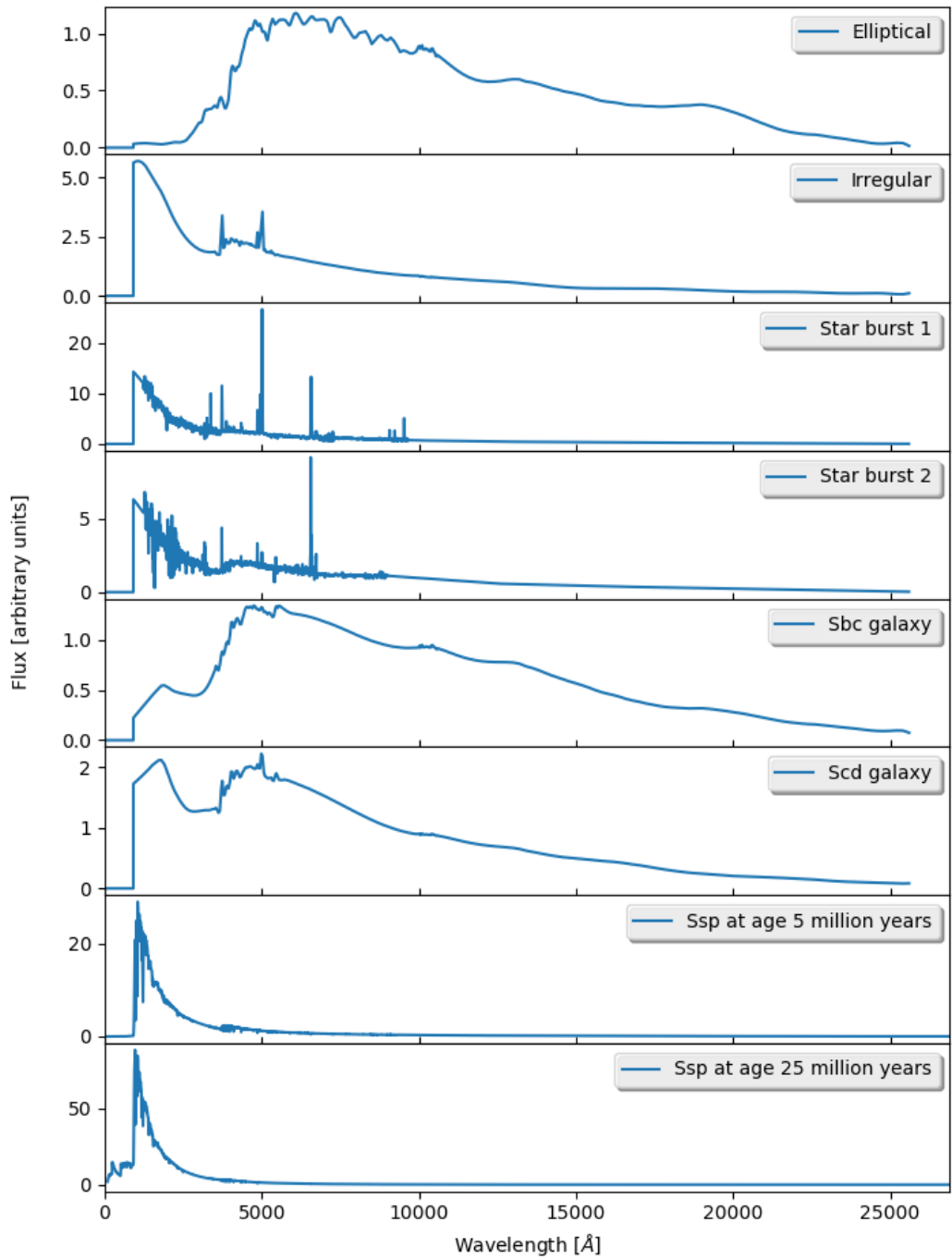
Figure 4.1: The 8 different template spectra used by the BPZ code. These are transformed based on estimated redshift and used to calculate the likelihood of a given spectra to be at a given redshift
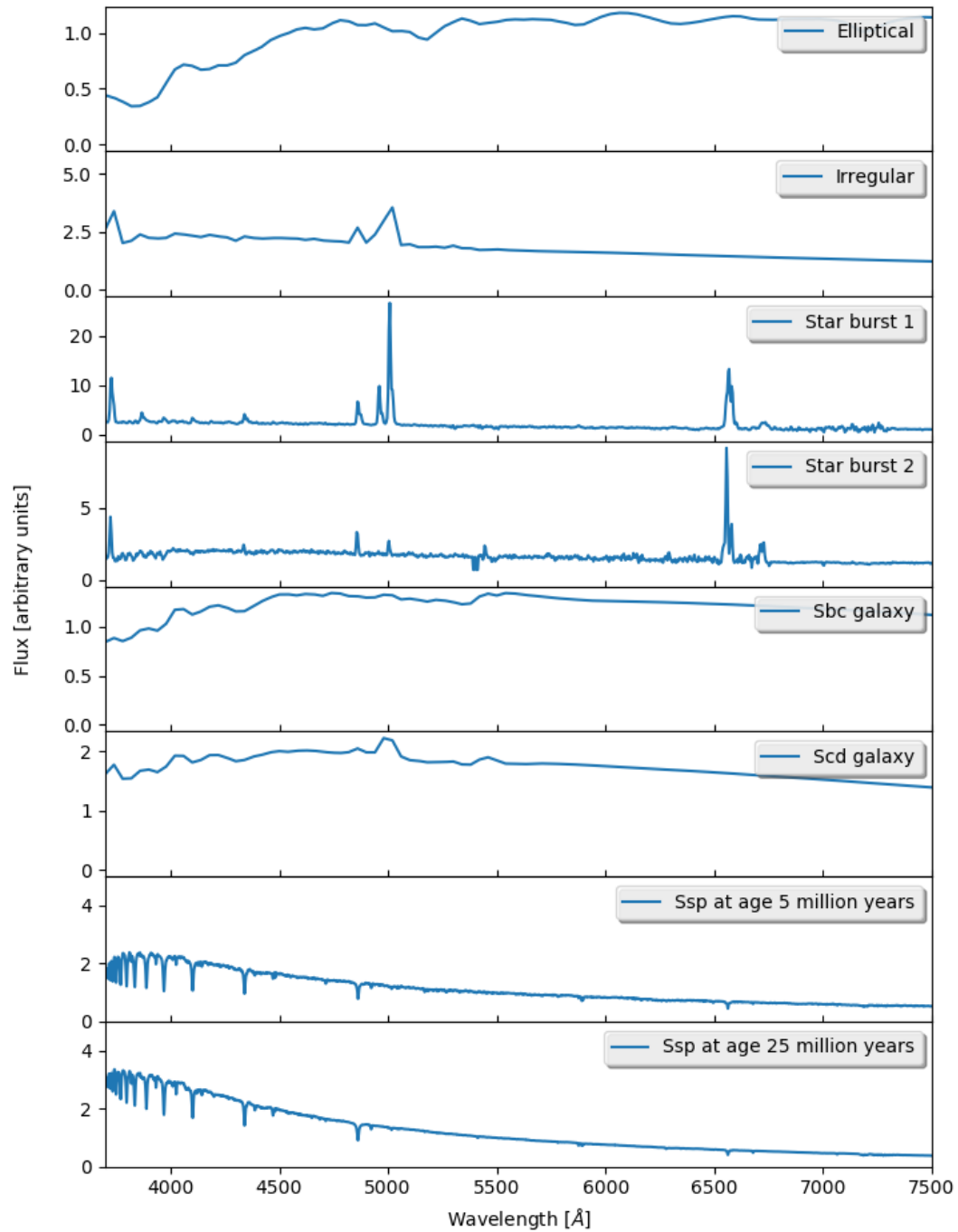
Figure 4.2: Zoom in on the optical part of the template spectra used by the BPZ code and presented in Fig. 4.1

morphological types of the templates used and can be written as

$$\phi(M) = 0.4\ln(10)\phi^\star(10^{0.4(M^\star-M)})^{\alpha+1}exp(-10^{0.4(M^\star-M)}). \qquad (4.2)$$

where $\phi^\star$ is the normalization density, M is the absolute magnitude, $M^\star$ is the characteristic absolute magnitude and α is the power law slope at low luminosity. Note here that the function the BPZ code uses has been transformed to use apparent magnitude, m_0, instead of absolute magnitude, M. Since Schechter's function depends on $M_\star$, the normalization density, ϕ^*, and the power law slope at low luminosity, α, as well as k and e corrections to transform the function to use apparent magnitude the code's prior depends on 8 different values which have been chosen from a large multicolour sample as described in Benítez (2000).

Besides the obvious difference of an existing prior this method has one more key difference compared to a maximum likelihood method. This lies in the fact that while we do not consider scenarios where the given galaxy is a mix between different types we do consider all types of galaxies and in cases where two different morphologies estimate roughly the same redshift that redshift has increased likelihood of being chosen compared to maximum likelihood that simply takes a single combination of redshift and morphological type.

By doing so for each galaxy template and multiplying the probabilities from these priors and the likelihood of the match with the data provided given the templates at each redshift we can then find several likelihood curves for each of the templates. We can then select most likely one as our result or several different results if there are several redshifts that are almost equally probable. While this approach gives the same results as a maximum likelihood approach if the prior is a flat line (i.e. it does not give preference to any redshift for any of the templates) it can give better results than a simple maximum likelihood method as Benítez (2000) shows which is why we use it.

We use purely SDSS data (which means SDSS magnitudes and therefore the SDSS $ugriz$ filters for the BPZ code, see Fig. 4.3) for a better comparison with the results from the other methods that also purely rely on SDSS, although less filters (that uses data transformed to estimate the Cousins R filter in the case of BL Lacs). The code then compares the magnitudes we have provided it with its database data and calculates a maximum likelihood redshift. This means that it finds a best fit for a redshift and a single template which it uses to compare with

a Bayesian method where all the templates are given a likelihood and a corresponding set of probable redshifts for each of those templates. Combining these two estimates then provides us with a total redshift estimate.

4.4.4   Tully-Fisher

The Tully-Fisher relation was first presented in Tully et al. (1975) and has since become a widely used method for finding the distance to an object independent of its redshift. The relation is a mass to light relation which has been empirically discovered by observing galaxies and measuring their flux and mass independently where the mass can be measured as either total mass or baryonic mass (Tully et al. 1975; Glowacki et al. (2020)). A common method of calculating the mass of a galaxy is by measuring its rotational speed since this should be directly related to its gravitational pull and therefore its mass. Once this is done we can easily measure its apparent flux and compare that to the flux a galaxy of the measured mass should have. As mentioned above there is no purely theoretical method of correlating the mass and its flux but by comparison with other galaxies for which we already know the flux through some other means and using those as a guideline we can get a relation between the two quantities.

4.5   Results

For the direct comparison between the BL Lac and SFR methods we find a total of 47 BL Lac objects near galaxy clusters within $z < 0.4$. Unfortunately most of these clusters are small and upon further testing have to be rejected as the method outlined in chapter 2 cannot be used on them even with lower requirements for the number of member galaxies. Once the tests are then done and objects with excessively large uncertainty have been removed we find 4 objects that can be measured using both methods (see Fig. 4.4). Two of the 4 objects are at lower redshift than what the SFR method has been calibrated to handle and as such we have evaluated the calibration based on the previous results and there being no shifts at this lower redshift. While it certainly is interesting that these results somewhat line up it is hardly a striking result due to the errors on both methods.
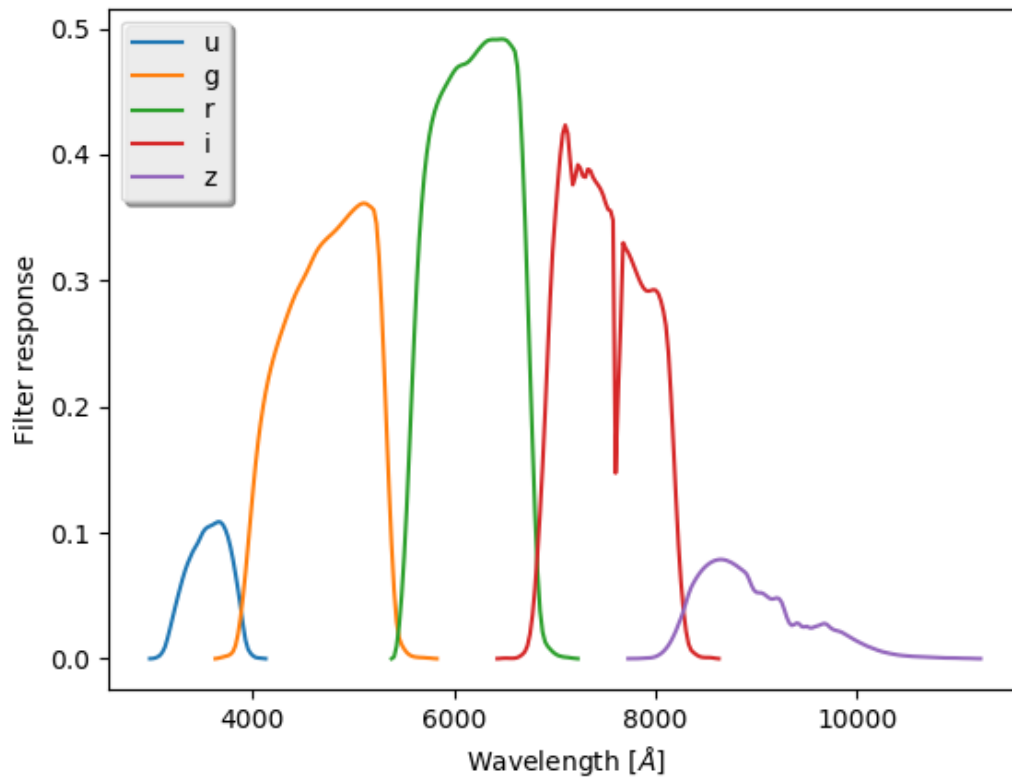
Figure 4.3: Filter response curves from each of the SDSS filters. These are the filters the code uses to compare its corrected templates to the magnitudes we use as input.
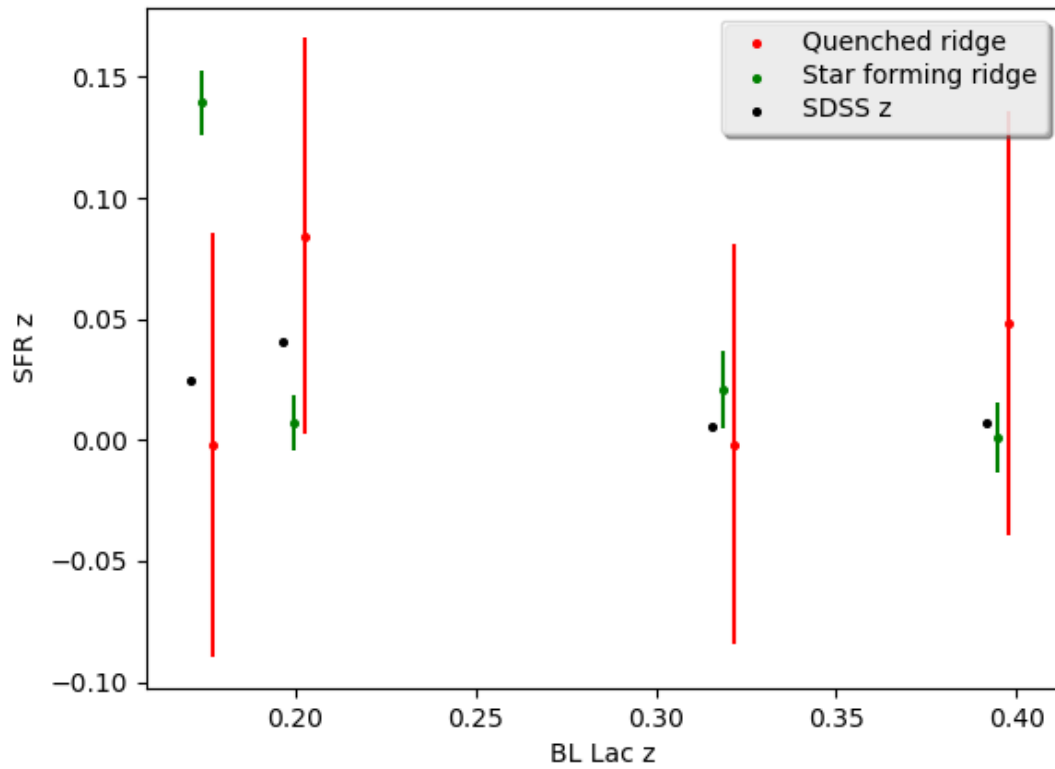
Figure 4.4: Comparison of the redshifts found using the two methods presented in chapter 2 and chapter 3. BL Lac redshift measurements have been offset for clarity. We have marked the redshifts obtained by each ridge separately as well as the redshift given by SDSS. While the SDSS redshift generally agrees with the one obtained by the SFR method, especially if we use the rather large error bars, we see that the BL Lac methods generally overestimates the redshift by a considerable amount.

4.5.1   Comparison with Bayesian Photometric Redshifts

Since we only find 4 objects that can be used for comparison between the other methods it is perhaps prudent to turn to BPZ in an attempt to get a better base for comparison. While the SFR method could be used here it makes for a poor subject to test BPZ against. This is due to it being less precise than the BL Lac method and because the SFR method looks at galaxy clusters compared to the single objects which the BL Lac and BPZ methods use. We therefore turn to look at the BL Lac method compared to the BPZ method. Since the BL Lac method is based primarily on SDSS data we are able to retrieve 5 magnitude filters, namely u,g,r,i,z, for each object that has been identified as a BL Lac. Using this we can get two independent measurements of photometric redshift which we have presented in Fig 4.5 and Fig. 4.6.

While the BPZ method gets more accurate at higher redshifts with less dispersion and a better median value for its difference between its estimate and the spectroscopic redshift the BL Lac method has an about constant level of dispersion starting out better than the BPZ method but becomes worse at above $z > 0.2$ as can be seen in Fig. 4.7. Another quite notable thing is that while the BPZ, on average, overestimates the redshift in each of the bins the BL Lac method does not systematically favour either higher or lower redshift in every bin even if it does underestimate redshifts on average when taking the complete sample.

4.5.2   Comparison with Tully-Fisher

Since the Tully-Fisher relation relies on spiral galaxies we do not expect there to be many, if any, opportunities for a direct comparison with the BL Lac method. However since the SFR method uses clusters of galaxies it is very likely that at least a couple of those galaxies will be spiral galaxies and have a measured distance using the Tully-Fisher method. By using the data from Sorce et al. (2014) we end up with 5 matches between the SFR method and their data which have been obtained using the Tully-Fisher method. As can be seen in Fig. 4.8 it is very clear that the Tully-Fisher method performs far better for these objects. This is however somewhat to be expected since the SFR method generally overestimates the redshift for clusters in this range by a large margin and then having a very large dispersion since clusters this close generally are messier and since it is generally harder for the method that
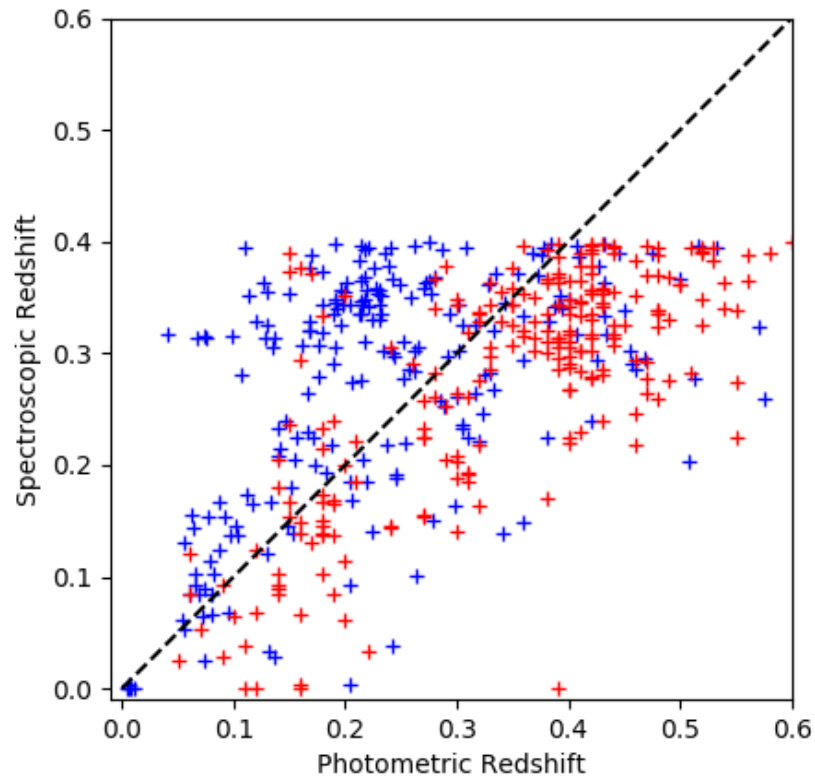
Figure 4.5: The redshifts of both the BPZ method (red crosses) and the BL Lac method (blue crosses) against the spectroscopic redshifts of each object. The dashed line represents 1 to 1. There are several very high photometric redshift blue crosses from the BL Lac method that have not been included here to make the graph easier to read. While the BL Lac method clearly seems to favour smaller redshifts the BPZ method seems to favour slightly higher redshifts even if it is slightly more accurate.
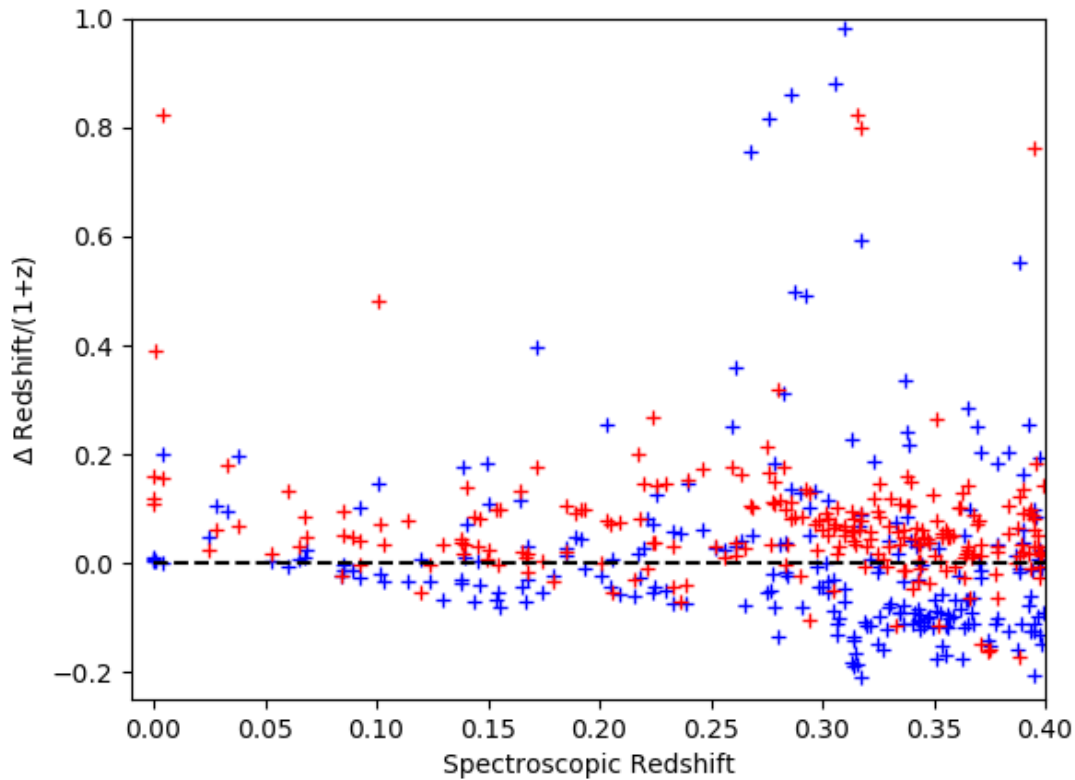
Figure 4.6: The difference from spectroscopic redshift per z for each of the methods. BPZ method is marked in red crosses while BL Lac method is marked in blue crosses. The dashed line represents 0 deviation. The BL Lac method has an about constant percentile deviation from the spectroscopic results while the BPZ method seems to get more accurate at higher redshifts. Some points at lower redshift are not represented in this plot to make it more readable.
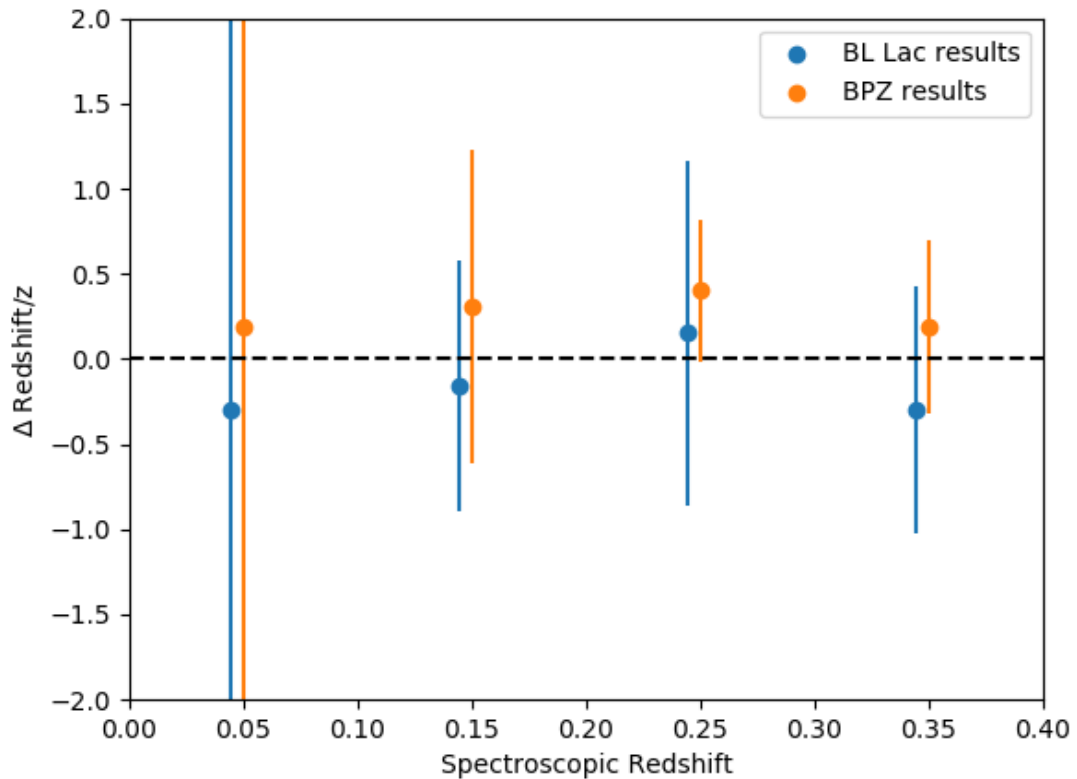
Figure 4.7: The statistics for each redshift bin with a width of $z = 0.1$. BPZ results are in orange while BL Lac results are in blue and the dashed line represent 0. The errorbars for BL Lac results have been moved slightly to lower redshift for readability. The first bin has extremely large error bars for both methods due to a few measurements at very low redshift having an extremely large value when looking at $\Delta z/z$. Looking at the other redshift bins we see that the BL Lac method sticks slightly closer to 0 for the second and third bin and its standard deviation does not get better or worse with distance. On the other hand the BPZ method does have less standard deviation in its results at higher redshifts.
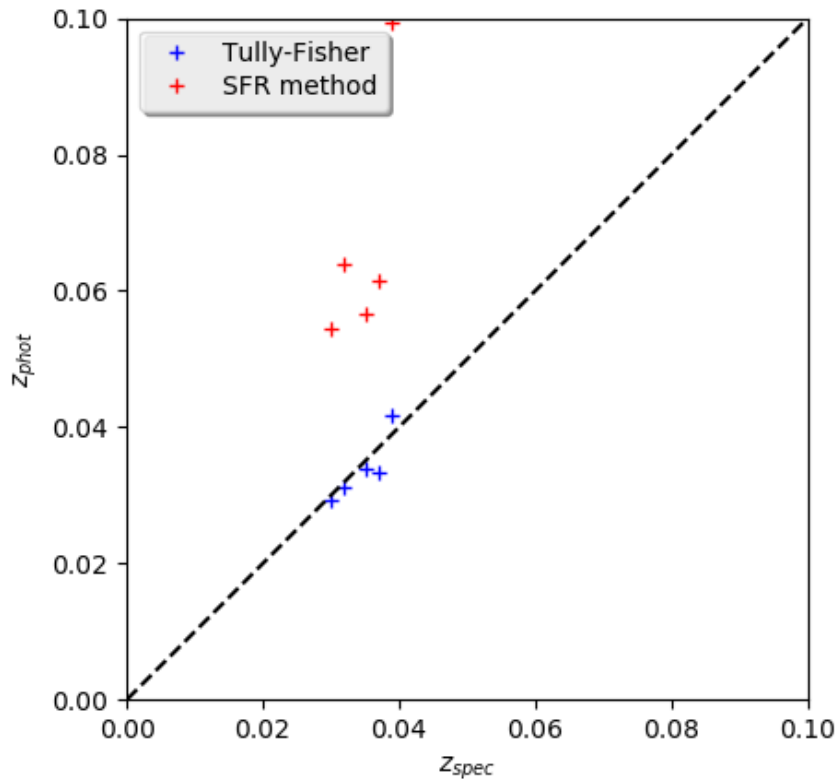
Figure 4.8: Plot of the 5 matches between the Tully-Fisher method and the SFR method. The dashed line represents 1 to 1. The SFR method clearly overestimates the distances by a lot, sometimes up to nearly double the value, while the Tully-Fisher method is much more precise. The main reason for this discrepancy is likely the redshift range of the objects used since the SFR method performs poorly here. Note that the spectroscopic redshift used here is taken from SDSS DR12.

picks out cluster members to be accurate at this distance. The clusters are also sparse to the point of being on the limit of this method being possible to use.

4.6   Discussion

We have made a comparison between the methods and while the SFR and BL Lac methods are not very accurate we do get results that fit within the uncertainty between the two methods. There clearly appears to be a systematic preference to higher redshift from the BL Lac method and as such star formation rates does not seem to be a valid calibration method for BL Lac objects. This is very likely due to the method of subtracting the AGN from the host galaxy not working very well at these low redshifts and where especially the aperture correction is unlikely to hold up. Overall this likely means that the difference in optimal redshift region between these two methods are too large, making the SFR method a poor choice for calibrating BL Lac measurements even if given better larger, higher quality amount of data unless that results in the limits of the methods being extended considerably.

The comparison with the BPZ results, however, show a much more interesting picture. Here we see that the BL Lac method holds up quite well in comparison. While we do see better results for the BPZ method at redshifts near $z = 0.4$ we also see better results for the BL Lac method at lower redshifts. While the BPZ method certainly would perform better with an increased number of filters and data available, the BL Lac method reaches its results through just using a single filter from which it gets its results. While it is rare that we would see photometric surveys with only single filters it is still worth mentioning this stark difference of data requirement.

Besides usability we also see an interesting systematic trend for both methods. The BPZ method favours overestimating redshifts while the BL Lac method underestimates them. For the BL Lac method this is echoing the results we discuss in chapter 3 where we find that the radio loud sample in general has a higher estimated absolute magnitude than the -22.9 often quoted in literature but despite this the measurements are sufficiently close to the actual redshift that in the redshift bin between $0.2 < z < 0.3$ we see an overestimation on average.

The reason for the BPZ method systematically favouring an overestimation is unclear but is likely due to the training set spanning far further than the redshift of $z < 0.4$ that we use the method for here. This means that it has likely sacrificed some precision at lower redshifts to attain better results at higher redshift which is then causing this systematic trend.

In all the BPZ and BL Lac methods are comparable in the redshift range we are looking at here. It should however be noted that the BPZ can certainly be more precise with more filter data added for each of the objects. This would however require multiple surveys as we are already using all the filters from the SDSS survey and more than 5 filters are not typically seen in catalogues based on single surveys. Compared to that the BL Lac method can be used based on line a single filter magnitude once the object has been identified as a BL Lac. It is in cases like these were we can clearly see the need for multiple methods of distance measuring as they each have their upsides and use cases.

Regarding the Tully-Fisher to SFR comparison we see a clear advantage from the Tully-Fisher method where it is clearly performing better at the redshift range we are comparing. Despite this difference in performance in the given distance interval it is however important to note that when comparing with the distance ladder the SFR method is a secondary method while the Tully-fisher is a tertiary method making the SFR less dependent on other results once it has been properly calibrated for these distances. It is also important to note that the Tully-Fisher method requires a measured spectra for the object in question while the SFR method has other requirements but can easily work on photometric data alone. Furthermore Sorce et al. (2014) and other Tully-Fisher catalogues generally do not go much beyond redshifts of $z = 0.06$ (see Theureau et al. 2007; Springob et al. 2007; Hong et al. 2019) which is unfortunately closer than where the SFR method is at its most precise between $z = 0.07$ and $z = 0.09$.

As a final comment we want to note that we tried to make a comparison between the BL Lac Lac method and type Ia supernovae measurements. To do this we used The Asiago Supernova Catalogue (see Barbon et al. 1999); The Open Supernova Catalog (see Guillochon et al. 2017; https://sne.space); Sternberg Astronomical Institute catalog of supernovae (see Tsvetkov et al. 2004) as well as A unified supernova catalogue (see Lennarz et al. 2012) but are unable to find

a match between any of our radio loud BL Lac objects and a supernovae presented in these catalogues. While there certainly is an overlap between several of these catalogues due to some of them being a compilation of several catalogues The Open Supernova Catalog alone has metadata for 67,618 supernovae which likely means that matches between our BL Lac objects and supernovae either do not exist or have not been used in enough research to the point where it would have become part of one of these catalogues.

In all we find that the BL Lac measurements perform quite well compared to other methods while the SFR method performs poorly, especially at the redshifts where we can compare with the Tully-Fisher method. Despite this we still believe there is some merit to the SFR method as it performs better at other redshifts. In all both methods have their own niche at which they perform well making them both useful enough that further optimization and appliance to new data will be useful.

Acknowledgements

---

[2]http://www.astropy.org

5. Conclusions and Possible Future Directions

Reach for the Moon, immortal smoke

– Jun'ya Ōta "ZUN", *Imperishable Night (2004)*

5.1 Prologue

This chapter goes through the results presented in this thesis. We also touch on some of the future directions continued research could take. Most of these require either more data or surveys going deeper than what has been available during the time the research was made. We also take the results as far as is possible and measure the Hubble constant. Although the result for this constant is very inaccurate it is theoretically possible to get a good prediction of the Hubble constant and as such the error on this result can be used as a measure of how close we are to having perfect data for the methods. For this measurement we have to assume that we have measured BL Lac host galaxy magnitudes using an H_0 independent method and that host galaxies are passively evolving as outlined in 3.2. Both of these assumptions are discussed in 3.

5.2 Summary

The goal of this thesis has been to discover and test methods to measure the distance of various objects. We have done so mainly through using optical data with a few additional tests in radio and X-ray. By testing out these methods we have made discoveries pertaining to how star formation in galaxies evolve as well raised some questions about the true nature of 'radio quiet BL Lacs' besides the main goals of better understanding of the limits of the methods and what they can be used for. More specifically the results presented in this thesis have been:

- Presentation of a new method to measure the distance to galaxy clusters by using only photometric data thus making it faster and more cost efficient compared to spectroscopic

133

methods and determination of a natural limit of about redshift $z < 0.2$ due to sparse observation of galaxies in given clusters.

- A relation between redshift and SFR in both the quenched ridge and the star forming ridge.

- Discovery of more than 4,000 BL Lac candidates in the BOSS catalogue as well as distance measurement to those within a redshift of $z < 0.4$ as BOSS data selection has completeness issues for BL Lacs beyond this point.

- A difference in host galaxy magnitude between 'radio quiet BL Lacs' and radio loud BL Lac that is consistent at all redshifts measurable using BOSS data.

Each of these points has added new knowledge to our understanding of the Universe or presents new methods making it possible to save costs on future observations and expand the possible uses of data that has already been made. The first two points are based on the work presented in chapter 2 where the first point presents a new method which has the potential to be cost and telescope time saving as it presents a method to get distances to objects observed only with photometry even if those distances are not as accurate as redshift is. While relations between SFR and redshift have been measured before they are typically only for small ranges of redshift and have never before been used for finding distance to galaxy clusters making it possible to include this as another step for determining accuracy of simulated models of galaxy clusters. The second point refers to the tightening of SFR measurements of the quenched and star forming ridges. While this has been measured before those measurements are typically only for a smaller range of redshifts and uses methods based on the shape of the ridges compared to our method that measures density slices of the ridges to determine a central point of the ridge.

The last two points are based on the results from chapter 3. The first of those points refer to the main goal of the chapter in searching for new BL Lac objects in the BOSS catalogue. Here we find more than 4,000 objects which have all the characteristics of what we classify as BL Lac objects. We also find more than 40,000 objects which satisfy all the optical characteristics but lack a radio signature. These objects have been noted by several previous authors but are

typically found in much smaller numbers and lack any general statistical analysis due to this. This leads us to the last point where we compare the radio loud and radio quiet objects and find that the radio quiet objects differ significantly from the radio loud objects when looked at as a whole rather than individually. They have about the same amount of dispersion but the host galaxy of the radio quiet objects have a somewhat lower absolute magnitude which is the key feature when using BL Lacs to measure distance.

We compare both the methods to each other but also to an independent method presented by Benítez et al. (2004). This is done to test our method for accuracy as well as any bias towards lower or higher results. Since our methods are limited to redshifts of $z < 0.4$ this is the area we test against and here we see no no significant bias towards any direction other than what we already knew from looking at our tests individually. As such throughout the thesis we have presented new methods of measuring distances to astronomical objects and therefore laid a base to measure, what is perhaps the most important constant in the question of distances, the Hubble constant.

5.3   Future observations

As with many other fields in astronomy our methods are mainly limited by observations. As such future observations either in the form of new surveys or telescopes are likely to improve upon the results presented in this thesis. For the method presented in chapter 2 the sparseness of observed galaxies in clusters further away than redshifts of $z > 0.2$ means that our method for using ridges to measure distances is limited to that redshift limit of $z < 0.2$. Similarly the method in chapter 3 is limited by the completeness of the BOSS survey and its observed AGN at redshift $z > 0.4$ does not seem to be complete. The improvement of the completeness of radio surveys and how well we can link radio sources to visible light sources is also likely to have an impact. Furthermore we expect the general redshift estimates of BL Lac objects to improve when we begin doing large scale surveys with high angular resolution on host galaxies to a degree such that the light from the nuclei can be excluded. This is unlikely to be in the immediate future making our approach of subtracting an estimated nuclei flux from the total flux a useful approach until such surveys are conducted. Given better surveys it seems

likely that the BL Lac method should be able to be used out to redshifts of $z < 3$ before k and e correction becomes a problem. For the rest of this section we will be going through some of the key surveys that are likely to improve on our results and how they are going to do so.

5.3.1 Legacy Survey of Space and Time

Future surveys such as the Legacy Survey of Space and Time (LSST, see Ivezić et al. 2019) promises data for 20 billion galaxies to a magnitude limit in the r band of $r \approx 27.5$ (compared to the SDSS survey which has a magnitude limit of $r \approx 22.2$). This survey will take use of the Vera C. Rubin Observatory which will start observing in October 2021 and be fully operational in October 2022. This telescope has a mirror 8.4 meters (6.5 meters effective) in diameter and a focal length of 10.31 meters which will feed its 3200 megapixel camera which will provide 20 terabytes of data every night. It will be using six filters (*ugrizy*) to observe wavelengths between 320 and 1050 nm.

LSST is very likely to provide many new targets for future observations, some of which will likely be BL Lacs and as such will indirectly improve on our BL Lac method but perhaps more interesting is the implications for the SFR method. By naively assuming that $m - M = 5\log(d_L/\text{Mpc}) + 25$ this change would mean a difference between the method working out to redshift $z < 0.2$ and to it now being usable out to redshifts of $z = 1.4$. Of course this large of a difference is unlikely due to the different types of corrections needed to be applied at larger redshifts such as k-corrections as well galaxy clusters being significantly different at these redshifts. Never the less there should be a significant increase in the limit of the method and especially given that LSST is purely photometric this gives the method a very good testing ground for providing crucial distance measurements where spectroscopic measurements are not made. Surveys such as LSST also showcase a good example of why it is important to be able to measure distance through photometric data only as it aims to repeatedly cover large areas of the sky and as such do not make any spectroscopic measurements making it impossible to directly measure redshifts of the observed objects. The depth that LSST might bring us could also potentially answer interesting questions regarding the development of the ridges in galaxy clusters at higher redshifts as well as giving

us insight on key questions such as the morphology of the ridges for a large number of clusters.

5.3.2   Euclid

Surveys such as the Euclid survey (Laureijs et al. 2011) promise to measure galaxy nuclei out to redshifts of $z = 2$ using the Euclid space telescope. This telescope has a diameter of 1.2 meters and a focal length of 24.5 meters which it will be using to observe in wavelengths between 550 and 2000 nm which it expects to start doing in July 2022. As such this might take us part of the way although there is still a long way to get completeness of galaxy nuclei all the way out to the apparent limit of $z = 3$. Even though it is unlikely that Euclid or any other survey in the immediate future is unlikely to provide completeness to this limit they do still give us more data to work with to analyse the difference in radio quiet and radio loud BL Lac objects.

Similarly since Euclid is expected to cover 400 square degrees every month it is very likely to provide us with better data on a large range of different galaxies as well as data on several new galaxies which have not been found currently due to being too dim. As such Euclid is also likely to provide better data on galaxies in galaxy clusters and observe them well enough to provide more test cases for the SFR method.

5.3.3   Square Kilometre Array

As we mention above a limiting factor for distinguishing BL Lacs from radio quiet BL Lac like objects is the radio flux they have. As such the various radio surveys which are currently under construction are especially important. Perhaps chief among these is the Square Kilometre Array (SKA, Johnston et al. 2007 Dewdney et al. 2009; Davidson 2012) which promises to deliver measurements in the 50 MHz to 15.3 GHz frequency range with a continuum rms of just 2 μJy at 1.4 GHz and is therefore very likely to give us a much better data on which of the BL Lac candidates are radio quiet as well as determining the compactness of the radio source of potential BL Lacs. To do so it will be using thousands of radio dishes and millions of low frequency antennas which will be situated in both South Africa and Australia which will have a total collecting area of 1 square kilometre. This will likely lead to a much clearer cut between

the radio loud and the radio quiet groups presented in chapter 3 and could give is a much better insight into what exactly these objects are. Although SKA will only begin operating in 2027 we are already seeing some results from precursors surveys like the Evolutionary Map of the Universe (EMU; Norris et al. 2011) survey which will be using the Australian Square Kilometre Array Pathfinder (ASKAP) telescope. This survey will observe 70 million objects up to redshift z 1 in the southern hemisphere at 1.3 GHz with rms 10μJy/beam. Another related survey is the LOFAR Two-metre Sky Survey (LoTSS; Shimwell et al. 2017; Shimwell et al. 2019) which uses radio telescopes spread over northern Europe and aims to observe the northern hemisphere. In preliminary images it measured 44,000 radio sources in the frequency range of 120-168 MHz with a typical noise level of <71 μJy/beam. The radio data this survey will provide, and its precursors are already providing, can also be used to measure star formation rates in galaxies. This means that a larger portion of already observed galaxies will have measured star formation rate and as such more less clusters will be discarded due to not having enough galaxy members with the required measurements.

5.3.4   Telescopes

Another factor that could potentially provide new data for this method are some of the telescopes which are currently under construction. Among these is The Maunakea Spectroscopic Explorer (MSE; see Saunders & Gillingham 2016; The MSE Science Team et al. 2019) Observatory which is designed to perform a spectroscopic survey which will provide spectra of millions of objects. This observatory has diameter of 11.25 meters and a focal length of 21.66 meters or greater and will be observing in wavelengths between 360 and 1800 nm and will be able to detect weak lines at the blue end of the spectra to a very high precision (spectral resolution of R 40,000) and will start operations in 2029. There is also the James Webb Space Telescope (JWST) which has a diameter of 6.5 meters and a focal length of 131.4 meters and is set to observe wavelengths between 600 and 28300 nm. Final design planning and construction of this telescope will begin in 2021.

Both of these telescopes are set to outperform current telescopes and especially the MSE is likely to make the search for BL Lacs easier but will also provide data on star formation

rate and masses of galaxies which are used by the SFR method. Meanwhile JWST is set to measure the infrared spectrum which makes it well suited for measuring star formation, especially in dusty galaxies where much of the visible light is blocked.

5.4   Measuring the Hubble constant

As an interesting point we would like to point to the fact that the work presented in this thesis can measure the Hubble constant even if the accuracy is not up to par of measurements such as supernovae methods (see section 1.2.5 for my quick notes on the subject as well or Grillo et al. (2018) for a newer method using supernovae) or measurements done on the CMB (see Ade et al. 2016). Measurements using observed objects usually result in Hubble constant somewhat higher than the results from the Planck satellite ($H_0 = 71.9^{+2.4}_{-3.0}$km s^{-1}Mpc^{-1} from Riess et al. (2016) compared to $H_0 = 67.74 \pm 0.46$km s^{-1}Mpc^{-1} from Ade et al. 2016). This discrepancy is an unsolved mystery in the astronomical community. It is however not one to which there are many good solutions. Some of the few prominent ones invoke early dark energy that acts mostly after matter-radiation equality but then becomes irrelevant after the recombination in order to avoid challenging what we have observed in the closer Universe (mostly $z < 2$ where we can use supernovae for measurement; Poulin et al. 2019), alternatively increased coupling and self interaction between neutrinos as well as a few new neutrino types in the early could delay the point in time where neutrinos become free streaming which then leads to a higher Hubble constant predicted by CMB measurements (Kreisch et al. 2020), or a completely new model which is separate from the ΛCDM model. Although these theories can technically explain the difference all of them have their own set of difficulties either due to our current understanding of particle physics or simply lacking observational evidence which might even be impossible to obtain by using contemporary methods. For a more complete discussion on this see Verde et al. (2019). While only mentioned briefly in Verde et al. (2019) the results could also be explained by systematic errors. However due to the difference in results it is unlikely that a single source of systematic error could result in current observations and as such it is likely that we need several sources of systematic errors (see Bernal & Peacock 2018). While we do not expect to be able to present a resolution to this difference it is still

an interesting result to check if we agree with either of the measurements and furthermore our methods could likely add to the discussion, especially if data from the future surveys described above are applied to them.

Similar to what we did in chapter 3 we will be splitting the groups of BL Lacs into radio loud and radio silent groups. This is done since the groups are distinct enough that there is some possibility that they are likely to be different types objects since they do not a have a similar absolute magnitude for their host galaxies. We will also be using the commonly cited absolute magnitude value of -22.9 for the host galaxy magnitude (Sbarufatti et al. 2005). This value comes from Sbarufatti et al. (2005), which as we mention in 3.2, is not an H_0 independent method. The reason we still use his value is that there are currently no commonly accepted measurements of BL Lac host galaxies that are H_0 independent and as we mention in the in the same section (3.2) there are possible ways to measure the absolute magnitude of the host galaxy in an H_0 independent manner.

Since we find that the radio loud population has a slightly higher (lower value) magnitude we can easily surmise that the resultant Hubble constant should be slightly higher. Similarly since the radio quiet objects generally have somewhat lower absolute magnitude we expect the resultant Hubble constant to be somewhat lower.

By fitting the absolute R magnitude of each population separately to a value of -22.9 we can set the Hubble constant as a free variable. In this case the formula is

$$M = m + 5 - 5\log_{10}(D_L(z)/\text{Mpc}). \tag{5.1}$$

Where M is the absolute R magnitude which we set to -22.9 in accordance with other literature, m is the apparent magnitude we have measured and D_L is the luminosity distance. By doing this we get a value for the Hubble constant of 75.5 ± 2.6 km/s/Mpc based on 181 objects which, as expected, is slightly higher than the value obtained from using supernovae but still very much within standard deviation of the results (see figure 5.1 for the absolute magnitudes of each of the objects calculated using this Hubble constant). It should however be noted that while this measurement is very much on line with previous results it does generates a chi-squared of 180.8 which suggests that the fit is not very good despite the low standard deviation which combined with the fact that we have not taken the error on the individual measurements

into account suggests that a more robust statistical method might produce a better result. In this case we apply a bootstrap method to data. This process involves resampling the population to achieve an equally large data set but with some repeated data points to make up for the data points that are not represented in the sub sample. In this case we chose use a completely random resampling process where any data point can appear any number of times without any weights applied based on how many times it has already appeared in the sub sample. By repeating this method more than 750,000 times we arrive at a much more likely value and error of 74.82 ± 5.37 km/s/Mpc.

When looking to the future it will be possible to us these methods to measure the Hubble constant even more precisely possibly making them part of the larger effort in the scientific community of measuring this constant to ever more precise values. This is important since the Hubble constant is one of the more fundamental values needed to understand how the Universe evolves and has evolved. Even on smaller scales the Hubble constant is incredibly important being a factor in converting redshifts to physical distances, being the basis of comparing objects observed close to us to those objects observed further away and as such it permeates throughout a large percentage of astronomical papers.

By going through a similar process we can in theory make measurements on the radio quiet population. In this case, however, the host galaxy magnitudes are significantly lower which is likely due to the fact that the radio quiet population are not BL Lacs. Despite the result from the radio quiet population not being useful it is still interesting that the radio loud population is able to predict the Hubble constant this well by only using data where the redshift follows $z < 0.4$. Better data, as we talked about previously, will likely be a great help in narrowing this measurement down to get a better fit as well as an overall more precise measurement. Especially considering that the standard deviation on this measurement was comparable to that of the supernovae measurement it seems likely that this can be another high quality method, comparable to supernovae, for measuring the Hubble constant in the future even if this method does rely on BL Lacs which generally are hard to identify making them much less obvious candidates than supernovae.
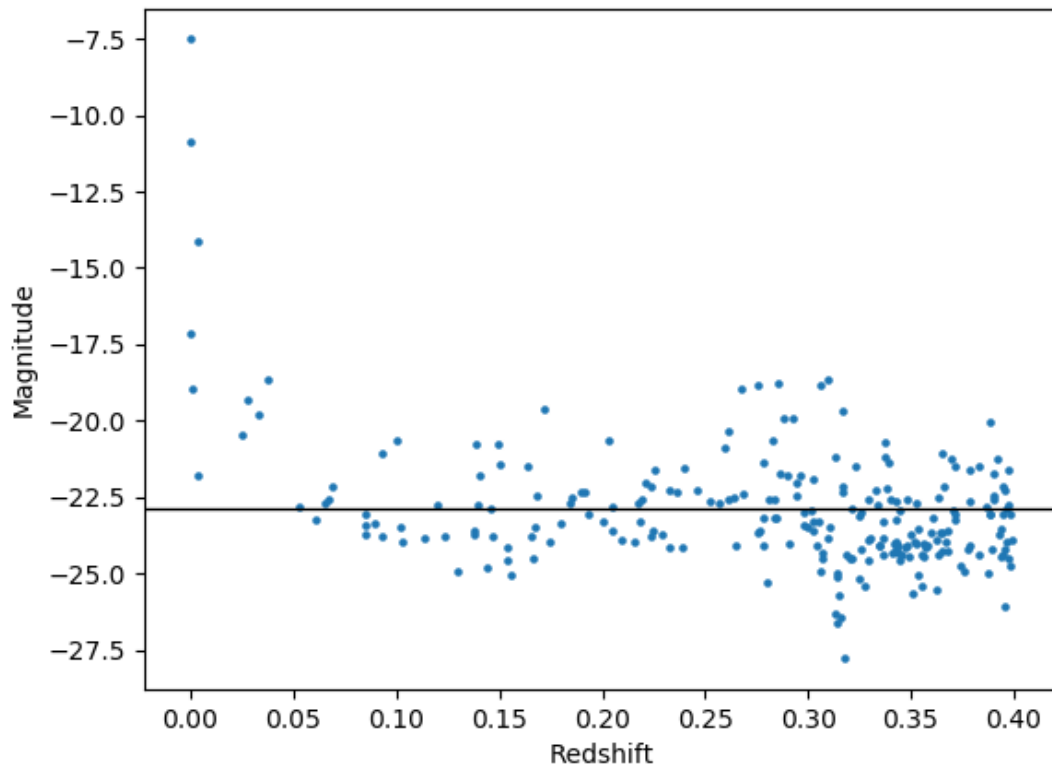
Figure 5.1: Absolute magnitudes of our radio loud sample if we assume a Hubble constant of 74.82 ± 5.37. We have included the dim objects towards low redshift for completeness sake.

Bibliography

Abazajian K., et al., 2004, The Astronomical Journal, 128, 502

Abraham R. G., McHardy I. M., Crawford C. S., 1991, Monthly Notices of the Royal Astronomical Society, 252, 482

Ade P. A. R., et al., 2014, Astronomy & Astrophysics, 571, A16

Ade P. A. R., et al., 2016, Astronomy & Astrophysics, 594, A13

Ahn C. P., et al., 2012, The Astrophysical Journal Supplement Series, 203, 21

Aird J., et al., 2010, Monthly Notices of the Royal Astronomical Society, 401, 2531

Alpher R. A., Herman R., 1948, Nature, 162, 774

Alpher R. A., Herman R., Gamow G. A., 1948, Physical Review, 74, 1198

Alpher R. A., Follin J. W., Herman R. C., 1953, Physical Review, 92, 1347

Anderson W., 1929, Zeitschrift für Physik, 56, 851

Angel J. R. P., Stockman H. S., 1980, Annual Review of Astronomy and Astrophysics, 18, 321

Antonucci R. R. J., 1984, The Astrophysical Journal, 278, 499

Antonucci R., 1993, Annual Review of Astronomy and Astrophysics, 31, 473

Antonucci R. R. J., Miller J. S., 1985, The Astrophysical Journal, 297, 621

Astropy Collaboration et al., 2013, Astronomy & Astrophysics, 558, A33

Astropy Collaboration et al., 2018, The Astronomical Journal, 156, 123

Baade W., Minkowski R., 1954, The Astrophysical Journal, 119, 206

Baade W., Zwicky F., 1934, Proceedings of the National Academy of Science, 20, 254

Bamford S. P., et al., 2009, Monthly Notices of the Royal Astronomical Society, 393, 1324

Barbon R., Buondí V., Cappellaro E., Turatto M., 1999, Astronomy & Astrophysics Supplement Series, 139, 531

Batten A. H., 1981, Journal of the Royal Astronomical Society of Canada, 75, 29

Beers T. C., Flynn K., Gebhardt K., 1990, The Astronomical Journal, 100, 32

Bell E. F., McIntosh D. H., Katz N., Weinberg M. D., 2003, The Astrophysical Journal Supplement Series, 149, 289

Bell E. F., et al., 2005, The Astrophysical Journal, 625, 23

Bellazzini M., Ferraro F. R., Pancino E., 2001, The Astrophysical Journal, 556, 635

Benítez N., 2000, The Astrophysical Journal, 536, 571

Benítez N., et al., 2004, The Astrophysical Journal Supplement Series, 150, 1

Bernal J. L., Peacock J. A., 2018, Journal of Cosmology and Astroparticle Physics, 2018, 002

Bernstein G., Jain B., 2004, The Astrophysical Journal, 600, 17

Bessel F. W., 1838, Monthly Notices of the Royal Astronomical Society, 4, 152

Best P. N., Kauffmann G., Heckman T. M., Brinchmann J., Charlot S., Ivezić Ž., White S. D. M., 2005, Monthly Notices of the Royal Astronomical Society, 362, 25

Binney J., 1998, Galactic Astronomy. Princeton University Press, Princeton

Blandford R. D., McKee C. F., 1982, The Astrophysical Journal, 255, 419

Blandford R. D., Rees M. J., 1978, in Wolfe A. M., ed., BL Lac Objects. Pittsburgh, Pa., University of Pittsburgh, pp 328–341

Błażejowski M., Sikora M., Moderski R., Madejski G. M., 2000, The Astrophysical Journal, 545, 107

Bondi H., Gold T., 1948, Monthly Notices of the Royal Astronomical Society, 108, 252

Bongiorno A., et al., 2012, Monthly Notices of the Royal Astronomical Society, 427, 3103

Borra E. F., Corriveau G., 1984, The Astrophysical Journal, 276, 449

Böttcher M., 2007, Astrophysics and Space Science, 309, 95

Bouche N., et al., 2010, The Astrophysical Journal, 718, 1001

Brammer G. B., et al., 2009, The Astrophysical Journal Letters, 706, L173

Brammer G. B., et al., 2011, The Astrophysical Journal, 739, 24

Brinchmann J., Ellis R., 2000, The Astrophysical Journal, 536, L77

Brinchmann J., Charlot S., White S. D. M., Tremonti C., Kauffmann G., Heckman T., Brinkmann J., 2004, Monthly Notices of the Royal Astronomical Society, 351, 1151

Bruzual G., Charlot S., 2003, Monthly Notices of the Royal Astronomical Society, 344, 1000

Budavari T., et al., 2009, The Astrophysical Journal, 694, 1281

Bundy K., et al., 2006, The Astrophysical Journal, 651, 120

Burbidge G. R., 1961, Nature, 190, 1053

Burbidge E. M., Burbidge G. R., Prendergast. K. H., 1959, The Astrophysical Journal, 130, 26

Burbidge E. M., Lynds C. R., Burbidge G. R., 1966a, The Astrophysical Journal, 144, 447

Burbidge G. R., Burbidge M., Hoyle F., Lynds C. R., 1966b, Nature, 210, 774

Busarello G., Capaccioli M., Capozziello S., Longo G., Puddu E., 1997, Astronomy & Astrophysics, 320, 415

Campbell L. A., et al., 2014, Monthly Notices of the Royal Astronomical Society, 443, 1231

Cananzi K., Augarde R., Lequeux J., 1993, Astronomy & Astrophysics Supplement Series, 101, 599

Carlberg R. G., Yee H. K. C., Ellingson E., Abraham R., Gravel P., Morris S., Pritchet C. J., 1996, The Astrophysical Journal, 462, 32

Cerruti M., Zech A., Boisson C., Inoue S., 2015, Monthly Notices of the Royal Astronomical Society, 448, 910

Christlein D., Zabludoff A. I., 2005, The Astrophysical Journal, 621, 201

Ciesla L., Elbaz D., Fensch J., 2017, Astronomy & Astrophysics, 608, A41

Coleman G. D., Wu C. C., Weedman D. W., 1980, The Astrophysical Journal Supplement Series, 43, 393

Colless M., Jones H., Proctor R., Harrison C., Campbell L., Lah P., 2007, Proceedings of the International Astronomical Union, 3, 399

Collin-Souffrin S., 1987, Astronomy & Astrophysics, 179, 60

Collinge M. J., et al., 2005, The Astronomical Journal, 129, 2542

Compton A. H., 1923, Physical Review, 21, 483

Condon J. J., Cotton W. D., Greisen E. W., Yin Q. F., Perley R. A., Taylor G. B., Broderick J. J., 1998, The Astronomical Journal, 115, 1693

Cowie L. L., Songaila A., Hu E. M., Cohen J. G., 1996, Astronomical Journal, 112, 839

Croom S. M., Smith R. J., Boyle B. J., Shanks T., Miller L., Outram P. J., Loaring N. S., 2004, Monthly Notices of the Royal Astronomical Society, 349, 1397

Curtis H. D., 1917, Publications of the Astronomical Society of the Pacific, 29, 206

Daddi E., et al., 2007, The Astrophysical Journal, 670, 173

Davidson D. B., 2012, in International Symposium on Antennas, Propagation &; EM Theory (ISAPE), 2012 10th International Symposium. Institute of Electrical and Electronics Engineers (IEEE), pp 1279–1282

Davies L. J. M., et al., 2016, Monthly Notices of the Royal Astronomical Society, 461, 458

Davis M., et al., 2007, The Astrophysical Journal, 660, L1

Dawson K. S., et al., 2012, The Astronomical Journal, 145, 10

Delvecchio I., et al., 2014, Monthly Notices of the Royal Astronomical Society, 439, 2736

Dermer C. D., Schlickeiser R., 1993, The Astrophysical Journal, 416, 458

Dewdney P., Hall P., Schilizzi R., Lazio T., 2009, Proceedings of the IEEE, 97, 1482

Diaferio A., 1999, Monthly Notices of the Royal Astronomical Society, 309, 610

Dickinson M., Papovich C., Ferguson H. C., Budavari T., 2003, The Astrophysical Journal, 587, 25

Dressler A., 1980, The Astrophysical Journal, 236, 351

Dunlop J. S., McLure R. J., Kukula M. J., Baum S. A., O'Dea C. P., Hughes D. H., 2003, Monthly Notices of the Royal Astronomical Society, 340, 1095

Dutton A. A., van den Bosch F. C., Dekel A., 2010, Monthly Notices of the Royal Astronomical Society, 405, 1690–1710

Dye S., et al., 2008, Monthly Notices of the Royal Astronomical Society, 386, 1107

Edelson R. A., Malkan M. A., 1987, The Astrophysical Journal, 323, 516

Edge D. O., Shakeshaft J. R., McAdam W. B., Baldwin J. E., Archer S., 1959, Memoirs of the Royal Astronomical Society, 68, 37

Einstein A., 1917, Sitzungsberichte der Königlich Preußischen Akademie der Wissenschaften (Berlin), pp 142–152

Eisenstein D. J., et al., 2005, The Astrophysical Journal, 633, 560

Elbaz D., et al., 2007, Astronomy & Astrophysics, 468, 33

Elbaz D., et al., 2011, Astronomy & Astrophysics, 533, A119

Eliche-Moral M. C., Prieto M., Gallego J., Zamorano J., 2010, Astronomy & Astrophysics, 519, A55

Falomo R., 1996, Monthly Notices of the Royal Astronomical Society, 283, 241

Falomo R., Kotilainen J. K., 1999, Astronomy & Astrophysics, 352, 85

Falomo R., Urry C. M., Pesce J. E., Scarpa R., Giavalisco M., Treves A., 1997, The Astrophysical Journal, 476, 113

Falomo R., Scarpa R., Treves A., Urry C. M., 2000, The Astrophysical Journal, 542, 731

Falomo R., Pian E., Treves A., 2014, The Astronomy and Astrophysics Review, 22, 73

Fanaroff B. L., Riley J. M., 1974, Monthly Notices of the Royal Astronomical Society, 167, 31P

Farouki R., Shapiro S. L., 1980, The Astrophysical Journal, 241, 928

Feltre A., et al., 2013, Monthly Notices of the Royal Astronomical Society, 434, 2426

Ferland G. J., Netzer H., Shields G. A., 1979, The Astrophysical Journal, 232, 382

Fixsen D. J., 2009, The Astrophysical Journal, 707, 916

Flesch E. W., 2016, Publications of the Astronomical Society of Australia, 33, 052

Flores H., et al., 1999, The Astrophysical Journal, 517, 148

Fontanot F., Lucia G. D., Monaco P., Somerville R. S., Santini P., 2009, Monthly Notices of the Royal Astronomical Society, 397, 1776

Freeman K. C., 1999, in Davies J. I., Impey C., Phillipps S., eds, Astronomical Society of the Pacific Conference Series Vol. 170, The Low Surface Brightness Universe. p. 3

Friedman A., 1922, Zeitschrift für Physik, 10, 377

Frieman J. A., 2008, AIP Conference Proceedings, 1057, 87

Gaia Collaboration et al., 2017, Astronomy & Astrophysics, 605, A79

Gamow G., 1948, Nature, 162, 680

Garcia-Bellido J., 2004, arXiv e-prints, pp hep–ph/0407111

Gieren W., et al., 2005, The Messenger, 121, 23

Gilbank D. G., et al., 2011, Monthly Notices of the Royal Astronomical Society, 414, 304

Glowacki M., Elson E., Davé R., 2020, arXiv e-prints, p. arXiv:2011.08866

Grillo C., et al., 2018, The Astrophysical Journal, 860, 94

Guillochon J., Parrent J., Kelley L. Z., Margutti R., 2017, The Astrophysical Journal, 835, 64

Gunn J. E., J. Richard I. G., 1972, The Astrophysical Journal, 176, 1

Guo K., Zheng X. Z., Fu H., 2013, The Astrophysical Journal, 778, 23

Guo K., Zheng X. Z., Wang T., Fu H., 2015, The Astrophysical Journal, 808, L49

Guzmán R., Gallego J., Koo D. C., Phillips A. C., Lowenthal J. D., Faber S. M., Illingworth G. D., Vogt N. P.,
    1997, The Astrophysical Journal, 489, 559

Hamblin J. D., 2005, Science in the Early Twentieth Century. ABC-CLIO, Santa Barbara

Hazard C., Mackey M. B., Shimmins A. J., 1963, Nature, 197, 1037

Heavens A., Panter B., Jimenez R., Dunlop J., 2004, Nature, 428, 625

Heckman T. M., Ptak A., Hornschemeier A., Kauffmann G., 2005, The Astrophysical Journal, 634, 161

Heidt J., Nilsson K., Sillanpää A., Takalo L. O., Pursimo T., 1999, Astronomy & Astrophysics, 341, 683

Herschel W., 1802, Philosophical Transactions of the Royal Society of London Series I, 92, 477

Hetherington N., 1993, Cosmology : historical, literary, philosophical, religious, and scientific perspectives.
    Garland Pub, New York

Hong T., et al., 2019, Monthly Notices of the Royal Astronomical Society, 487, 2061

Hoyle F., 1948, Monthly Notices of the Royal Astronomical Society, 108, 372

Hoyle F., Fowler W. A., 1963, Monthly Notices of the Royal Astronomical Society, 125, 169

Hsieh B. C., Yee H. K. C., 2014, The Astrophysical Journal, 792, 102

Hubble E. P., 1927, in Publications of the American Astronomical Society. pp 261–264

Hubble E., 1929, Proceedings of the National Academy of Science, 15, 168

Hubble E. P., 1936, Realm of the Nebulae. Yale university press ; H. Milford, Oxford University Press, New Haven

Hubble E., Humason M. L., 1931, The Astrophysical Journal, 74, 43

Hutchings J. B., Janson T., Neff S. G., 1989, The Astrophysical Journal, 342, 660

Impey C. D., Brand P. W. J. L., 1982, Monthly Notices of the Royal Astronomical Society, 201, 849

Impey C. D., Neugebauer G., 1988, The Astronomical Journal, 95, 307

Impey C. D., Malkan M. A., Tapia S., 1989, The Astrophysical Journal, 347, 96

Inserra C., et al., 2021, Monthly Notices of the Royal Astronomical Society, 504, 2535

Ivezić Ž., et al., 2019, The Astrophysical Journal, 873, 111

Jannuzi B. T., Green R. F., French H., 1993, The Astrophysical Journal, 404, 100

Jansky K., 1932, Proceedings of the Institute of Radio Engineers, 20, 1920

Jansky K., 1933, Proceedings of the IRE, 21, 1387

Jarvis M. J., Rawlings S., Eales S., Blundell K. M., Bunker A. J., Croft S., McLure R. J., Willott C. J., 2001, Monthly Notices of the Royal Astronomical Society, 326, 1585

Johnson H. L., 1964, The Astrophysical Journal, 139, 1022

Johnston S., et al., 2007, Publications of the Astronomical Society of Australia, 24, 174

Jones D. H., et al., 2004, Monthly Notices of the Royal Astronomical Society, 355, 747

Jones D. H., et al., 2009, Monthly Notices of the Royal Astronomical Society, 399, 683

Karim A., Schinnerer E., the VLA-COSMOS collaborations C., 2011, The Astrophysical Journal, 730, 61

Kauffmann G., et al., 2003, Monthly Notices of the Royal Astronomical Society, 346, 1055

Kauffmann G., White S. D. M., Heckman T. M., Menard B., Brinchmann J., Charlot S., Tremonti C., Brinkmann J., 2004, Monthly Notices of the Royal Astronomical Society, 353, 713

Kewley L. J., Dopita M. A., Sutherland R. S., Heisler C. A., Trevena J., 2001, The Astrophysical Journal, 556, 121

Khachikian E. Y., Weedman D. W., 1974, The Astrophysical Journal, 192, 581

Kinney A. L., Calzetti D., Bohlin R. C., McQuade K., Storchi-Bergmann T., Schmitt H. R., 1996, The Astrophysical Journal, 467, 38

Kish G., 1978, A Source book in geography. Harvard University Press, Cambridge

Kohyama T., Shibai H., Fukagawa M., Hibi Y., 2010, The Astrophysical Journal, 719, 873

Kragh H., 2013, Astronomy and Geophysics, 54, 2.28

Krauss L. M., 2003, Science, 299, 65

Kreisch C. D., Cyr-Racine F.-Y., Doré O., 2020, Physical Review D, 101, 123505

Kuehr H., Witzel A., Pauliny-Toth I. I. K., Nauber U., 1981, Astronomy and Astrophysics, Supplement, 45, 367

Laing R. A., Riley J. M., Longair M. S., 1983, Monthly Notices of the Royal Astronomical Society, 204, 151

Landt H., Padovani P., Giommi P., 2002, Monthly Notices of the Royal Astronomical Society, 336, 945

Landt H., Padovani P., Perlman E. S., Giommi P., 2004, Monthly Notices of the Royal Astronomical Society, 351, 83

Lapuente P., 1997, Thermonuclear Supernovae. Springer Netherlands Imprint Springer, Dordrecht

Laureijs R., et al., 2011, arXiv e-prints, p. arXiv:1110.3193

Leavitt H. S., 1908, Annals of Harvard College Observatory, 60, 87

Lemaître G., 1927, Annales de la Société Scientifique de Bruxelles, 47, 49

Lemaître A. G., 1931, Monthly Notices of the Royal Astronomical Society, 91, 483

Lennarz D., Altmann D., Wiebusch C., 2012, Astronomy & Astrophysics, 538, A120

Lindholmer M. O., Pimbblet K. A., 2019, Astronomy & Astrophysics, 629, A7

Londish D., et al., 2002, Monthly Notices of the Royal Astronomical Society, 334, 941

Londish D., et al., 2007, Monthly Notices of the Royal Astronomical Society, 374, 556

Lovelock D., 1971, Journal of Mathematical Physics, 12, 498

Low F. J., Johnson H. L., 1965, The Astrophysical Journal, 141, 336

Lynden-Bell D., 1969, Nature, 223, 690

Madau P., Dickinson M., 2014, Annual Review of Astronomy and Astrophysics, 52, 415

Magoulas C., Colless M., Jones D., Springob C., Mould J., 2009, Proceedings of the International Astronomical Union, 5, 376

Mahmood F., Jeganathan J., Saraf R., Shahul S., Swaminathan M., Mackensen G. B., Knio Z., Matyal R., 2016, Journal of Cardiothoracic and Vascular Anesthesia, 30, 470

Mannucci F., Basile F., Poggianti B., Cimatti A., Daddi E., Pozzetti L., Vanzi L., 2001, Monthly Notices of the Royal Astronomical Society, 326, 745

Maraschi L., Ghisellini G., Celotti A., 1992, Astrophysical Journal Letters, 397, L5

Maraston C., Pforr J., Renzini A., Daddi E., Dickinson M., Cimatti A., Tonini C., 2010, Monthly Notices of the Royal Astronomical Society, 407, 830

Marchesini D., van Dokkum P. G., Schreiber N. M. F., Franx M., Labbé I., Wuyts S., 2009, The Astrophysical Journal, 701, 1765

Marshall D. J., Robin A. C., Reylé C., Schultheis M., Picaud S., 2006, Astronomy & Astrophysics, 453, 635

Massaro E., Giommi P., Leto C., Marchegiani P., Maselli A., Perri M., Piranomonte S., Sclavi S., 2008, Astronomy & Astrophysics, 495, 691

Matthews T. A., Sandage A. R., 1963, The Astrophysical Journal, 138, 30

McGaugh S. S., 2005, The Astrophysical Journal, 632, 859

McGaugh S. S., Schombert J. M., Bothun G. D., de Blok W. J. G., 2000, The Astrophysical Journal, 533, L99

Messier C., 1781, Catalogue des Nébuleuses et des Amas d'Étoiles (Catalog of Nebulae and Star Clusters), Connoissance des Temps ou des Mouvements Célestes

Miller J. S., Antonucci R. R. J., 1983, The Astrophysical Journal, 271, L7

Minkowski R., 1941, Publications of the Astronomical Society of the Pacific, 53, 224

Mitchell P. D., Lacey C. G., Baugh C. M., Cole S., 2013, Monthly Notices of the Royal Astronomical Society, 435, 87

Mücke A., Protheroe R. J., Engel R., Rachen J. P., Stanev T., 2003, Astroparticle Physics, 18, 593

Muriel H., Donzelli C., Rovero A. C., Pichel A., 2015, Astronomy & Astrophysics, 574, A101

Murphy T., Mauch T., Green A., Hunstead R. W., Piestrzynska B., Kels A. P., Sztajer P., 2007, Monthly Notices of the Royal Astronomical Society, 382, 382

Muzzin A., et al., 2013, The Astrophysical Journal, 777, 18

Nesci R., Sclavi S., Massaro E., 2005, Astronomy & Astrophysics, 434, 895

Neugebauer G., Becklin E. E., Oke J. B., Searle L., 1976, The Astrophysical Journal, 205, 29

Noeske K. G., et al., 2007a, The Astrophysical Journal, 660, L43

Noeske K. G., et al., 2007b, The Astrophysical Journal, 660, L47

Norris R. P., et al., 2011, Publications of the Astronomical Society of Australia, 28, 215

O'Dowd M., Urry C. M., 2005, The Astrophysical Journal, 627, 97

Obreja A., Brook C. B., Stinson G., Domínguez-Tenreiro R., Gibson B. K., Silva L., Granato G. L., 2014, Monthly Notices of the Royal Astronomical Society, 442, 1794

Ochsenbein F., 1996, The VizieR database of astronomical catalogues, doi:10.26093/CDS/VIZIER

Oke J. B., 1963, Nature, 197, 1040

Oke J. B., Sargent W. L. W., 1968, The Astrophysical Journal, 151, 807

Osterbrock D. E., 1978, Proceedings of the National Academy of Science, 75, 540

Osterbrock D. E., Parker R. A. R., 1965, The Astrophysical Journal, 141, 892

Outram P., Smith R., Shanks T., Boyle B., Croom S., Loaring N., Miller L., 2001, Monthly Notices of the Royal Astronomical Society, 328, 805

Padmanabhan N., et al., 2008, The Astrophysical Journal, 674, 1217

Padovani P., Giommi P., 1995, Monthly Notices of the Royal Astronomical Society, 277, 1477

Paegert M., et al., 2015, The Astronomical Journal, 149, 186

Pannella M., et al., 2015, The Astrophysical Journal, 807, 141

Pâris I., et al., 2012, Astronomy & Astrophysics, 548, A66

Pawlak M., et al., 2019, Monthly Notices of the Royal Astronomical Society, 487, 5932–5945

Peebles P. J. E., 1966, The Astrophysical Journal, 146, 542

Peebles P. J. E., Ratra B., 2003, Reviews of Modern Physics, 75, 559

Penzias A. A., Wilson R. W., 1965, The Astrophysical Journal, 142, 419

Pigatto L., 2005, Island Universes, Novae and Supernovae. A Great Debate of the XX Century. Astronomical Society of the Pacific, p. 43

Pimbblet K. A., Penny S. J., Davies R. L., 2014, Monthly Notices of the Royal Astronomical Society, 438, 3049

Plotkin R. M., Anderson S. F., Hall P. B., Margon B., Voges W., Schneider D. P., Stinson G., York D. G., 2008, The Astronomical Journal, 135, 2453

Plotkin R. M., et al., 2010, The Astronomical Journal, 139, 390

Poe E. A., 1848, Eureka. Leavitt, Trow & Co. Prs., 33 Ann-street.

Pogson N., 1856, Monthly Notices of the Royal Astronomical Society, 17, 12

Poulin V., Smith T. L., Karwal T., Kamionkowski M., 2019, Physical Review Letters, 122, 221301

Pruzhinskaya M. V., Lisakov S. M., 2016, Journal of Astronomical History and Heritage, 19, 203

Ptolemy 1998, Ptolemy's Almagest. Princeton University Press, Princeton

Quilis V., 2000, Science, 288, 1617

Ramazani V. F., Lindfors E., Nilsson K., 2017, Astronomy & Astrophysics, 608, A68

Reddy N. A., Steidel C. C., Fadda D., Yan L., Pettini M., Shapley A. E., Erb D. K., Adelberger K. L., 2006, The Astrophysical Journal, 644, 792

Renzini A., Peng Y., 2015, The Astrophysical Journal, 801, L29

Rieke G. H., 1978, The Astrophysical Journal, 226, 550

Rieke G. H., Low F. J., 1972, The Astrophysical Journal Letters, 176, L95

Riess A. G., Press W. H., Kirshner R. P., 1996, The Astrophysical Journal, 473, 88

Riess A. G., et al., 2016, The Astrophysical Journal, 826, 56

Robertson H. P., 1935, The Astrophysical Journal, 82, 284

Roche N., Bernardi M., Hyde J., 2009, Monthly Notices of the Royal Astronomical Society, 398, 1549

Rodighiero G., et al., 2011, The Astrophysical Journal, 739, L40

Rodighiero G., et al., 2014, Monthly Notices of the Royal Astronomical Society, 443, 19

Roos M., 2008, arXiv e-prints, p. arXiv:0802.2005

Rosario D., et al., 2012, Astronomy & Astrophysics, 545, A45

Ross N. P., et al., 2012, The Astrophysical Journal Supplement Series, 199, 3

Rowan-Robinson M., 1977, The Astrophysical Journal, 213, 635

Ryden B., 2003, Introduction to cosmology. Addison-Wesley, San Francisco

Sadat R., Blanchard A., Mendiboure C., Kneib J. P., 2004, Advances in Space Research, 34, 2516

Sakai S., 1999, in Cosmological Parameters and the Evolution of the Universe. p. 48

Salim S., et al., 2007, The Astrophysical Journal Supplement Series, 173, 267

Salmi F., Daddi E., Elbaz D., Sargent M., Dickinson M., Renzini A., Bethermin M., Borgne D. L., 2012, The Astrophysical Journal, 754, L14

Salpeter E. E., 1955, The Astrophysical Journal, 121, 161

Salpeter E. E., 1964, The Astrophysical Journal, 140, 796

Sandage A., 1965, The Astrophysical Journal, 141, 1560

Sandage A. R., 1971, in Study Week on Nuclei of Galaxies. p. 271

Saunders W., Gillingham P. R., 2016, in Hall H. J., Gilmozzi R., Marshall H. K., eds, Society of Photo-Optical Instrumentation Engineers (SPIE) Conference Series Vol. 9906, Ground-based and Airborne Telescopes VI. p. 990638

Sbarufatti B., Treves A., Falomo R., 2005, The Astrophysical Journal, 635, 173

Scarpa R., Urry C. M., Falomo R., Pesce J. E., Treves A., 2000a, The Astrophysical Journal, 532, 740

Scarpa R., Urry C. M., Padovani P., Calzetti D., O'Dowd M., 2000b, The Astrophysical Journal, 544, 258

Schechter P., 1976, The Astrophysical Journal, 203, 297

Schlegel D. J., Finkbeiner D. P., Davis M., 1998, The Astrophysical Journal, 500, 525

Schmidt M., 1963, Nature, 197, 1040

Schmitt J. L., 1968, Nature, 218, 663

Schreiber C., et al., 2014, Astronomy & Astrophysics, 575, A74

Seo H.-J., Eisenstein D. J., 2003, The Astrophysical Journal, 598, 720

Serjeant S., 2010, Observational cosmology. Cambridge University Press Open University, Cambridge

Seyfert C. K., 1943, The Astrophysical Journal, 97, 28

Seyfert C. K., 1948, The Astronomical Journal, 53, 203

Shankar F., Weinberg D. H., Miralda-Escudé J., 2009, The Astrophysical Journal, 690, 20

Shao L., et al., 2010, Astronomy & Astrophysics, 518, L26

Shapley H., Curtis H. D., 1921, Bulletin of the National Research Council, 2, 171

Shemmer O., Brandt W. N., Anderson S. F., Diamond-Stanic A. M., Fan X., Richards G. T., Schneider D. P., Strauss M. A., 2009, The Astrophysical Journal, 696, 580

Shields G. A., 1974, The Astrophysical Journal, 191, 309

Shields G. A., 1977, Astrophysical Letters, 18, 119

Shields G. A., 1978, Nature, 272, 706

Shields G. A., 1999, Publications of the Astronomical Society of the Pacific, 111, 661

Shimwell T. W., et al., 2017, Astronomy & Astrophysics, 598, A104

Shimwell T. W., et al., 2019, Astronomy & Astrophysics, 622, A1

Shklovskii I. S., 1964, Soviet Astronomy, 8, 132

Sikora M., Begelman M. C., Rees M. J., 1994, The Astrophysical Journal, 421, 153

Slipher V. M., 1915, Popular Astronomy, 23, 21

Smith R. W., 2009, The Expanding Universe. Cambridge University Press, Cambridge

Smith H. J., Hoffleit D., 1963, The Astronomical Journal, 68, 292

Smith E. P., Heckman T. M., Bothun G. D., Romanishin W., Balick B., 1986, The Astrophysical Journal, 306, 64

Sorce J. G., Tully R. B., Courtois H. M., Jarrett T. H., Neill J. D., Shaya E. J., 2014, Monthly Notices of the Royal Astronomical Society, 444, 527

Souffrin S., 1969, Astronomy & Astrophysics, 1, 414

Sparre M., Hayward C. C., Feldmann R., Faucher-Giguère C.-A., Muratov A. L., Kereŝ D., Hopkins P. F., 2016, Monthly Notices of the Royal Astronomical Society, 466, 88

Speagle J. S., Steinhardt C. L., Capak P. L., Silverman J. D., 2014, The Astrophysical Journal Supplement Series, 214, 15

Spergel D. N., et al., 2007, The Astrophysical Journal Supplement Series, 170, 377

Spitzer Lyman J., Saslaw W. C., 1966, The Astrophysical Journal, 143, 400

Springob C. M., Masters K. L., Haynes M. P., Giovanelli R., Marinoni C., 2007, The Astrophysical Journal Supplement Series, 172, 599

Springob C. M., et al., 2014, Monthly Notices of the Royal Astronomical Society, 445, 2677

Stein W. A., Weedman D. W., 1976, The Astrophysical Journal, 205, 44

Stein W. A., O'Dell S. L., Strittmatter P. A., 1976, Annual review of astronomy and astrophysics, 14, 173

Stensbo-Smidt K., Gieseke F., Igel C., Zirm A., Pedersen K. S., 2016, Monthly Notices of the Royal Astronomical Society, 464, 2577

Stickel M., Meisenheimer K., Kühr H., 1994, Astronomy & Astrophysics Supplement Series, 105, 211

Stoner E. C., 1929, The London, Edinburgh, and Dublin Philosophical Magazine and Journal of Science, 7, 63

Straatman C. M. S., et al., 2016, The Astrophysical Journal, 830, 51

Tasca L. A. M., et al., 2015, Astronomy & Astrophysics, 581, A54

Taubenberger S., et al., 2019, Astronomy & Astrophysics, 628, L7

Taylor E. N., et al., 2011, Monthly Notices of the Royal Astronomical Society, 418, 1587

Terlevich R., Melnick J., 1985, Monthly Notices of the Royal Astronomical Society, 213, 841

Terlevich R., Tenorio-Tagle G., Franco J., Melnick J., 1992, Monthly Notices of the Royal Astronomical Society, 255, 713

The MSE Science Team et al., 2019, arXiv e-prints, p. arXiv:1904.04907

Theureau G., Hanski M. O., Coudreau N., Hallet N., Martin J. M., 2007, Astronomy & Astrophysics, 465, 71

Thomas D., Maraston C., Bender R., de Oliveira C. M., 2005, The Astrophysical Journal, 621, 673

Tremonti C. A., et al., 2004, The Astrophysical Journal, 613, 898

Trumpler R. J., 1930, Lick Observatory Bulletins, 14, 154

Tsvetkov D. Y., Pavlyuk N. N., Bartunov O. S., 2004, Astronomy Letters, 30, 729

Tully R. B., Courtois H. M., 2012, The Astrophysical Journal, 749, 78

Tully R. B., de Marseille O., Fisher J. R., 1975, in Bulletin of the American Astronomical Society. p. 426

Ulrich M. H., et al., 1984, Monthly Notices of the Royal Astronomical Society, 206, 221

Urry M., 1999, in Takalo L. O., Sillanpää A., eds, Astronomical Society of the Pacific Conference Series Vol. 159, BL Lac Phenomenon. p. 3 (arXiv:astro-ph/9812420)

Urry C. M., Padovani P., 1995, Publications of the Astronomical Society of the Pacific, 107, 803

Urry C. M., Falomo R., Scarpa R., Pesce J. E., Treves A., Giavalisco M., 1999, The Astrophysical Journal, 512, 88

Urry C. M., Scarpa R., O'Dowd M., Falomo R., Pesce J. E., Treves A., 2000, The Astrophysical Journal, 532, 816

Uzan J.-P., 2016, arXiv e-prints, p. arXiv:1606.06112

Verde L., Treu T., Riess A. G., 2019, Nature Astronomy, 3, 891

Visvanathan N., Oke J. B., 1968, The Astrophysical Journal Letters, 152, L165

Voute J., 1917, Monthly Notices of the Royal Astronomical Society, 77, 650

Walker M. F., 1968, The Astrophysical Journal, 151, 71

Weinberg 1972, Gravitation and Cosmology. John Wiley & Sons, Hoboken

Weiner B. J., et al., 2007, The Astrophysical Journal, 660, L39

Weinmann S. M., van den Bosch F. C., Yang X., Mo H. J., 2006, Monthly Notices of the Royal Astronomical Society, 366, 2

Weinmann S. M., Kauffmann G., van den Bosch F. C., Pasquali A., McIntosh D. H., Mo H., Yang X., Guo Y., 2009, Monthly Notices of the Royal Astronomical Society, 394, 1213

Weymann R. J., 1970, The Astrophysical Journal, 160, 31

Whitaker K. E., van Dokkum P. G., Brammer G., Franx M., 2012, The Astrophysical Journal, 754, L29

White R. L., Becker R. H., Helfand D. J., Gregg M. D., 1997, The Astrophysical Journal, 475, 479

Wilkinson C. L., Pimbblet K. A., Stott J. P., 2017, Monthly Notices of the Royal Astronomical Society, 472, 1447

Willott C. J., Rawlings S., Blundell K. M., Lacy M., 1998, Monthly Notices of the Royal Astronomical Society, 300, 625

Willott C. J., Rawlings S., Jarvis M. J., Blundell K. M., 2003, Monthly Notices of the Royal Astronomical Society, 339, 173

Wisniewski W. Z., Wing R. F., Spinard H., Johnson H. L., 1967, The Astrophysical Journal, 148, L29

Woltjer L., 1959, The Astrophysical Journal, 130, 38

Wurtz R., Stocke J. T., Yee H. K. C., 1996, The Astrophysical Journal Supplement Series, 103, 109

Wuyts S., et al., 2011, The Astrophysical Journal, 742, 96

Xu Y.-D., Cao X., Wu Q., 2009, The Astrophysical Journal, 694, L107

Yahil A., Vidal N. V., 1977, The Astrophysical Journal, 214, 347

Yuan T.-T., Kewley L. J., Swinbank A. M., Richard J., 2012, The Astrophysical Journal, 759, 66

Zabludoff A. I., Huchra J. P., Geller M. J., 1990, The Astrophysical Journal Supplement Series, 74, 1

Zamojski M. A., et al., 2007, The Astrophysical Journal Supplement Series, 172, 468

Zasov A. V., Khoperskov A. V., Saburova A. S., 2011, Astronomy Letters, 37, 374

Zasowski G., et al., 2013, The Astronomical Journal, 146, 81

Zel'dovich Y. B., 1964, Soviet Physics Doklady, 9, 195

Zheng X. C., et al., 2020, Astronomy & Astrophysics, 644, A12

Zhu G., Blanton M. R., Moustakas J., 2010, The Astrophysical Journal, 722, 491

Zibetti S., Charlot S., Rix H.-W., 2009, Monthly Notices of the Royal Astronomical Society, 400, 1181

de Vaucouleurs G., 1948, Annales d'Astrophysique, 11, 247

van Leeuwen F., 2013, Astronomy & Astrophysics, 550, L3

van Leeuwen F., Feast M. W., Whitelock P. A., Laney C. D., 2007, Monthly Notices of the Royal Astronomical Society, 379, 723

van den Bosch F. C., Pasquali A., Yang X., Mo H. J., Weinmann S., McIntosh D. H., Aquino D., 2008, arXiv e-prints, p. arXiv:0805.0002